

**A STUDY OF NUCLEATION BY ATTRITION IN
AGITATED DRAFT-TUBE BAFFLE
CRYSTALLIZERS**

Thirawat Mueansichai

A Thesis Submitted in Partial Fulfillment of the Requirements for the

Degree of Doctor of Philosophy in Chemical Engineering

Suranaree University of Technology

Academic Year 2012

การศึกษาการเกิดนิเวศเสียจากการสึกกร่อนในเครื่องตกผลึก
แบบกวนที่มีกราฟต์-ทิวบ์และแผ่นกั้น

นายธีระวัฒน์ เหมือนศรีชัย

วิทยานิพนธ์นี้เป็นส่วนหนึ่งของการศึกษาตามหลักสูตรปริญญาวิศวกรรมศาสตรดุษฎีบัณฑิต
สาขาวิชาวิศวกรรมเคมี
มหาวิทยาลัยเทคโนโลยีสุรนารี
ปีการศึกษา 2555

A STUDY OF NUCLEATION BY ATTRITION IN AGITATED DRAFT-TUBE BAFFLE CRYSTALLIZERS

Suranaree University of Technology has approved this thesis submitted in partial fulfillment of the requirements for the Degree of Doctor of Philosophy.

Thesis Examining Committee

(Dr. Terasut Sookkumnerd)

Chairperson

(Prof. Dr. Adrian Evan Flood)

Member (Thesis Advisor)

(Asst. Prof. Dr. Atichat Wongkoblap)

Member

(Asst. Prof. Dr. Boris Golman)

Member

(Asst. Prof. Dr. Sopark Sonwai)

Member

(Prof. Dr. Sukit Limpijumnong)

Vice Rector for Academic Affairs

(Assoc. Prof. Flt. Lt. Dr. Kontom Chamniprasart)

Dean of Institute of Engineering

ธีระวัฒน์ เหมือนศรีชัย : การศึกษาการเกิดนิวเคลียสจากการสึกกร่อนในเครื่องตกผลึกแบบกวนที่มีดราฟต์-ทิวบ์และแผ่นกั้น (A STUDY OF NUCLEATION BY ATTRITION IN AGITATED DRAFT-TUBE BAFFLE CRYSTALLIZERS) อาจารย์ที่ปรึกษา : ศาสตราจารย์ ดร. เอเดรียน ฟลัด, 164 หน้า.

การสึกกร่อนเป็นกลไกสำคัญอันหนึ่งในการสร้างนิวเคลียสชนิดทุติยภูมิในเครื่องตกผลึกระดับอุตสาหกรรม งานวิจัยนี้มีวัตถุประสงค์เพื่อให้เกิดความเข้าใจพฤติกรรมการสึกกร่อนและสร้างแบบจำลองทางคณิตศาสตร์จากการทดลองสำหรับพยากรณ์อัตราการเกิดนิวเคลียสที่เกิดจากกลไกการสึกกร่อน โดยทำการทดลองศึกษาผลกระทบของรูปทรงทางเรขาคณิตของเครื่องตกผลึกและสภาวะการทำงานของเครื่องตกผลึก (เส้นผ่านศูนย์กลางของใบพัด (Impeller diameter) เส้นผ่านศูนย์กลางของดราฟต์-ทิวบ์ (Draft-tube diameter) ชนิดของใบพัด (Impeller type) วัสดุที่ใช้ในการทำใบพัด (Impeller material) และ ความเร็วรอบของใบพัด (Impeller speed)) คุณสมบัติของผลึก (ชนิดของผลึกตั้งต้น (Parent crystal type) ได้แก่ น้ำตาลซูโครส (Sucrose) เกลือโซเดียมคลอไรด์ (Sodium chloride, NaCl) และขนาดของผลึกตั้งต้น (Parent crystal size)) คุณสมบัติของการแขวนลอยและคุณสมบัติของสารละลาย (ความหนาแน่นของการแขวนลอย (Suspension density) ความหนาแน่นของสารละลาย (Solution density) และความหนืดของสารละลาย (Solution viscosity)) ที่มีต่ออัตราการเกิดขึ้นและการกระจายขนาดของชิ้นส่วนจากการสึกกร่อน (Attrition fragment) โดยที่ทำการทดลองแบบกะในระดับห้องปฏิบัติการ

การหาจำนวนของชิ้นส่วนจากการสึกกร่อนและการกระจายขนาดของชิ้นส่วนจากการสึกกร่อนทำการวัดโดยใช้เครื่อง Multisizer 3 Coulter Counter และเครื่อง Malvern Mastersizer S จากนั้นสร้างกราฟแสดงความสัมพันธ์ระหว่างจำนวนชิ้นส่วนจากการสึกกร่อนและเวลาเพื่อทำการหาค่าอัตราการเกิดนิวเคลียสจากค่าความชันของกราฟดังกล่าว จากผลการทดลองของอัตราการสึกกร่อนแสดงให้เห็นว่าตัวแปรที่มีความสำคัญสำหรับการสร้างแบบจำลองทางคณิตศาสตร์ได้แก่ ความเร็วรอบของใบพัด ขนาดของผลึกตั้งต้น ความหนาแน่นของการแขวนลอย ระยะห่างระหว่างใบพัดกับก้นถัง (Off-bottom clearance) และระยะห่างระหว่างดราฟต์-ทิวบ์กับใบพัด (Draft-tube impeller clearance) แบบจำลองทางคณิตศาสตร์จากการทดลองนี้ได้ใช้ตัวแปรที่มีผลต่ออัตราการสึกกร่อนและคุณสมบัติของสารละลายและคุณสมบัติของผลึกมาสร้างเป็นกลุ่มตัวแปรไร้มิติเพื่ออธิบายถึงอัตราการเกิดนิวเคลียสที่เกิดจากการสึกกร่อน กลุ่มตัวแปรไร้มิติที่ใช้ได้แก่ ตัวเลขการสึกกร่อน (Attrition number) ตัวเลขกำลัง (Power number) ตัวเลขเรย์โนลด์ (Reynolds number) ตัวเลขขนาดผลึกตั้งต้น (Parent crystal size number) ตัวเลขความหนาแน่นการแขวนลอย

(Suspension density number) ตัวเลขกราฟต์-ทิวป์ (Draft-tube number) และตัวเลขระยะห่างระหว่างใบพัดกับก้นถัง (Off-bottom clearance) แบบจำลองทางคณิตศาสตร์จากการทดลองแบบยกกำลังให้ผลสอดคล้องกับค่าอัตราการเกิดนิวเคลียสจากข้อมูลการทดลอง แบบจำลองทางคณิตศาสตร์จากการทดลองสามารถใช้อธิบายอัตราการสึกกร่อนของสารสองชนิด คือ น้ำตาลซูโครสและเกลือ โซเดียมคลอไรด์ได้เป็นอย่างดี

ประโยชน์จากงานวิจัยนี้คือ สามารถสร้างแบบจำลองทางคณิตศาสตร์จากการทดลองสำหรับประมาณการจำนวนนิวเคลียสชนิดทุติยภูมิที่เกิดจากการสึกกร่อน และความรู้จากการศึกษาครั้งนี้สามารถนำไปใช้ในการปรับปรุงคุณภาพของผลิตภัณฑ์เพราะความรู้เกี่ยวกับแบบจำลองทางคณิตศาสตร์ของการสึกกร่อนจะทำให้สามารถควบคุมอัตราการเกิดการสึกกร่อนในเครื่องตกผลึกระดับอุตสาหกรรมได้



THIRAWAT MUEANSICHAJ : A STUDY OF NUCLEATION BY
ATTRITION IN AGITATED DRAFT-TUBE BAFFLE CRYSTALLIZERS.
THESIS ADVISOR : PROF. ADRIAN FLOOD, Ph.D., 164 PP.

NUCLEATION/ATTRITION/FRAGMENT NUMBER/EMPIRICAL
MODEL/INDUSTRIAL CRYSTALLIZATION

Attrition is the main mechanism that produces secondary nuclei in industrial crystallizers. This work helps to understand the attrition behavior and model the empirical equation to predict the nucleation rate from this mechanism. The experiments studied the effect of crystallizer geometry and operating conditions (impeller diameter, draft tube diameter, impeller type, impeller material, and impeller speed), crystal properties (type of parent crystal: sucrose, NaCl and size of parent crystal), and suspension and solution properties (suspension density, solution density, and solution viscosity) on the rate of generation and size distribution of attrition fragments with a batch process on a laboratory scale.

Determination of the number of attrition fragments and attrition fragment size distribution was performed using a Multisizer 3 Coulter Counter and a Malvern Mastersizer S. The number of attrition fragment versus time was plotted to find the nucleation rate from the slope of the curve. The results of attrition rate show significant parameters for modeling of empirical correlation are impeller speed, parent crystal size, suspension density, and draft-tube impeller clearance. Then, the dimensionless groups were calculated and used for data fitting to get the empirical model. The dimensionless groups are attrition number, power number, Reynolds

number, parent crystal size number, suspension density number, draft-tube number, and off-bottom clearance number. The value of the nucleation rate from the experimental data was compared with an empirical power law model. The empirical model can fit the attrition rate for the two species (sucrose and NaCl) very well.

The benefits from this work are the model of secondary nucleation from attrition and the improvement in the product quality, because knowledge of the attrition model will allow us to control the attrition rate in industrial crystallizers.



School of Chemical Engineering

Academic Year 2012

Student's Signature _____

Advisor's Signature _____

ACKNOWLEDGEMENTS

First of all, I would like to express my sincere gratitude to my thesis advisor, Prof. Dr. Adrian E. Flood for his invaluable help, supporting information and encouragement throughout the course of this research. I would like to thank him for providing me with the opportunity to undertake a program of study Ph.D. and for his tireless effort in correcting my English and encouraging me to complete my work.

Special thanks go to Prof. Dr.-Ing. habil. Dr. h.c. Joachim Ulrich and Dr.-Ing. Torsten Stelzer, the Thermal Process Technology (TVT) at Martin Luther University Halle-Wittenberg (MLU) in Halle (Saale), Germany, for their advice, patience, supporting information and useful materials during my oversea research at MLU.

I would also like to thank the entire thesis examining committee: Dr. Terasut Sookkumnerd, Asst. Prof. Dr. Boris Golman, Asst. Prof. Dr. Atichat Wongkoblaph, and Asst. Prof. Dr. Sopark Sonwai for their advice and wonderful questions.

In addition, I would like to thank all of the lecturers at the School of Chemical Engineering, Suranaree University of Technology (SUT) for their suggestion and help. Special thanks go to Prof. Dr. Chaiyot Tangsathitkulchai, Asst. Prof. Dr. Chalongsri Flood, Asst. Prof. Dr. Panarat Rattanaphanee, and Dr. Supunnee Junpirom for their invaluable assistance and great advice.

I would like to thank all the member of the technical staff in the Center for Scientific and Technology Equipment (CSTE), SUT, for their support and guideline

for use of the laboratory equipment, and occasional help in characterization of the sample properties and construction of equipment. Special thanks go to Mr. Saran Dokmaikun, Mr. Prasit Ngamsantia, Mr. Manop Jansanitsri, Mr. Anuchit Ruangvittayanon and Mr. Komsun Pasayadej for their skillful technical work and assistance. Many thanks go to Mrs. Amporn Ladnongkhun, our lovely secretary of Chemical Engineering School, for her skillful secretarial work and assistance.

Thanks are also due to my colleagues and friends who are graduate students in the School of Chemical Engineering, SUT and graduate students in the group of Thermal Process Technology (TVT), MLU. Special thanks go to Dr. Kesarin Chaleepa for helping me during my time in Halle (Saale), Germany and Ph.D. candidate in industrial crystallization group, SUT, especially Dr. Sukanya Srisa-nga, Ms. Natthaya Punsuwan and Dr. Lek Wantha for sharing experiences and information.

Financial support both from the Thailand Research Fund (TRF) through the Royal Golden Jubilee Ph.D. Program (RGJ-Ph.D.), grant number 1.C.TS/46/B.2, and the Commission on Higher Education, the Ministry of Education through the scholarship for development of new faculty staff at Rajamangala University of Technology Thanyaburi are greatly appreciated.

Finally, I most gratefully acknowledge my family for their love, supporting, and care. For the invaluable help of everyone I may have forgotten to mention here, I also gratefully acknowledge.

Thirawat Mueansichai

TABLE OF CONTENTS

	Page
ABSTRACT (THAI).....	I
ABSTRACT (ENGLISH).....	III
ACKNOWLEDGEMENTS.....	V
TABLE OF CONTENTS.....	VII
LIST OF TABLES.....	XVI
LIST OF FIGURES.....	XVII
SYMBOLS AND ABBREVIATIONS.....	XXXVII
CHAPTER	
I INTRODUCTION	1
1.1 Background problem and significance of the study.....	1
1.2 Research objectives.....	7
1.3 Scope and limitation of the study.....	8
1.3.1 Design the equipment and the experimental conditions.....	8
1.3.2 Determine the effect of parameters on the attrition rate.....	9
1.3.3 Modeling of crystal attrition equation.....	9
1.4 Output.....	10

TABLE OF CONTENTS (Continued)

	Page
II LITERATURE REVIEW	11
2.1 Industrial Crystallization.....	11
2.1.1 General considerations.....	11
2.1.2 Supersaturation.....	12
2.1.3 Nucleation.....	15
2.2 Secondary Nucleation	17
2.2.1 Origin of secondary nucleation.....	17
2.2.2 Mechanism of secondary nucleation.....	20
2.2.3 Parameters Affecting Secondary Nucleation Rate.....	21
2.2.3.1 Supersaturation.....	21
2.2.3.2 Temperature.....	22
2.2.3.3 The degree of agitation.....	22
2.2.3.4 The hardness of the contact material	24
2.2.4 Secondary nucleation kinetics.....	25
2.3 Attrition Models.....	27
2.3.1 Offermann and Ulrich model.....	27
2.3.2 Gahn and Mersmann model.....	28
2.3.3 Yokota et al. model.....	35
2.3.4 Gharidi and Zhang model.....	37

TABLE OF CONTENTS (Continued)

	Page
2.4 Case study of attrition experiment.....	38
2.4.1 The effect of repeated impacts of individual Crystals.....	38
2.4.2 The effect of crystal-wall or crystal-stirrer impact.....	39
2.4.3 The effect of impact energy and shape of crystal.....	41
2.4.4 Mechanical properties of the crystal.....	42
2.4.4.1 Young's modulus.....	43
2.4.4.2 Vickers hardness.....	43
III RESEARCH PROCEDURE.....	46
3.1 Instrumentation.....	46
3.1.1 The crystallizer.....	46
3.1.2 Multisizer 3 COULTER COUNTER®.....	48
3.1.3 Malvern Mastersizer S.....	50
3.1.4 Wireless Rotary Torque Transducer.....	51
3.1.5 Scanning Electron Microscope (SEM).....	52
3.2 Materials.....	53
3.2.1 Sucrose.....	53
3.2.2 Sodium Chloride.....	54
3.2.3 Cellulose Acetate Membrane	55
3.2.4 Methanol.....	55

TABLE OF CONTENTS (Continued)

	Page
3.2.5 Lithium Chloride.....	55
3.2.6 Deionized water (DI water).....	55
3.3 Experimental Methods.....	56
3.3.1 Determination of significant parameters on attrition rate.....	56
3.3.1.1 Determination of attrition fragment by Malvern Mastersizer S.....	57
3.3.1.2 Determination of attrition fragment by Multisizer 3 Coulter Counter	59
3.3.2 Determination of the attrition fragment size distribution and number per unit volume.....	60
3.3.2.1 Malvern Mastersizer S.....	61
3.3.2.2 Multisizer 3 Coulter Counter.....	61
3.3.3 Determination of attrition rate.....	63
3.3.4 Scale-up crystallizer study.....	65
3.3.5 Determination of power input in the crystallizer and suspension properties.....	68
3.4 Data analysis method and empirical modeling procedure.....	70
3.4.1 Determination of dimensionless groups	70
3.4.2 Determination of the empirical model.....	73

TABLE OF CONTENTS (Continued)

	Page
IV RESULTS AND DISCUSSION.....	74
4.1 Attrition of sucrose crystal in a mixed-suspension crystallizer.....	74
4.1.1 Parent crystal and attrition fragment size distribution.....	75
4.1.2 Effect of impeller speed on attrition rate.....	82
4.1.3 Effect of parent crystal size on attrition rate.....	83
4.1.4 Effect of suspension density on attrition rate.....	84
4.1.5 Effect of impeller material on attrition rate.....	85
4.1.6 Effect of impeller type on attrition rate.....	86
4.1.7 Effect of impeller and draft tube clearance on attrition rate.....	88
4.1.8 Effect of off-bottom impeller clearance on attrition rate.....	89
4.2 Attrition of Sodium Chloride crystals in mixed suspension crystallizers.....	91
4.2.1 Parent crystal and attrition fragment size distribution.....	91
4.2.2 Effect of impeller speed on attrition rate.....	93
4.2.3 Effect of parent crystal size on attrition rate.....	93

TABLE OF CONTENTS (Continued)

	Page
4.2.4 Effect of suspension density on attrition rate.....	95
4.2.5 Effect of draft tube impeller clearance on attrition rate.....	96
4.2.6 Effect of impeller type on attrition rate.....	97
4.2.7 Effect of impeller material on attrition rate.....	98
4.2.8 Effect of off-bottom clearance on attrition rate.....	99
4.3 The effect of scale-up on attrition rate.....	101
4.3.1 The effect of parent crystal size for small scale crystallizer.....	101
4.3.2 The effect of parent crystal size for large scale crystallizer.....	105
4.4 A study of power input and solution properties.....	109
4.4.1 Torque measurement for NaCl system.....	109
4.4.1.1 Effect of impeller speed.....	109
4.4.1.2 Effect of suspension density.....	111
4.4.1.3 Effect of parent crystal size.....	112
4.4.1.4 Effect of off-bottom impeller clearance.....	113
4.4.1.5 Effect of draft tube diameter.....	114

TABLE OF CONTENTS (Continued)

	Page
4.4.2 Torque measurement for sucrose system.....	115
4.4.2.1 Effect of impeller speed.....	115
4.4.2.2 Effect of suspension density.....	116
4.4.2.3 Effect of parent crystal size.....	117
4.4.2.4 Effect of off-bottom impeller clearance.....	118
4.4.2.5 Effect of draft tube diameter.....	119
4.4.3 Power input calculation results.....	120
4.4.4 Solution properties.....	123
4.5 Data analysis for modeling of crystal attrition.....	124
4.5.1 Dimensionless groups.....	124
4.5.1.1 Power number.....	124
4.5.1.2 Reynolds number.....	124
4.5.1.3 Parent crystal size and impeller diameter ratio.....	126
4.5.1.4 Draft tube impeller clearance and impeller diameter ratio.....	127
4.5.1.5 Off-bottom clearance and impeller diameter ratio.....	129
4.5.1.6 Suspension density and crystal density ratio.....	130

TABLE OF CONTENTS (Continued)

	Page
4.5.2 Empirical engineering model.....	133
4.5.2.1 Power law modeling of NaCl.....	133
4.5.2.2 Power law modeling of sucrose.....	135
4.5.2.3 Power law modeling for both system (sucrose and NaCl).....	137
V CONCLUSIONS AND RECOMMENDATIONS.....	140
5.1 Conclusions.....	140
5.1.1 The attrition fragments size distribution.....	140
5.1.2 The effect of parameters from crystallizer properties, crystal properties, and solution properties on the attrition rate.....	141
5.1.3 The effect of scale up on attrition rate.....	142
5.1.4 The suitable dimensionless groups for data fitting.....	142
5.1.5 The empirical engineering model for nucleation rate.....	142
5.2 Recommendations.....	143
5.2.1 Experimental design for study of secondary nucleation.....	143

TABLE OF CONTENTS (Continued)

	Page
5.2.2 Parameters for further study of secondary nucleation.....	143
5.2.3 The general equation for secondary nucleation.....	144
REFERENCES.....	145
APPENDIX PUBLICATIONS.....	154
BIOGRAPHY.....	164



LIST OF TABLES

Table	Page
1.1 Sources of nuclei in industrial crystallization.....	6
2.1 Driving forces for growth and nucleation.....	14
2.2 Hardness values for NaCl crystals.....	45
3.1 Dimensions of the crystallizers.....	47
3.2 General dimensions and characteristics of crystallizer.....	67
4.1 Power input and torque from NaCl experiment.....	121
4.2 Power input and torque from sucrose experiment.....	122
4.3 Viscosity and density of the solution in this work.....	123
4.4 Dimensionless groups for NaCl system.....	131
4.5 Dimensionless groups for sucrose system.....	132
4.6 Attrition number from experiments and empirical model for NaCl system.....	135
4.7 Attrition number from experiments and empirical model for sucrose.....	137

LIST OF FIGURES

Figure	Page
1.1	Distribution of nature of problems encountered..... 1
1.2	The influence of magnitude and direction of a force on the breakage mechanism.....3
2.1	General schematic of a crystallization process..... 12
2.2	Method of supersaturation creation in solution crystallizations.....13
2.3	Mechanism of nucleation.....15
2.4	Example of growth regimes for magnesium sulfate heptahydrate..... 16
2.5	Differentiation of the secondary nucleation mechanisms using enantiomorphous crystals. The fraction of the crystals with the same modification as that of the parent crystal is denoted as percent..... 18
2.6	Nuclei size distribution from contact nucleation..... 19
2.7	Dependence of number of secondary nuclei produced on stirrer speed and supercooling in secondary nucleation of potassium chloride.....23
2.8	Trend of volume percentage of fine fragments (less than 32 μm) vs. time at two different stirring rate: symbols, experimental data; line, calculated curves..... 24
2.9	Effect of agitator speed on secondary nucleation rate for steel and plastic impellers.....25

LIST OF FIGURES (Continued)

Figure	Page
2.10	Contacts of a harder and softer material: a) a cone being deformed by a hard plate, b) a hard cone contacting a softer material. (Gahn and Mersmann, 1999).....29
2.11	Representation of theoretical attrition process. (Gahn and Mersmann, 1997).....30
2.12	Theoretical and experimental values of abraded volumes..... 33
2.13	Theoretical and experimental values of abraded volumes. The substances meet the requirement for the brittle fracture..... 34
2.14	Comparison of experimental results with the prediction of the original model by Gahn and Mersmann (with original, non-tuned material properties) and the proposed extended model..... 35
2.15	Influence of the number of impacts on the attrition of sodium glutamate crystals at an impact velocity of 7 ms^{-1} 39
2.16	Comparison between the size distribution (in number) of the NaCl crystals before and after the impact (pressure 2 bars, inject-target distance 8 cm).....40
2.17	Picture of examples of NaCl crystals before the impact (a) and after the impact (b) (pressure 2 bars, inject-target distance 8 cm).....40
2.18	Mass of attrition fragments as a function of impact energy.....42
2.19	Volume of fragments as a function of impact energy.....42
2.20	Compression profile obtained for NaCl single crystal..... 44

LIST OF FIGURES (Continued)

Figure	Page
2.21	Geometry of the indentation in the Vickers test and obtained pattern on a single crystal surface with 1 N load..... 45
3.1	Schematic diagram of a crystallizer used in the study and experimental set-up Key: (1) motor, (2) wireless rotary torque transducer, (3) data recording, (4) impeller, (5) draft tube, (6) baffles, and (7) crystallizer.....47
3.2	The types of the impeller in the study..... 48
3.3	Diagrammatic illustration of the Coulter Principle applied in the Multisizer 3 and electrical sensing zone technique..... 49
3.4	Multisizer 3 COULTER COUNTER®..... 50
3.5	The Malvern Mastersizer S and its accessories Key: (1) the optical unit, (2) one or more sample preparation accessories, and (3) a computer system.....51
3.6	Rotary torque transducer and wireless force indicator..... 52
3.7	SEM micrograph of a sucrose parent crystal size range 300 - 425 μm 53
3.8	SEM micrograph of a NaCl parent crystal size range 300 - 425 μm54

LIST OF FIGURES (Continued)

Figure	Page
3.9 Changes in the number-based and volume-based particle size distributions for a sample taken from the 500 mL batch crystallizer (slightly supersaturated solution of NaCl in 80% methanol; 300-425 μm NaCl parent crystals; suspension density 0.1 g/mL; stainless steel marine upflow impeller; impeller speed 1000 rpm; crystallizer diameter 90 mm; draft tube diameter 64 mm; impeller diameter 50 mm; off-bottom clearance 10 mm).....	63
3.10 Increase in number counts with respect to time for a sample taken from the 500 mL batch crystallizer (slightly supersaturated solution of NaCl in 80% methanol; 300-425 μm NaCl parent crystals; suspension density 0.025, 0.050, and 0.100 g/mL; stainless steel marine upflow impeller; impeller speed 1000 rpm; crystallizer diameter 90 mm; draft tube diameter 64 mm; impeller diameter 50 mm; off-bottom clearance 10 mm).....	64
3.11 Schematic diagram of the crystallizer for scale up study.....	68

LIST OF FIGURES (Continued)

Figure	Page
4.1 Changes in the volume-based and number-based particle size distribution for a sample taken from the 500 mL batch crystallizer. (saturated solution of sucrose in methanol; 425 - 600 μm NaCl parent crystals; suspension density 0.1 g/mL; stainless steel marine upflow impeller; impeller speed 1200 rpm; crystallizer diameter 90 mm; draft tube diameter 64 mm; impeller diameter 50 mm; off-bottom clearance 10 mm).....	76
4.2 Number of attrition fragments as a function of time for calculation of attrition rate. (saturated solution of sucrose in methanol; 425 – 600 and 600 - 850 μm NaCl parent crystals; suspension density 0.1 g/mL; stainless steel marine upflow impeller; impeller speed 1000 rpm; crystallizer diameter 90 mm; draft tube diameter 64 mm; impeller diameter 50 mm; off-bottom clearance 10 mm).....	77
4.3 Attrition fragment geometric mean versus time and average size as a function of impeller speed. (saturated solution of sucrose in methanol; 425 – 600 μm NaCl parent crystals; suspension density 0.1 g/mL; stainless steel marine upflow impeller; impeller speed 800, 1000, 1200 rpm; crystallizer diameter 90 mm; draft tube diameter 64 mm; impeller diameter 50 mm; off-bottom clearance 10 mm).....	79

LIST OF FIGURES (Continued)

Figure	Page
4.4 Rate of increase in fragment volume per mL suspension. (saturated solution of sucrose in methanol; 425 – 600 μm NaCl parent crystals; suspension density 0.1 g/mL; stainless steel marine upflow impeller; impeller speed 800, 1000, 1200 rpm; crystallizer diameter 90 mm; draft tube diameter 64 mm; impeller diameter 50 mm; off-bottom clearance 10 mm).....	80
4.5 Parent crystal of sucrose size range 300 – 425 μm	81
4.6 Attrition fragment of sucrose for a sample taken from the 500 mL batch crystallizer (saturated solution of sucrose in methanol; 300-425 μm parent crystals; suspension density 0.1 g/mL; stainless steel marine upflow impeller; impeller speed 1000 rpm; crystallizer diameter 90 mm; draft tube diameter 64 mm; impeller diameter 50 mm; off-bottom clearance 10 mm).....	82
4.7 Attrition rate as a function of impeller speed at standard conditions. (saturated solution of sucrose in methanol; 425 - 600 μm parent crystals; suspension density 0.1 g/mL; stainless steel marine upflow impeller; impeller speed 1000 rpm; crystallizer diameter 90 mm; draft tube diameter 64 mm; impeller diameter 50 mm; off-bottom clearance 10 mm).....	83

LIST OF FIGURES (Continued)

Figure	Page
4.8 Attrition rate as a function of parent crystal size at standard conditions. (saturated solution of sucrose in methanol; 300 – 425, 425 – 600, 600 - 850 μm parent crystals; suspension density 0.1 g/mL; stainless steel marine upflow impeller; impeller speed 1000 rpm; crystallizer diameter 90 mm; draft tube diameter 64 mm; impeller diameter 50 mm; off-bottom clearance 10 mm).....	84
4.9 Attrition rate as a function of suspension density at standard conditions. (saturated solution of sucrose in methanol; 425 – 600 μm parent crystals; suspension density 0.1 and 0.15 g/mL; stainless steel marine upflow impeller; impeller speed 1000 rpm; crystallizer diameter 90 mm; draft tube diameter 64 mm; impeller diameter 50 mm; off-bottom clearance 10 mm).....	85
4.10 Attrition rate as a function of impeller material at standard conditions. (saturated solution of sucrose in methanol; 425 – 600 μm parent crystals; suspension density 0.1 g/mL; stainless steel and resin marine upflow impeller; impeller speed 1000 rpm; crystallizer diameter 90 mm; draft tube diameter 64 mm; impeller diameter 50 mm; off-bottom clearance 10 mm).....	86

LIST OF FIGURES (Continued)

Figure	Page
4.11 Attrition rate as a function of impeller speed for marine impeller. (saturated solution of sucrose in methanol; 425 – 600 μm parent crystals; suspension density 0.1 g/mL; stainless steel marine upflow impeller; impeller speed 1000 and 1200 rpm; crystallizer diameter 90 mm; draft tube diameter 64 mm; impeller diameter 50 mm; off-bottom clearance 10 mm).....	87
4.12 Attrition rate as a function of impeller speed for pitch blade impeller. (saturated solution of sucrose in methanol; 425 – 600 μm parent crystals; suspension density 0.1 g/mL; stainless steel pitch blade upflow impeller; impeller speed 1000 and 1200 rpm; crystallizer diameter 90 mm; draft tube diameter 64 mm; impeller diameter 50 mm; off-bottom clearance 10 mm).....	88
4.13 Attrition rate as a function of impeller and draft tube ratio at standard conditions. (saturated solution of sucrose in methanol; 425 – 600 μm parent crystals; suspension density 0.1 g/mL; stainless steel pitch blade upflow impeller; impeller speed 1000 rpm; crystallizer diameter 90 mm; draft tube diameter 64 and 75 mm; impeller diameter 50 mm; off-bottom clearance 10 mm).....	89

LIST OF FIGURES (Continued)

Figure	Page
4.14 Attrition rate as a function of clearance and draft tube ratio at standard conditions. (saturated solution of sucrose in methanol; 425 – 600 μm parent crystals; suspension density 0.1 g/mL; stainless steel pitch blade upflow impeller; impeller speed 1000 rpm; crystallizer diameter 90 mm; draft tube diameter 64 mm; impeller diameter 50 mm; off-bottom clearance 10 and 20 mm).....	90
4.15 SEM photographs of parent crystals before and after the experiment and attrition fragments. (slightly supersaturated solution of NaCl in 80% methanol; 300 - 425 μm NaCl parent crystals; suspension density 0.1 g/mL; stainless steel marine upflow impeller; impeller speed 1000 rpm; crystallizer diameter 90 mm; draft tube diameter 64 mm; impeller diameter 50 mm; off-bottom clearance 10 mm).....	92
4.16 The attrition rate as a function of impeller speed, (slightly supersaturated solution of NaCl in 80% methanol; 300-425 μm NaCl parent crystals; suspension density 0.10 g/mL; stainless steel marine upflow impeller; impeller speed 800, 1000, 1200 rpm; crystallizer diameter 90 mm; draft tube diameter 64 mm; impeller diameter 50 mm; off-bottom clearance 10 mm).....	94

LIST OF FIGURES (Continued)

Figure	Page
4.17 The attrition rate as a function of parent crystal size. (slightly supersaturated solution of NaCl in 80% methanol; 150 – 300, 300-425, 425 - 600 μm NaCl parent crystals; suspension density 0.10 g/mL; stainless steel marine upflow impeller; impeller speed 1000 rpm; crystallizer diameter 90 mm; draft tube diameter 64 mm; impeller diameter 50 mm; off-bottom clearance 10 mm).....	95
4.18 The attrition rate as a function of suspension density. (slightly supersaturated solution of NaCl in 80% methanol; 300-425 μm NaCl parent crystals; suspension density 0.05, 0.10, and 0.15 g/mL; stainless steel marine upflow impeller; impeller speed 1000 rpm; crystallizer diameter 90 mm; draft tube diameter 64 mm; impeller diameter 50 mm; off-bottom clearance 10 mm).....	96
4.19 The attrition rate as a function of impeller diameter and draft tube diameter ratio (slightly supersaturated solution of NaCl in 80% methanol; 300-425 μm NaCl parent crystals; suspension density 0.10 g/mL; stainless steel marine upflow impeller; impeller speed 1000 rpm; crystallizer diameter 90 mm; draft tube diameter 64 and 75 mm; impeller diameter 50 mm; off-bottom clearance 10 mm).....	97

LIST OF FIGURES (Continued)

Figure	Page
4.20 The attrition rate as a function of impeller type (slightly supersaturated solution of NaCl in 80% methanol; 300-425 μm NaCl parent crystals; suspension density 0.10 g/mL; stainless steel marine upflow impeller and pitch blade; impeller speed 1000 rpm; crystallizer diameter 90 mm; draft tube diameter 64 mm; impeller diameter 50 mm; off-bottom clearance 10 mm).....	98
4.21 The attrition rate as a function of impeller material (slightly supersaturated solution of NaCl in 80% methanol; 300-425 μm NaCl parent crystals; suspension density 0.10 g/mL; stainless steel and resin marine upflow impeller; impeller speed 1000 rpm; crystallizer diameter 90 mm; draft tube diameter 64 mm; impeller diameter 50 mm; off-bottom clearance 10 mm).....	99
4.22 The attrition rate as a function of off-bottom clearance. (slightly supersaturated solution of NaCl in 80% methanol; 300-425 μm NaCl parent crystals; suspension density 0.10 g/mL; stainless steel marine upflow impeller; impeller speed 1000 rpm; crystallizer diameter 90 mm; draft tube diameter 64 mm; impeller diameter 50 mm; off-bottom clearance 10 and 20 mm).....	100

LIST OF FIGURES (Continued)

Figure	Page
4.23 Attrition fragment size distribution for different the parent crystal size. (saturated solution of sucrose in methanol; 250 – 355, 355 – 450, 450 - 600 μm parent crystals; suspension density 0.1 g/mL; stainless steel marine impeller; impeller speed 1700 rpm; crystallizer diameter 80 mm; draft tube diameter 57 mm; impeller diameter 25 mm; off-bottom clearance 15 mm).....	102
4.24 Illustration of log-normal 3 parameters fitting for volume distribution. (Saturated solution of sucrose in methanol; 355 – 450 μm parent crystals; suspension density 0.1 g/mL; stainless steel marine impeller; impeller speed 1700 rpm; crystallizer diameter 80 mm; draft tube diameter 57 mm; impeller diameter 25 mm; off-bottom clearance 15 mm).....	103
4.25 Normalized volume concentrations of attrition fragments as a function of parent crystal size for the small scale crystallizer. (saturated solution of sucrose in methanol; 250 – 355, 355 – 450, 450 - 600 μm parent crystals; suspension density 0.1 g/mL; stainless steel marine impeller; impeller speed 1700 rpm; crystallizer diameter 80 mm; draft tube diameter 57 mm; impeller diameter 25 mm; off-bottom clearance 15 mm).....	104

LIST OF FIGURES (Continued)

Figure	Page
4.26 Normalized attrition rate per seed crystal as a function of parent crystal size for the small scale crystallizer. (saturated solution of sucrose in methanol; 250 – 355, 355 – 450, 450 - 600 μm parent crystals; suspension density 0.1 g/mL; stainless steel marine impeller; impeller speed 1700 rpm; crystallizer diameter 80 mm; draft tube diameter 57 mm; impeller diameter 25 mm; off-bottom clearance 15 mm).....	105
4.27 Size distribution of the attrition fragments for the large scale crystallizer. (saturated solution of sucrose in methanol; 250 – 355, 355 – 450, 450 - 600 μm parent crystals; suspension density 0.1 g/mL; stainless steel marine impeller; impeller speed 850 rpm; crystallizer diameter 100 mm; draft tube diameter 57 mm; impeller diameter 50 mm; off-bottom clearance 27 mm).....	106
4.28 Normalized volume concentrations as a function of parent crystal size for the large scale crystallizer. (saturated solution of sucrose in methanol; 250 – 355, 355 – 450, 450 - 600 μm parent crystals; suspension density 0.1 g/mL; stainless steel marine impeller; impeller speed 850 rpm; crystallizer diameter 100 mm; draft tube diameter 57 mm; impeller diameter 50 mm; off-bottom clearance 27 mm).....	107

LIST OF FIGURES (Continued)

Figure	Page
<p>4.29 Normalized attrition rate as a function of parent crystal size for the large scale crystallizer.</p> <p>(saturated solution of sucrose in methanol; 250 – 355, 355 – 450, 450 - 600 μm parent crystals; suspension density 0.1 g/mL; stainless steel marine impeller; impeller speed 850 rpm; crystallizer diameter 100 mm; draft tube diameter 57 mm; impeller diameter 50 mm; off-bottom clearance 27 mm).....</p>	108
<p>4.30 The relationship between torque and time for a standard condition.</p> <p>(slightly supersaturated solution of NaCl in 80% methanol; 300-425 μm NaCl parent crystals; suspension density 0.050 g/mL; stainless steel marine upflow impeller; impeller speed 800, 1000, 1200 rpm; crystallizer diameter 90 mm; draft tube diameter 64 mm; impeller diameter 50 mm; off-bottom clearance 10 mm).....</p>	110
<p>4.31 The effect of impeller speed on torque. (slightly supersaturated solution of NaCl in 80% methanol; 300-425 μm NaCl parent crystals; suspension density 0, 0.025, 0.050 g/mL; stainless steel marine upflow impeller; impeller speed 800, 1000, 1200 rpm; crystallizer diameter 90 mm; draft tube diameter 64 mm; impeller diameter 50 mm; off-bottom clearance 10 mm).....</p>	111

LIST OF FIGURES (Continued)

Figure	Page
4.32 The effect of suspension density on torque. (slightly supersaturated solution of NaCl in 80% methanol; 150-300, 300-425, and 425-600 μm NaCl parent crystals; suspension density 0.025, 0.050, and 0.100 g/mL; stainless steel marine upflow impeller; impeller speed 1000 rpm; crystallizer diameter 90 mm; draft tube diameter 64 mm; impeller diameter 50 mm; off-bottom clearance 10 mm).....	112
4.33 The effect of mean parent crystal size on torque. (slightly supersaturated solution of NaCl in 80% methanol; 150-300, 300-425, and 425-600 μm NaCl parent crystals; suspension density 0.025, 0.050, and 0.100 g/mL; stainless steel marine upflow impeller; impeller speed 1000 rpm; crystallizer diameter 90 mm; draft tube diameter 64 mm; impeller diameter 50 mm; off-bottom clearance 10 mm).....	113
4.34 The effect of off-bottom impeller clearance on torque. (slightly supersaturated solution of NaCl in 80% methanol; 300-425 μm NaCl parent crystals; suspension density 0.025 g/mL; stainless steel marine upflow impeller; impeller speed 800, 1000, and 1200 rpm; crystallizer diameter 90 mm; draft tube diameter 64 mm; impeller diameter 50 mm; off-bottom clearance 10 mm).....	114

LIST OF FIGURES (Continued)

Figure	Page
4.35 The effect of draft tube diameter on torque. (slightly supersaturated solution of NaCl in 80% methanol; 300-425 μm NaCl parent crystals; suspension density 0.025 g/mL; stainless steel marine upflow impeller; impeller speed 800, 1000, and 1200 rpm; crystallizer diameter 90 mm; draft tube diameter 64 and 75 mm; impeller diameter 50 mm; off-bottom clearance 10 mm).....	115
4.36 The effect of impeller speed on torque. (saturated solution of sucrose in methanol; 425 – 600 μm sucrose parent crystals; suspension density 0.1, 0.15, 0.2 g/mL; stainless steel marine upflow impeller; impeller speed 800, 1000, 1200 rpm; crystallizer diameter 90 mm; draft tube diameter 64 mm; impeller diameter 50 mm; off-bottom clearance 10 mm).....	116
4.37 The effect of suspension density on torque. (saturated solution of sucrose in methanol; 425 – 600 μm sucrose parent crystals; suspension density 0.1, 0.15, 0.2 g/mL; stainless steel marine upflow impeller; impeller speed 600, 800, and 1000 rpm; crystallizer diameter 90 mm; draft tube diameter 64 mm; impeller diameter 50 mm; off-bottom clearance 10 mm).....	117

LIST OF FIGURES (Continued)

Figure	Page
<p>4.38 The effect of mean parent crystal size on torque. (saturated solution of sucrose in methanol; 300 – 425, 425 – 600, 600 - 850 μm sucrose parent crystals; suspension density 0.1 g/mL; stainless steel marine upflow impeller; impeller speed 600, 800, and 1000 rpm; crystallizer diameter 90 mm; draft tube diameter 64 mm; impeller diameter 50 mm; off-bottom clearance 10 mm).....</p>	118
<p>4.39 The effect of off-bottom impeller clearance on torque. (saturated solution of sucrose in methanol; 425 - 600 μm sucrose parent crystals; suspension density 0.1 g/mL; stainless steel marine upflow impeller; impeller speed 600, 800, and 1000 rpm; crystallizer diameter 90 mm; draft tube diameter 64 mm; impeller diameter 50 mm; off-bottom clearance 10 and 20 mm).....</p>	119
<p>4.40 The effect of draft tube diameter on torque. (saturated solution of sucrose in methanol; 425 - 600 μm sucrose parent crystals; suspension density 0.1 g/mL; stainless steel marine upflow impeller; impeller speed 600, 800, and 1000 rpm; crystallizer diameter 90 mm; draft tube diameter 64 and 75 mm; impeller diameter 50 mm; off-bottom clearance 10 mm).....</p>	120

LIST OF FIGURES (Continued)

Figure	Page
4.41 The attrition number as a function of power number. (slightly supersaturated solution of NaCl in 80% methanol; 300-425 μm NaCl parent crystals; suspension density 0.10 g/mL; stainless steel marine upflow impeller; impeller speed 800, 1000, 1200 rpm; crystallizer diameter 90 mm; draft tube diameter 64 mm; impeller diameter 50 mm; off-bottom clearance 10 mm).....	125
4.42 The attrition number as a function of Reynolds number. (slightly supersaturated solution of NaCl in 80% methanol; 300-425 μm NaCl parent crystals; suspension density 0.10 g/mL; stainless steel marine upflow impeller; impeller speed 800, 1000, 1200 rpm; crystallizer diameter 90 mm; draft tube diameter 64 mm; impeller diameter 50 mm; off-bottom clearance 10 mm).....	126
4.43 The attrition number as a function of parent crystal size and impeller diameter ratio. (slightly supersaturated solution of NaCl in 80% methanol; 150 – 300, 300-425, 425 - 600 μm NaCl parent crystals; suspension density 0.10 g/mL; stainless steel marine upflow impeller; impeller speed 1000 rpm; crystallizer diameter 90 mm; draft tube diameter 64 mm; impeller diameter 50 mm; off-bottom clearance 10 mm).....	127

LIST OF FIGURES (Continued)

Figure	Page
4.44 The attrition number as a function of draft tube number. (slightly supersaturated solution of NaCl in 80% methanol; 300-425 μm NaCl parent crystals; suspension density 0.10 g/mL; stainless steel marine upflow impeller; impeller speed 1000 rpm; crystallizer diameter 90 mm; draft tube diameter 64 and 75 mm; impeller diameter 50 mm; off-bottom clearance 10 mm).....	128
4.45 The attrition number as a function of off-bottom clearance number. (slightly supersaturated solution of NaCl in 80% methanol; 300-425 μm NaCl parent crystals; suspension density 0.10 g/mL; stainless steel marine upflow impeller; impeller speed 1000 rpm; crystallizer diameter 90 mm; draft tube diameter 64 mm; impeller diameter 50 mm; off-bottom clearance 10 and 20 mm).....	129
4.46 The attrition number as a function of suspension density and crystal density ratio. (slightly supersaturated solution of NaCl in 80% methanol; 300-425 μm NaCl parent crystals; suspension density 0.05, 0.10, and 0.15 g/mL; stainless steel marine upflow impeller; impeller speed 1000 rpm; crystallizer diameter 90 mm; draft tube diameter 64 mm; impeller diameter 50 mm; off-bottom clearance 10 mm).....	130

LIST OF FIGURES (Continued)

Figure	Page
4.47 Comparison of experimental attrition number with the empirical attrition number estimated by power law model a) overall data b) focus on small values.....	134
4.48 Comparison of experimental attrition number with the empirical attrition number estimated by power law model (for sucrose system).....	136
4.49 Comparison of experimental attrition number with the empirical attrition number estimated by power law model (for sucrose system and NaCl system).....	139

SYMBOLS AND ABBREVIATIONS

B_i	=	Secondary nucleation rate, nuclei/seed-min
B	=	Nucleation rate, $\#/m^3s$
B	=	Baffles width, m
C	=	Attrition coefficient, $m^3 J^{-4/3}$
C	=	Solution concentration, $kmol/m^3$
C	=	Calibration constant of the viscometer, $(mm^2/s)/s$
C^*	=	The equilibrium saturation at the given temperature, $kmol/m^3$
ΔC	=	The concentration driving force, $kmol/m^3$
C_D	=	Draft tube clearance, m
C_{OB}	=	Off-bottom impeller clearance, m
c	=	The solution concentration, kg/m^3
c^*	=	The equilibrium saturation at the given temperature, kg/m^3
Δc	=	Concentration driving force, kg/m^3
D_b	=	Size of the blade, m
D_D	=	Draft tube diameter, m
D_I	=	Impeller diameter, m
D_T	=	Crystallizer diameter, m
d	=	Impeller diameter, m
d_p	=	Crystal size, μm
E	=	Young's modulus, Pa

SYMBOLS AND ABBREVIATIONS (Continued)

E_p	=	Impact energy, J
F	=	Force acting after complete loading of the cone, N
H	=	Hardness of brittle solid, N/m ² (Pa)
H _D	=	Draft tube height, m
H _T	=	Liquid height, m
H _v	=	Vicker's hardness, Pa
J_{c-i}	=	Secondary nucleation rate caused by collisions of particles with impeller, m ⁻³ s ⁻¹
K _c	=	Fracture toughness, N m ^{-3/2}
K _r	=	The efficiency factor in radial direction, -
k'	=	Coefficient, -
k_N	=	A rate constant (dependent on many factors including stirring speed, T, M _T)
k'_N	=	A rate constant (it is a function of temperature)
L	=	Fragment size, m
L_p	=	Parent crystal size, m
$\overline{L}_{3,0}$	=	Volume – number average size, m
l	=	A characteristic particle size, m
M _T	=	Suspension density, kg/m ³
m	=	Mass of the colliding crystal, kg
m	=	Mass of suspension, kg

SYMBOLS AND ABBREVIATIONS (Continued)

N	=	Number of nuclei
N	=	Impeller speed, rev/min (rpm)
N_{Att}	=	Attrition number, -
N_{CF}	=	Crystal density and fluid density ratio, -
N_{DT}	=	Draft tube impeller clearance and impeller diameter ratio, -
N_{Lp}	=	Parent crystal size and impeller diameter ratio, -
N_{MT}	=	Suspension density and crystal density ratio, -
N_{OB}	=	Off-bottom clearance and impeller diameter ratio, -
N_P	=	Power number, -
N_{Re}	=	Reynolds number, -
N_{SF}	=	Suspension density and fluid density ratio, -
N_T	=	Total number of attrition fragment
n	=	Number density, $\#/\mu\text{m}$
n	=	Impeller revolutions, min^{-1}
n_s	=	Number of seed crystals used to commence contact nucleation
P	=	Power input, Watt
p	=	Number of impeller blades
$q_0(L)$	=	Number density distribution, m^{-1}
S	=	Supersaturation ratio, -
T^*	=	The solid-liquid equilibrium temperature, $^{\circ}\text{C}$
T	=	Temperature that is less than T^* , $^{\circ}\text{C}$
ΔT	=	Temperature driving force (supercooling), $^{\circ}\text{C}$

SYMBOLS AND ABBREVIATIONS (Continued)

t	=	Mean flow time, s
u	=	Tip speed of impeller, m/s
V	=	Volume of solution, m ³
V	=	Volume of suspension, m ³
V_a	=	Total volume removed by attrition, m ³
V_c	=	Tank volume, m ³
V_T	=	Total volume of attrition fragment, m ³
v	=	Impact velocity, m/s
W	=	A measure of mechanical agitation
W_p	=	Impact energy, J
AB	=	The distance from A to B
AC	=	The distance from A to C
AD	=	The distance from A to D
ASTM	=	American Society for Testing and Materials
CSD	=	Crystal size distribution
DI	=	De-ionized
PSD	=	Particle size distribution
SEM	=	Scanning electron microscope
Γ	=	Fracture surface energy, J/m ²
α	=	Volume shape factor, -
α	=	Proportionality constant, -
η	=	Dynamic viscosity, mPa.s

SYMBOLS AND ABBREVIATIONS (Continued)

η	=	Target efficiency, - (defined by Eq. 2.17)
η_{geo}	=	Probability that the crystal is on a streamline moving towards the impeller, -
η_T	=	Target efficiency, -
μ	=	Shear modulus, N/m ²
μ_{gN}	=	Geometric mean of the number distribution, m
μ_{gV}	=	Geometric mean of the volume distribution, m
ν	=	Kinematic viscosity, mm ² /s
ξ	=	Fractional loss from a particle, -
ρ	=	Particle density, kg/m ³
σ	=	Absolute or relative supersaturation
σ_{g}	=	Geometric standard deviation
ϕ	=	Volume concentration of the solid phase
$\omega_{\text{eff}}(d_p)$	=	Effective collision frequency of particles per blade on the frontside, s ⁻¹
$\omega_{\text{id}}(d_p)$	=	Ideal collision frequency of particles per blade on the frontside, s ⁻¹
*	=	Equilibrium
b	=	Parameters from curve fitting
c	=	Parameters from curve fitting
d	=	Parameters from curve fitting

SYMBOLS AND ABBREVIATIONS (Continued)

e	=	Parameters from curve fitting
f	=	Parameters from curve fitting
g	=	Parameters from curve fitting
i	=	The exponents can be found from experimental data,
j	=	The exponents can be found from experimental data,
Att	=	Attrition
b	=	Blade
c	=	Crystal
D	=	Draft tube
eff	=	Effective
f	=	Fluid
g	=	Geometric
I	=	Impeller
min	=	Minimum
max	=	Maximum
N	=	Number
OB	=	Off-bottom
P	=	Parent crystal
P	=	Power
s	=	Seed crystal
T	=	Total
V	=	Volume

CHAPTER I

INTRODUCTION

1.1 Background problem and significance of the study

Crystallization is known as a separation process and as a polishing step. There are a lot of technologies and mature processes involving crystallization in the chemical industry (Seader and Henley, 1998). However some areas of crystallization are still not well understood. Secondary nucleation is one of the mechanisms that still need investigation. An overview of Japanese industrial crystallization research found that the problems in industrial crystallization are from four sources; equipment, operation, measurements, and quality of crystals. The largest problem is from operation and product quality as can be seen in Figure 1.1 (Kubota and Ooshima, 2001).

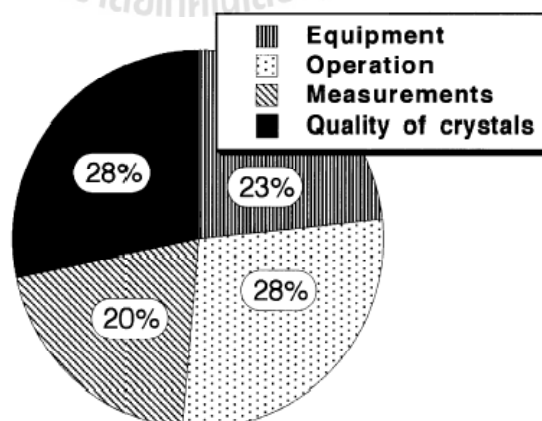


Figure 1.1 Distribution of nature of problems encountered. (Kubota and Ooshima, 2001)

Secondary nucleation can be produced by many mechanisms, especially from contact between crystals and crystallizer parts such as walls and the impeller. When secondary nucleation occurs in the crystallization processes, it will influence the product quality because the shape and the size distribution of the parent crystal change as well as producing larger populations of crystals and therefore smaller sizes. In many industrial crystallization applications, attrition is the major source of secondary nucleation. Thus, we should know the attrition behavior to identify the important crystal properties, crystallizer properties, and solution properties in order to minimize attrition. Attrition produces nuclei in industrial crystallizers, and needs to be very carefully controlled to avoid excess numbers of particles.

The mechanisms occurring in the crystallizer that can produce fragments are not only attrition. For example, Beekman et al. (2002) proposed four mechanisms of breakage as shown in Figure 1.2. The mechanism depends on the direction and the magnitude of the force acting on the parent crystal. In fact, we cannot specify the exact mechanism in the crystallizer but we can separate the mechanisms into two groups. The very small fragment should be from attrition or abrasion mechanism but is usually known as attrition rather than abrasion. The big fragments are from fragmentation or breakage mechanisms. All the mechanisms are shown here because the name of the different mechanisms are not always clearly defined or correctly used.

Several possible mechanisms of secondary nucleation were proposed by Strickland-Constable (1968) as well. They separated secondary nucleation mechanisms into four types, initial breeding, needle breeding, polycrystalline breeding, and collision breeding. Initial breeding occurs when crystalline dust is swept off a newly introduced seed crystal. Needle breeding occurs because of the

detachment of weak out-growths. Polycrystalline breeding occurs when a weak polycrystalline mass break into small pieces. Collision breeding occurs when the crystal contact with other crystals or with parts of crystallizer.

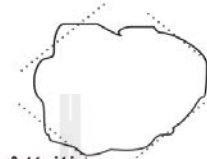
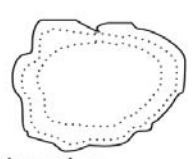
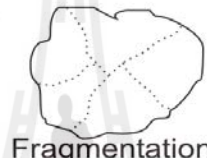
Magnitude	Direction	
	Normal	Tangential
Low Force <i>“Wear”</i>	 Attrition	 Abrasion
High force <i>“Fracture”</i>	 Fragmentation	 Chipping

Figure 1.2 The influence of magnitude and direction of a force on the breakage mechanism. (Beekman et al., 2002 and van Laarhoven et al., 2010)

Many investigators have studied the secondary nucleation behavior of crystals. For example, Melia and Moffitt (1964) proposed a study of secondary nucleation from aqueous solution; Cayey and Estrin (1967) studied secondary nucleation in agitated magnesium sulfate solutions; Denk and Botsaris (1972) presented the mechanism of contact nucleation and fundamental studies in secondary nucleation from solution; Ottens and De Jong (1973) proposed a model for secondary nucleation in a stirred vessel cooling crystallizer; Garside and Davey (1980) studied secondary contact nucleation (kinetics, growth, and scale-up); Offermann and Ulrich (1980a, 1980b, 1982, and 1983) proposed a secondary nucleation model and the mechanical attrition of crystals; Grootscholten et al. (1982) presented factors affecting

secondary nucleation rate of sodium chloride in an evaporative crystallizer; Yuregir et al. (1987) studied impact attrition of sodium chloride crystals; Mersmann et al. (1988) proposed attrition and secondary nucleation in crystallizer; Daudey et al. (1990) presented secondary nucleation kinetics of ammonium sulfate in a CMSMPR crystallizer; Ghadiri et al. (1991) studied the influence of processing conditions on attrition of NaCl crystals; Mazzarotta (1992) proposed abrasion and breakage phenomena in agitated crystal suspension; Biscans et al. (1996) also proposed abrasion and breakage phenomena in mechanically stirred crystallizers; Gahn and Mersmann (1997) presented theoretical prediction and experimental determination of attrition rates and proposed brittle fracture in crystallization processes in 1999; Marrot and Biscans (2001) studied about impact of single crystal in solution, on an immersed target, in condition which simulate impact attrition in crystallizer; Zhang and Ghadiri (2002) proposed impact attrition of particulate solids; Briesen (2007) showed model-based analysis of the effect of particle and impact geometry on attrition of brittle material and proposed two-dimensional population balance modeling for shape dependent crystal attrition in 2009; and a mechanism influencing crystal breakage experiments in stirred vessels was proposed by Reeves and Hill (2012). Table 1.1 shows the example sources of secondary nucleation and prevention. There are three cases of collisions between crystals and either other crystals or surfaces i.e. crystallizer.

Attrition or collision breeding is the most important mechanism in industrial crystallizers because it can produce a lot of attrition fragments and it can occur in industrial crystallizers more than other mechanisms (Gharidi et al., 1991, Gharidi and Zhang, 2002, Yuregir et al., 1987, Zhang and Gharidi, 2002, and Bravi et al., 2003).

Generation of attrition fragments due to collisions between crystals and the internals of the crystallizer are an important source of secondary nucleation in industrial crystallizers. This phenomenon must be understood and be adequately modeled when designing industrial crystallization units in order to obtain a design that will produce a suitable particle size distribution. It has been suggested that attrition-based secondary nucleation is one of the key features in determining the process stability and product quality in suspension crystallizers (Kail et al., 2005).

Theoretical models of attrition were proposed by many researchers. Fasoli and Conti (1976) and Nienow and Conti (1978) developed energy-impact models from the results of attrition and breakage studies in agitated vessels using crystals suspended in inert liquids. A generalized model of nucleation by mechanical attrition has been proposed by Kuboi, Nienow, and Conti (1984). They developed the model based on Rittinger's law for the energy required for producing new surface and the additivity of two attrition processes due to crystal-crystal and crystal-impeller collisions.

Jager et al. (1991) proposed an empirical attrition model which relates crystal attrition to crystal size and hold-up. They developed the model from data obtained with a 20 liter continuous evaporative crystallizer using ammonium sulphate. However, the models of attrition which have been proposed by these researchers are not accurate enough for industrial crystallization. The model needs more parameters to predict the attrition behavior such as crystallizer properties, crystal properties, and solution properties. A model developed by a study of all properties in crystallization processes will improve predictive capabilities.

Table 1.1 Sources of nuclei in industrial crystallization (Myerson, 2002)

Source of Nuclei	Type of Nucleation	Prevention
Crystal/crystallizer contacts 1. Collisions with moving parts (impellers, pumps etc.) 2. Collisions with crystallizer walls	Secondary	Adjust tip speed and design configuration, coat impellers with soft materials, reduce if possible magma density and mean crystal size
Crystal/crystal contacts Crystal grinding in small clearance spaces (impeller/draft tube, pump rotator/rotor)	Secondary, attrition breakage	Carefully specify all clearances and hydrodynamics of two-phase flow therein
Crystal/solution interaction Fluid shear, effect of impurities, etc.	Primary or secondary	Reduce jetting, get to know the effect of impurities for each particular system, prevent incrustation

While there have been several attempts at creating fundamental models of attrition fragmentation (Biscans, 2004, Briesen, 2005, Briesen 2007, Gahn and Mersmann, 1997, Gahn and Mersmann, 1999a and 1999b, and Marrot and Biscans, 2001), models created thus far have been difficult to apply to suspension crystallizers due to a lack of knowledge about the fluid and particle dynamics in the impeller

region which makes accurate prediction of the collision frequency and forces involved in the collision difficult. Gahn and Mersmann (1999) proposed an attrition model equation to explain the fracture behavior of crystalline solid for the attrition process in suspension crystallizers. Then, they developed a model equation for the processes of attrition and abrasion of brittle solid to predict the whole crystallization process in a quantitative manner. There are four groups of assumptions for the attrition model. They are the loading conditions, the material properties, the elastic stress field in the solid, and a law to describe the fracture process (Gahn and Mersmann, 1997, Gahn and Mersmann, 1999a and 1999b). This model can be used to estimate the correct values of abraded volumes of brittle solids which have the ratio of E/H_v (Young's modulus/Vicker's hardness) less than 100. So, the models which Gahn and Mersmann proposed are accurate for brittle substances only and the information for the model is not available, for example, the efficiency factor in radial direction and the fracture surface energy.

1.2 Research Objectives

This work is a project to describe attrition in industrial crystallizers using an empirical engineering model based on dimensionless groups (derived from Buckingham-Pi theory for example) describing crystal properties, suspension properties, mother liquor properties, and groups describing crystallizer geometry and operation. The aim of this study is to understand the attrition behavior and to model the crystal attrition equation. There are four objectives as follows

1. To determine the parameters that have a significant effect on the attrition mechanism.

2. To determine the attrition rate and the size distribution of the attrition fragments.
3. To determine the non-dimensional groups from parameters in the crystallization process to use in data fitting.
4. To determine an empirical engineering model for calculation of the attrition rate.

1.3 Scope and limitation of the study

The work is separated into three parts; design the equipment and experimental conditions, determine the effect of parameters on the attrition rate by using the number of attrition fragment per unit volume and attrition fragment size distribution, and model the crystal attrition equation.

1.3.1 Design the equipment and the experimental conditions

The crystallizer is made from glass and stirred by an impeller. The detail of the crystallizer is shown in Figure 3.1. The base of the crystallizer is a profiled bottom. The design of crystallizer is adapted from Bauer et al. (1974). We will do the experiment on the laboratory scale and use a batch process to operate the crystallizer. The detail of experimental condition is in section 3.3.1. There are three groups of parameters; (1) crystallizer geometry and operating conditions, (2) crystal properties, and (3) solution and suspension properties.

1.3.2 Determine the effect of parameters on the attrition rate

The effect of all parameters will be studied in the same crystallizer by a partial factorial design, with standard conditions (low value : high value). The attrition fragment size distribution will be used two techniques to measure.

1. Using the Malvern Mastersizer S, and
2. Using the Multisizer 3 Coulter Counter.

The attrition fragment will be measured in the unit of number of attrition fragments per unit volume. Then, the number of attrition fragment per unit volume and experimental time will be used to calculate the attrition rate in the unit of number of attrition fragments produced per unit volume per time. The number of the parent crystal will be considered too, because the number of the parent crystal will change if the breakage mechanism occurs in the crystallizer so if we found that the size and number of parent crystal are not change that mean only attrition mechanism occurs in the system. The size distribution of the fragment can be determined directly from Malvern Mastersizer S and Multisizer 3 Coulter Counter and we will use the SEM photograph to check the average size of the fragment and parent crystal as well.

1.3.3 Modeling of crystal attrition equation

There are two parts of the modeling; (1) to determine dimensionless groups of significant parameters on attrition rate by using dimensional analysis (Buckingham Pi Theorem) and (2) to develop the empirical engineering model. We will use only the data from parameters that have an effect on the attrition behavior to model the equation to calculate the attrition number. A power law model will be used and SigmaPlot will be used to help fitting the equation.

1.4 Output

According to the objectives of the work, this research expects to obtain the effect of parameters from crystallizer geometry and operation conditions, crystal properties, and solution and suspension properties on the attrition rate and the effect of each parameter on the size distribution of the attrition fragments. The data from experiment of attrition rate will be used to determine the suitable dimensionless groups to use in the data fitting. Finally, the dimensionless groups will be used to develop an empirical engineering model to calculate the attrition number.



CHAPTER II

LITERATURE REVIEW

2.1 Industrial Crystallization

2.1.1 General considerations

There are a lot of different methods of crystallization in industrial crystallization, for example, crystal growth from melts, crystal growth from solution, crystal growth from the vapor phase (for instance desublimation), crystal growth from supercritical fluids, and liquid or vapor phase epitaxy (Flood, 2009). In this research, we consider only crystallization from solution. A general schematic of a crystallization process can be drawn as in Figure 2.1. For a particular crystallizer, any of the streams may be present, or absent. The example of crystallization processes are continuous, steady-state crystallizer, batch crystallizer, seeded crystallizer, non-solvent and salting-out crystallizations, cooling and heating crystallization, evaporative crystallization, precipitation (Flood, 2009).

In this research, we consider only batch crystallizer because we want to know attrition rate as a function of time without it being made more complex by presence of outflow streams (which would remove parent crystals and/or fragments) and we want to minimize other mechanisms (true nucleation, growth, agglomeration, etc.). For batch crystallizer from Figure 2.1, neither the inflow nor the outflow streams are present but at the beginning and at the end of operation of the batch we need to fill the raw material and to remove the product (Flood, 2009).

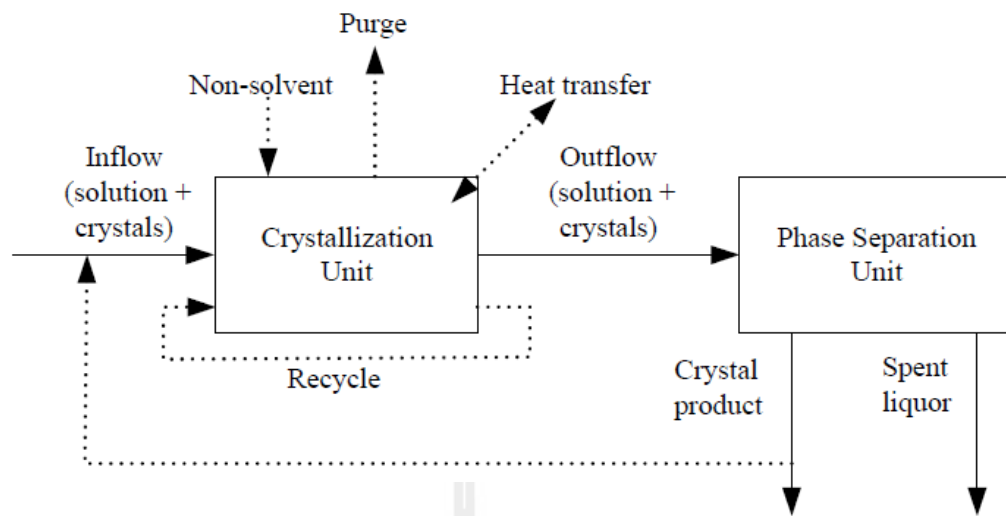


Figure 2.1 General schematic of a crystallization process. (Flood, 2009)

2.1.2 Supersaturation

In crystallization process, supersaturation is one of the most important parameters because it is the driving force for the nucleation and crystal growth processes. There are a lot of expressions of supersaturation or supercooling. The most common expressions of supersaturation are the concentration driving force, Δc , the supersaturation ratio, S , and the absolute or relative supersaturation, σ (Mullin, 2001). Supersaturation or supercooling is usually defined by

$$\Delta c = c - c^* \quad (2.1)$$

$$S = \frac{c}{c^*} \quad (2.2)$$

$$\sigma = \frac{\Delta c}{c^*} = S - 1 \quad (2.3)$$

where c = the solution concentration

c^* = the equilibrium saturation at the given temperature

There are several ways to create supersaturation, for example, cooling, evaporation, salting out, and chemical reaction (Nyvlt, 1992). Figure 2.2 shows the popular techniques of supersaturation creation for crystallization from solution. From Figure 2.2, path AB is cooling process, path AC is evaporation process, and path AD is salting out by addition of non-solvent.

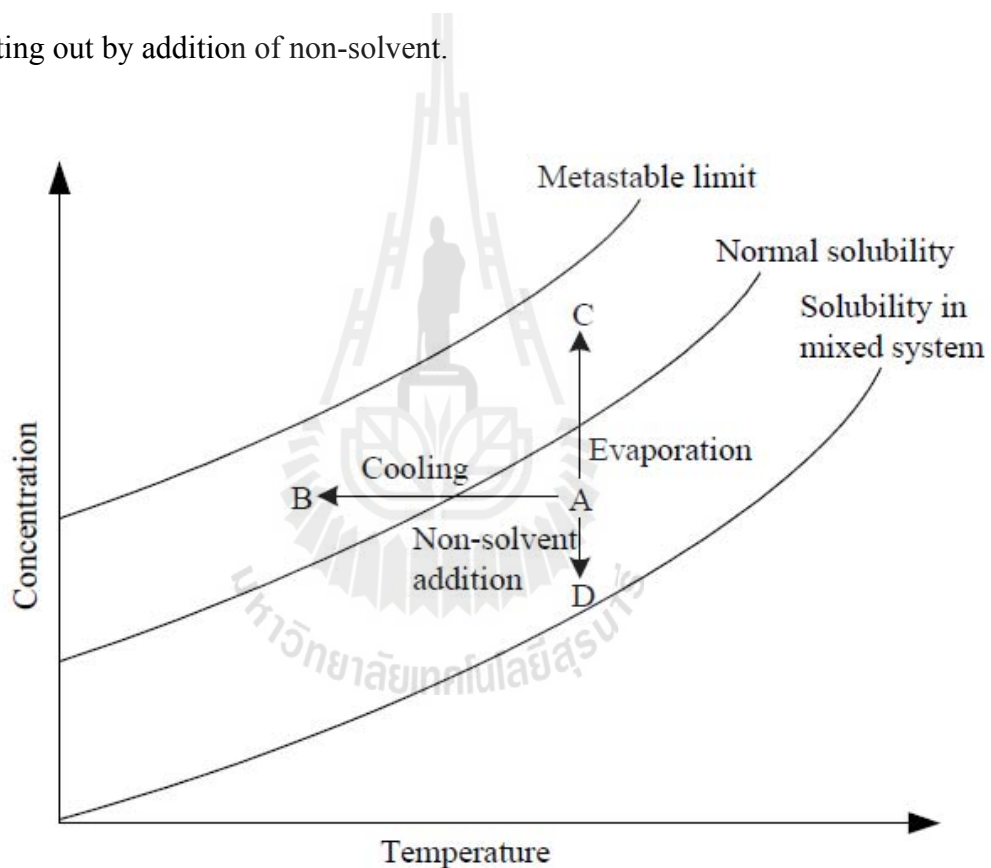


Figure 2.2 Method of supersaturation creation in solution crystallizations. (Flood, 2009)

Another expression of supersaturation is the supercooling, that is defined by

$$\Delta T = T^* - T \quad (2.4)$$

where T^* = the solid-liquid equilibrium temperature

T = the temperature that is less than T^*

The commonly used definitions of driving force in crystallization processes are shown in Table 2.1. It is shown that the driving force of secondary nucleation is supersaturation (σ) (Mersmann, 2001). In this research, we focus on secondary nucleation by attrition; attrition is the only source of secondary nuclei that does not depend on supersaturation (McCabe et al., 2001). By the way, generation of fragments may not depend on σ , but survival of fragments does depend on σ .

Table 2.1 Driving forces for growth and nucleation. (Mersmann, 2001)

Kinetic parameter		Driving force
Growth	Diffusion controlled	ΔC [kmol/m ³] or Δc [kg/m ³]
	Surface integration controlled	$\sigma = \Delta c/c^*$ or $\Delta C/C^*$
Nucleation	Primary	$S = 1 + \sigma$
	Secondary	σ

2.1.3 Nucleation

There are two types of nucleation in crystallization processes. They are primary nucleation and secondary nucleation as shown in Figure 2.3. J.W.Mullin said if there are no crystals in the crystallizer, the nucleation that occurs is by primary nucleation. There are two mechanisms of primary nucleation. They are homogeneous for spontaneous nucleation and heterogeneous nucleation where nuclei are induced by foreign particles (Mullin, 2001). When solute crystals are present in the supersaturated solution, secondary nucleation is likely to occur. The nucleation phenomena depends on these parent crystals, and thus, nucleation occurs at a lower supersaturation than needed for spontaneous nucleation. There are many investigations on secondary nucleation but the mechanisms and kinetics are poorly understood (Myerson, 2002).

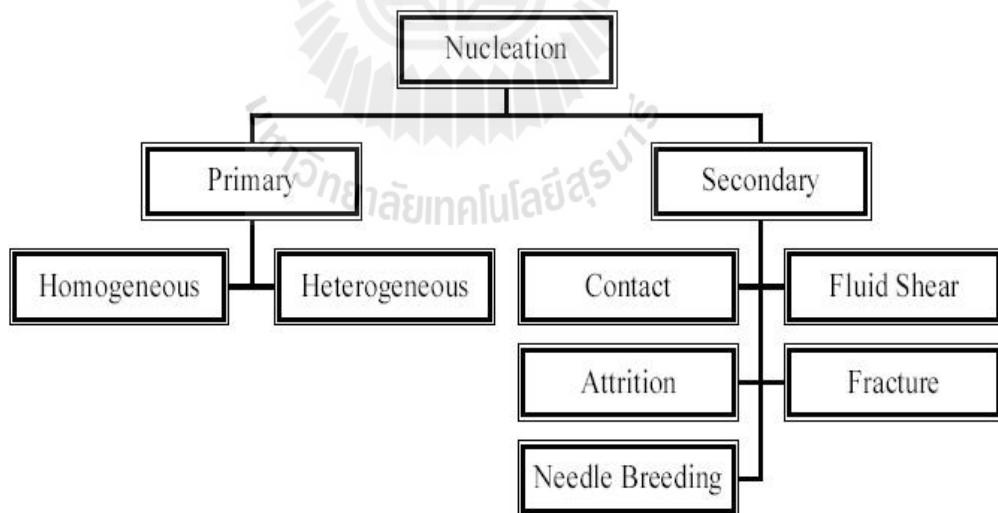


Figure 2.3 Mechanism of nucleation (Randolph and Larson, 1988)

Figure 2.4 shows the appearance of good and inferior crystals and variation of product quality at various supersaturation for $\text{MgSO}_4 \cdot 7\text{H}_2\text{O}$. As can be seen, at $\Delta T < 4^\circ\text{C}$ is the best operation region but attrition can still occur. If the operation is at $\Delta T > 4^\circ\text{C}$, secondary nucleation is very easy to occur. This is the reason that the most industrial crystallizers need to operate at low supersaturation and using only well-designed and operated pumps and agitators (McCabe et al., 2001). In this research, we consider only secondary nucleation by attrition which is the most important mechanism in industrial crystallizers.

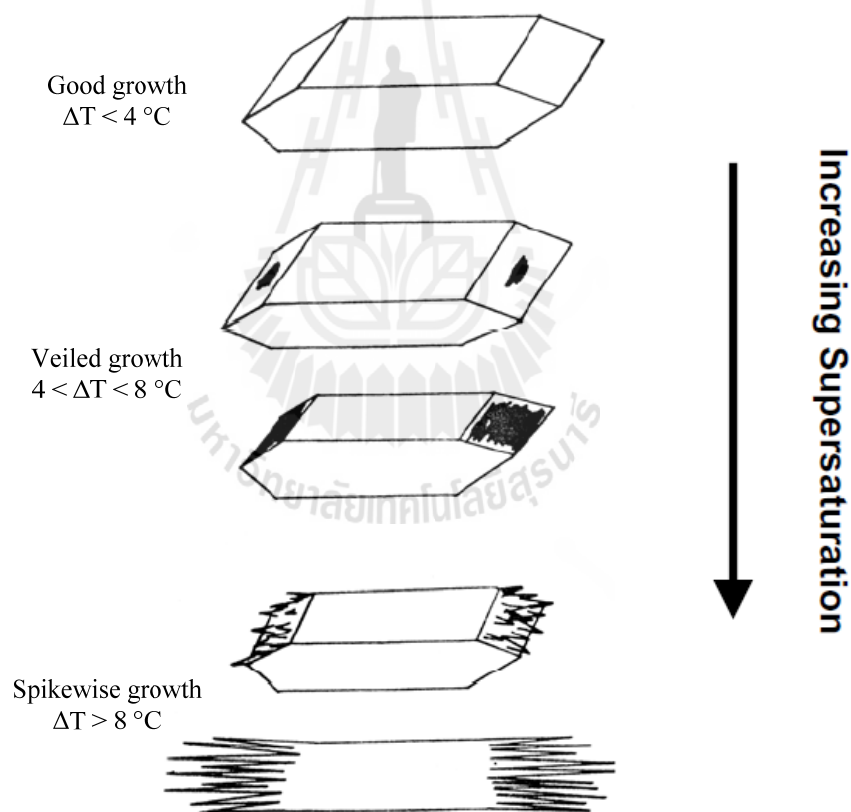


Figure 2.4 Example of growth regimes for magnesium sulfate heptahydrate. (Clontz and McCabe, 1971)

2.2 Secondary Nucleation

2.2.1 Origin of secondary nucleation

From the mechanisms of secondary nucleation discussed in the previous section it can be seen that secondary nuclei originate either from the parent seed crystal or from the solute in the liquid phase around or adsorbed to the parent crystal.

Powers (1963) is the first person who proposed the presence of an adsorbed layer as a source of secondary nuclei. Later, several investigators (Clontz and McCabe, 1971 and Strickland-Contable, 1972) performed experiments to verify this hypothesis. They slid a crystal along a solid surface, and studied the nucleation and crystallization behavior. They found that generation of nuclei needs a growing crystal. The nucleation rate was a function of the contact energy and degree of supersaturation.

The experiment for study secondary nuclei was performed by Denk and Botsaris (1972). They performed an experiment which used the optical activity of the sodium chlorate crystals to investigate the origin of nuclei. They grew a crystal from aqueous solution in the presence of seed crystals with and without the presence of impurities. Figure 2.5 shows the results for crystals grown from pure stagnant solutions. If the resulting crystals have the same form as the parent crystal, it means the solid phase was the source of the secondary nuclei. If the ratio of optically different nuclei is similar to the ratio obtained during spontaneous nucleation, the liquid or transition phase was the source of the secondary nuclei. As shown in Figure 2.5, the source of nuclei changes around a supercooling of 3 °C and the ratio

approached to that of spontaneous nucleation at higher supersaturation. So, we can conclude that there is more than one mechanism to explain secondary nucleation.

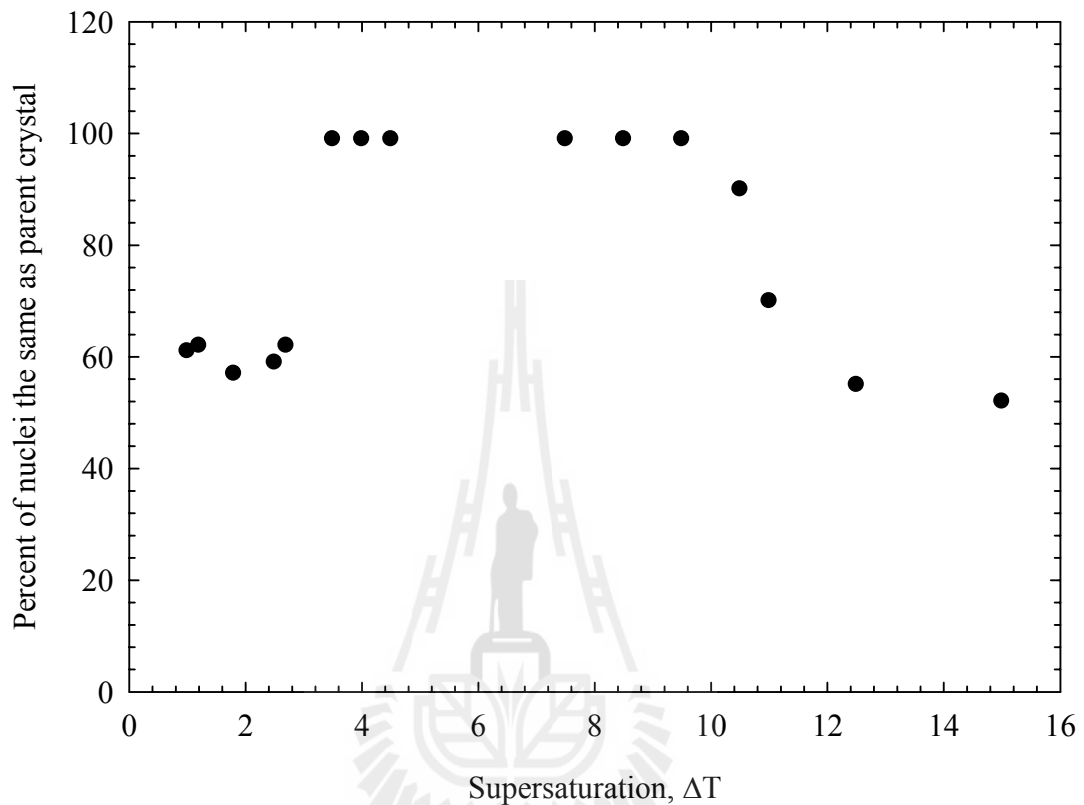


Figure 2.5 Differentiation of the secondary nucleation mechanisms using enantiomorphous crystals. The fraction of the crystals with the same modification as that of the parent crystal is denoted as percent. (Denk and Botsaris, 1972a)

An experiment was developed by Garside et al. (1979) to study the contact of crystal with a fixed energy. The results are shown in Figure 2.6. They are the crystal size distribution (CSD) in a potassium-alum system as a function of population density. Similar equipment was used by Larson and Bendig (1976) to determine the dependence of nucleation on contact frequency. It was found that the adsorbed layer

requires time for regeneration and the nucleation rate declines by several orders of magnitude if proper regeneration times cannot be met.

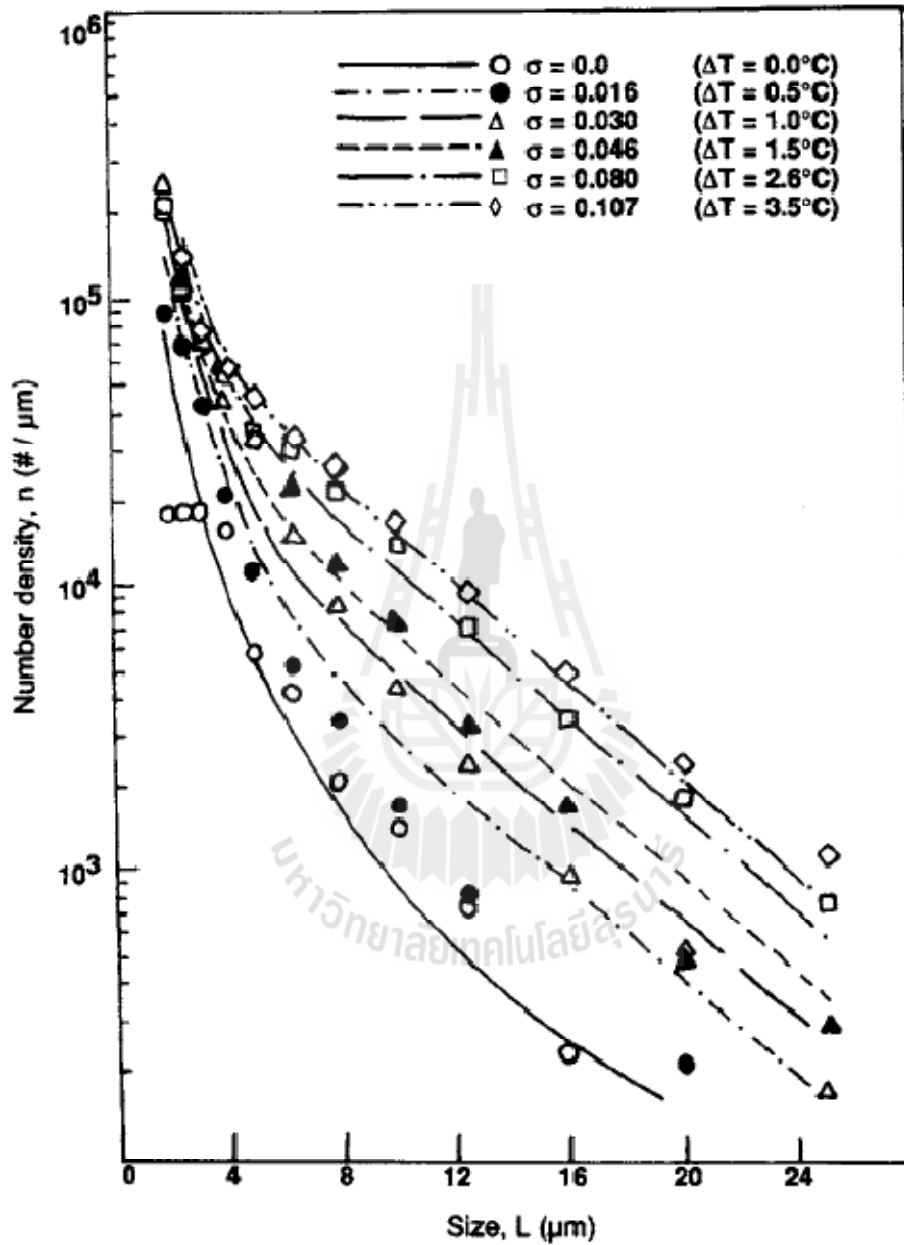


Figure 2.6 Nuclei size distribution from contact nucleation. (Garside et al., 1979)

2.2.2 Mechanism of secondary nucleation

Several mechanisms have been proposed to explain secondary nucleation. Randolph and Larson (1988) described sources of secondary nucleation by six mechanisms, but we mention only five mechanisms here, because the initial breeding mechanism occurs only in seeded systems and secondary nuclei from this mechanism are not from parent crystals, it is the fragment that comes with parent crystal so it is easy to remove by washing. Hence, we will not discuss it.

1. Fracture; if we have the production of brittle crystals in a system where the suspension is very dense and it is subjected to violent agitation or high-velocity pumping, nucleation will occur in the system by the fracture process. The shape of the crystalline product usually has a rounded appearance and usually shows a deficiency of crystals in the large size range. This is because of the high rate of fracture in the system. The most damage is done by crystal-impeller interaction or sharp changes in the flow path. Fracture by impact between crystals probably does not occur to any significant extent.

2. Attrition; this mechanism happens by crystal-crystal collision or crystal-apparatus contact at high suspension densities. The effect of this mechanism to the shape of crystalline product is limited. The visible damage on the parent crystal is usually slight. The main sources of attrition are from agitation or pumping, suspension density, and crystallizer walls and impeller. If agitation or pumping is reduced and suspension density or soft linings and coverings are used on the crystallizer walls and impeller, the attrition mechanism can be reduced.

3. Needle breeding; this mechanism occurs because of a crystal habit that is called 'dendritic' [It is branching growth of crystals usually on a surface or as an inclusion that forms plant-like patterns]. Dendritic crystals will break at high agitation so we can reduce needle breeding by reducing agitation, and we can control by reducing the driving force for growth such as supersaturation or using appropriate additives to change the crystal habit or tendency to form dendrites.

4. Fluid shear; nucleation by fluid shear is due to the effect of the relative velocity between fluid and crystal. The adsorbed layer is removed when the fluid velocity relative to the crystal velocity is large. This mechanism is not an important source of nuclei because Sung, Estrin, and Youngquist (1973) showed that the shear created nuclei must be contained in a much higher supersaturation than the one in which they were created, in order to grow.

5. Contact; contact nucleation is the most important source of nuclei in mixed suspension for the system that has high supersaturation. It occurs when the crystal contact with the agitator, pump, flow lines or other crystals. Contact nucleation can occur at very low impact energies compared to fraction or attrition.

2.2.3 Parameters Affecting Secondary Nucleation Rate

2.2.3.1 Supersaturation

The critical parameter to control the nucleation rate is the degree of supersaturation. At high supersaturation, the number of nuclei is very large because the adsorbed layer is thicker and when the supersaturation increase the size of nuclei will decrease, so the chance of a critical nucleus surviving to form crystals is

higher. The microroughness of the surface of the crystal increases at high supersaturation: thus, the number of nuclei is high because it is generated from the crystal surfaces.

2.2.3.2 Temperature

The effect of temperature on secondary nucleation is not fully understood. However the temperature is very important to kinetic processes. Genck and Larson (1972) studied a potassium chloride system and a potassium nitrate system. They found that the nucleation rate decreased when temperature increased in the potassium nitrate system but for the potassium chloride system the nucleation rate increased when the temperature increased. In 1981, Nývlt showed that the nucleation rate is not sensitive to temperature variation.

2.2.3.3 The degree of agitation

It was found by Sikdar and Randolph (1976) that for smaller crystals of magnesium sulfate (8-10 μm), the nucleation rate increased with the degree of stirring and the degree of agitation had no effect on nucleation rate for larger crystals.

Melia and Moffitt (1964a, 1964b) studied the secondary nucleation of potassium chloride. Their results are shown in Figure 2.7. It was found that when the supersaturation, the degree of supercooling and agitation were increased, the nucleation rate also increased.

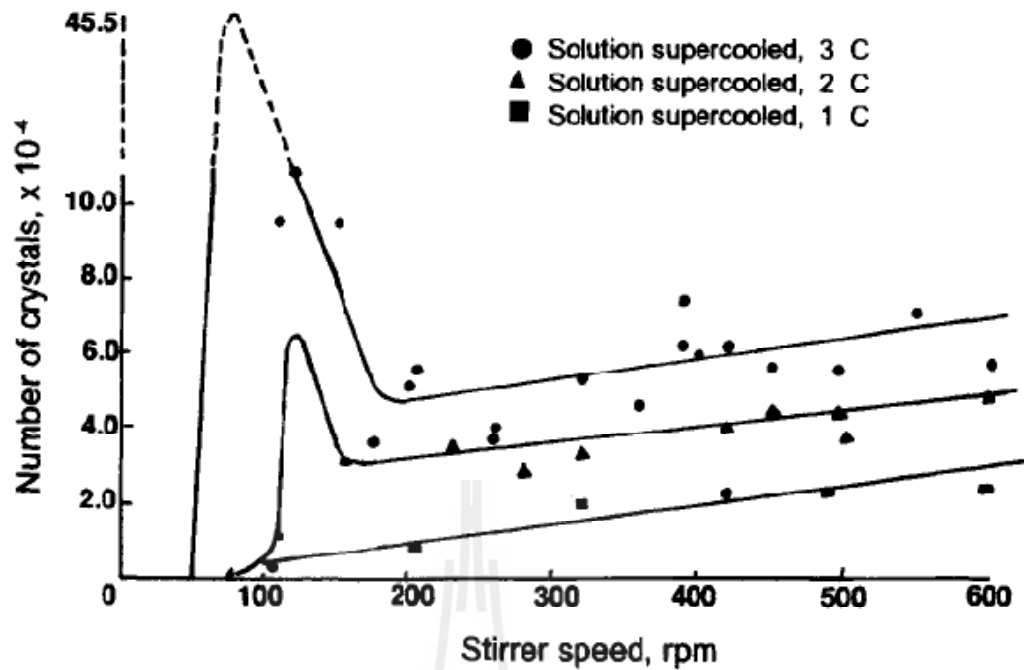


Figure 2.7 Dependence of number of secondary nuclei produced on stirrer speed and supercooling in secondary nucleation of potassium chloride. (Melia and Moffitt, 1964a)

The influence of the stirring rate was proposed by Biscans et al. (1996). They studied monosized sodium chloride crystals (500–560 μm) at low concentration crystal suspensions (3 kg m^{-3}) for two different stirring rates (960 and $1154 \text{ rev min}^{-1}$). The results are shown in Figure 2.8. It is clear that the extent of the attrition phenomena increases with the agitation.

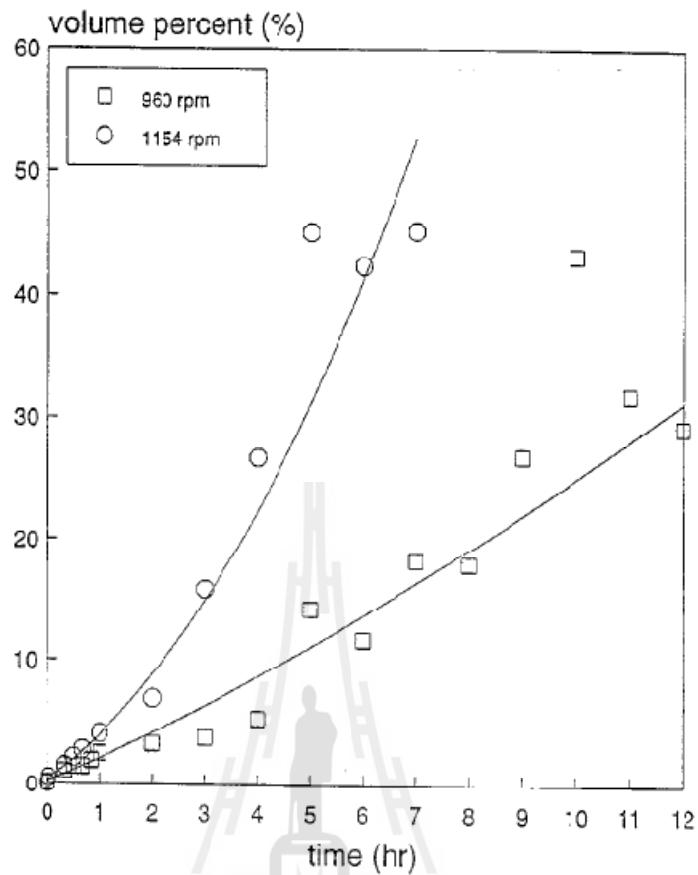


Figure 2.8 Trend of volume percentage of fine fragments (less than 32 μm) vs. time at two different stirring rates: symbols, experimental data; line, calculated curves. (Biscans et al., 1996)

2.2.3.4 The hardness of the contact material

Several investigators studied the effect of hardness of the contact material and the crystal hardness on the secondary nuclei generation. A harder material usually increases the nucleation rates (Myerson, 2002). Ness and White (1976) studied the effect of agitator speed on secondary nucleation rate for steel and plastic impellers as shown in Figure 2.9. They found that a polyethylene stirrer reduced the nucleation rate by a factor of 4 – 10, depending on the stirring.

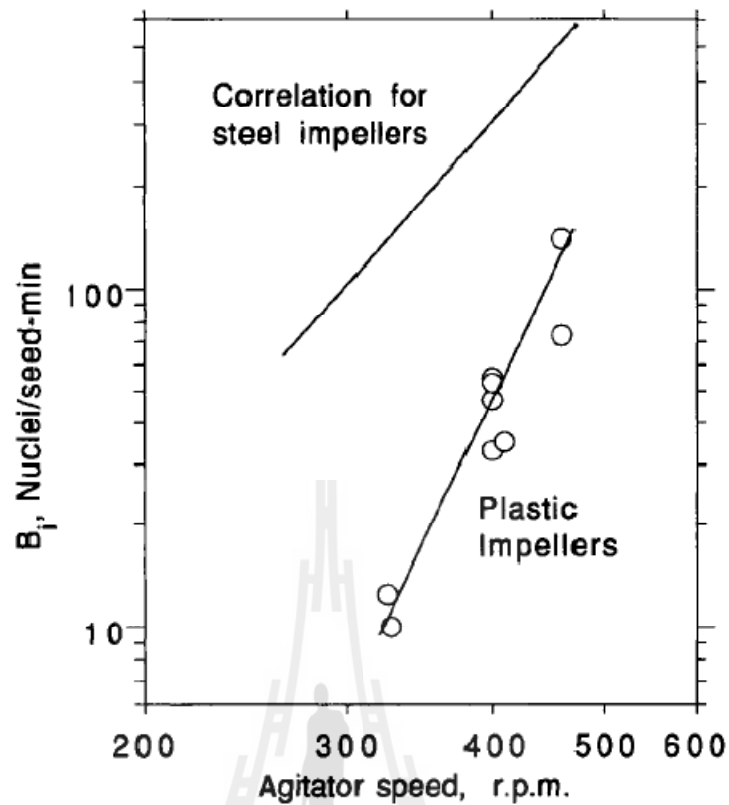


Figure 2.9 Effect of agitator speed on secondary nucleation rate for steel and plastic impellers. (Ness and White, 1976)

2.2.4 Secondary nucleation kinetics

Ploß and Mersmann (1989) have proposed a model for secondary nucleation rate with the mechanism of contact nucleation. The secondary nucleation by attrition occurs when crystals collide with each other or crystallizer parts and fine particles are abraded. The main affecting parameters are (Ploß and Mersmann, 1989):

- geometry and volume of the crystallizer,
- type of stirrer,
- operating parameter such as tip speed velocity,
- physical properties of solution and crystals,

- supersaturation and kinetics of growth.

Several mechanisms are involved in secondary nucleation and the behavior is not well understood. The nucleation rate cannot be predicted because a general theory does not exist (Myerson, 2002). Most experimental data is explained by correlations that are based on the power law model. From the Decker-Doering relationship, the power law is shown as

$$B = k_N \Delta C^n \quad (2.5)$$

where B = the nucleation rate in units of $\#/m^3s$

k_N = a rate constant (dependent on many factors including stirring speed, T, M_T)

ΔC = the degree of supersaturation.

If the adsorption layer mechanism is the source of the nucleation, we can use equation (2.5) to calculate the nucleation rate but this equation is not suitable for other mechanisms because only the adsorption layer mechanism has the nucleation rate independent of the suspension concentration.

From section 2.2.2, contact nucleation is the primary source of new crystal formation in mixed suspension crystallizers. Crystals are generated very fast at measurable sizes. Bennett, Fiedelman, and Randolph (1973) proposed that the rate of nucleation can be correlated with the degree of agitation as expressed by the tip speed of a pump impeller or vessel agitator.

The correlation for calculating the nucleation rate in the case where most of the nuclei are generated by contact nucleation is

$$B = k'_N W^i M_T^j (\Delta C)^n \quad (2.6)$$

where the rate constant k'_N is a function of temperature, W is a measure of mechanical agitation, M_T is the suspension density, and ΔC is the degree of supersaturation.

The size distribution must be taken into account in the equation if it is wide. The exponents can be found from experimental data, but j is usually 1 and i is usually from 1 to 3.

2.3 Attrition Models

2.3.1 Offermann and Ulrich model

Offerman and Ulrich (1981) studied secondary nucleation empirical model by attrition both in mixed-suspension crystallizers and in a stirred fluidized bed. In the mixed-suspension crystallizer work the authors used a dimensional analysis approach similar to the approach used in this study. For a range of salts (NaCl, $MgSO_4 \cdot 7H_2O$, $KAl(SO_4)_2 \cdot 12H_2O$, and K_2SO_4) undergoing attrition in a mixed-suspension crystallizer they predicted the following relationship (where variable names have been adjusted to agree with those in the current study):

$$\frac{N_{Ab}}{V} \cdot D_I^3 = 1.93 \times 10^6 \left(\frac{L_P}{D_I} \right)^{-1.37} \left(\frac{\rho_C - \rho_S}{\rho_S} \right)^{-3.6} (N \cdot t_R)^{1.4} (Re)^{0.85} \phi^{0.47} (H_V)^{-0.7} \quad (2.7)$$

where N_{Ab} is the number of attrition fragments generated, V is the volume of the suspension, L_P is the size of the parent crystals, ρ_C and ρ_S are the densities of the

crystal and solution respectively, N is the impeller speed, t_R is the time period the parent crystals are under stress conditions, Re is the impeller Reynolds number, ϕ is the crystal volume fraction, and H_V is the hardness of the crystal. This equation is the first case of the use of dimensionless groups as an aid to model attrition in a crystallizer.

To develop this correlation, they investigated the effect of impeller tip speed, impeller diameter, volume concentration of the solid phase, the crystal size, and temperature (simulated by variation of density and viscosity) on number of nuclei generated per unit volume of solution. They suggested that the information beyond these experiments is required for a qualitative equation of design and operation in real crystallizers (Offermann and Ulrich, 1981).

2.3.2 Gahn and Mersmann model

Gahn and Mersmann (1997) proposed a physical attrition model equation to explain the fracture behavior of crystalline solid for the attrition process in suspension crystallizers. Then, they developed a model equation for the processes of attrition and abrasion of a brittle solid to predict the whole crystallization process in a quantitative manner (Gahn and Mersmann, 1999). There are four groups of assumptions for the attrition model. They are the loading conditions, the material properties, the elastic stress field in the solid, and a law to describe the fracture process (Gahn and Mersmann, 1997). The major simplifying assumptions are listed below.

A1. Only the contact between a crystal corner and a much harder and flat object is considered. Figure 2.10 shows examples of attrition process, the crystal corner impacting on the harder target is replaced by a cone having a semi-apical angle of $\Theta =$

60° (Figure 2.10a). If a cone is harder than a flat surface, an abrasion occurs as shown in Figure 2.10b.

A2. The force is acting in the normal direction to the contact area and there is no sliding contact or rotation of the crystal.

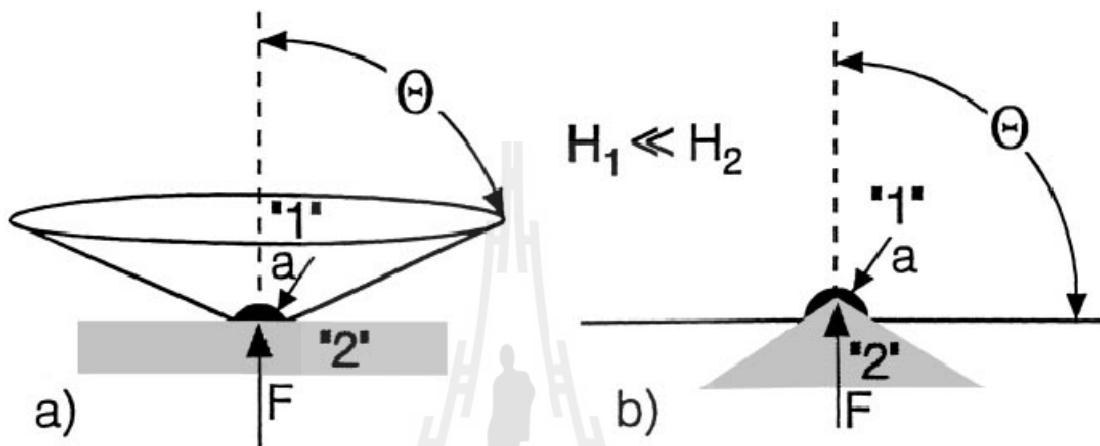


Figure 2.10 Contacts of a harder and softer material: a) a cone being deformed by a hard plate, b) a hard cone contacting a softer material. (Gahn and Mersmann, 1999)

A3. It is assumed that ductility is restricted to a region limited by the area of contact and that the deformation is linear elastic elsewhere because the plastic deformation required high pressure. This plastically deformation region is assumed to be under hydrostatic pressure, which corresponds to the hardness of the material.

A4. After complete loading, fracture of the corner is assumed to begin. The formation and propagation of cracks occurs instantaneously and is only determined by this quasi-static stress field.

A5. The average isotropic values which are assumed to be independent of the strain rate are used as the mechanical properties of the crystalline substance.

A6. From Rittinger's law, the newly created surface cause by the formation of a fragment is proportional to the elastic strain energy stored in the volume of this fragment.

A7. The elastic field at a distance $r > a$ is calculated as if the load was acting as a point force at $a = 0$. The elastic field of this loading condition is given by Michell (1900), in which the point force caused stresses and strains proportional to $1/r^2$.

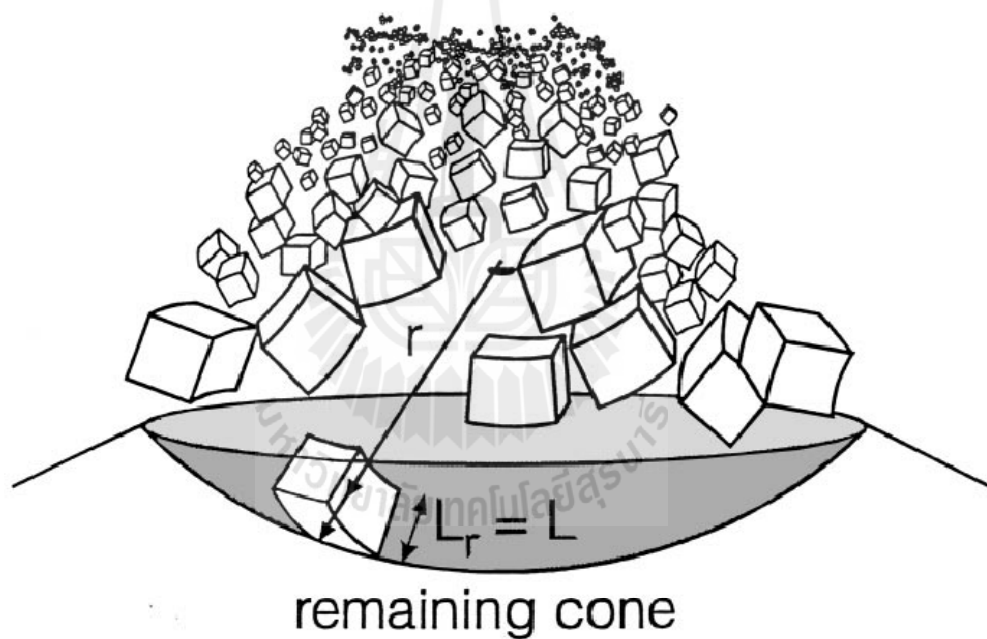


Figure 2.11 Representation of theoretical attrition process. (Gahn and Mersmann, 1997)

A8. The attrition model is based on a simple energetic consideration, and does not consider the influence of the strain rate on plastic deformation.

A9. It is assumed that the characteristic size a is only determined by the hardness of the crystal and not by the ratio of the hardness to shear modulus.

The following equations are attrition model that proposed by Ganh and Mersmann (1999).

Total volume of fragments as a function of the impact energy, W_p

$$V_a = CW_p^{4/3} \quad (2.8)$$

Attrition coefficient C :

$$C = \frac{2 H^{2/3} K_r}{3 \mu \Gamma} \quad (2.9)$$

where H is the hardness of brittle solid (N/m^2)

K_r is the efficiency factor in radial direction (-)

μ is the shear modulus (N/m^2)

Γ is the fracture surface energy (J/m^2)

The energy of impact can be approximated by

$$W_p \approx 0.05 \sqrt{\frac{F^3}{H}} \quad (2.10)$$

where F is the force acting after complete loading of the cone. (N)

H is the hardness of brittle solid (N/m^2)

The impact energy below which material removal will not occur is given by

$$W_{p,\min} = 64 \frac{\mu^3 \Gamma^3}{H^5 K_r^3} \quad (2.11)$$

The smallest size of the fragments produced is given by

$$L_{\min} = \frac{32}{3} \frac{\mu \Gamma}{H^2 K_r} \quad (2.12)$$

The maximum size of fragments produced is given by

$$L_{\max} = \frac{1}{2} \left(\frac{H^{2/3} K_r}{\mu \Gamma} \right)^{1/3} W_p^{4/9} \quad (2.13)$$

The number density distribution of the fragments produced is given by

$$q_0(L) = \frac{2.25}{L_{\min}^{-2.25} - L_{\max}^{-2.25}} L^{-3.25} \quad (2.14)$$

The total number of fragments produced is given by

$$N = \frac{\pi}{21} \frac{H^{1/2} K_r^{3/4}}{\alpha \mu^{3/4} \Gamma^{3/4}} \left(\frac{1}{L_{\min}^{2.25}} - \frac{1}{L_{\max}^{2.25}} \right) W_p \quad (2.15)$$

where α is the volume shape factor, which is dimensionless

The total number of fragments for the case $L_{\min} \ll L_{\max}$ is given by

$$N = 7 \times 10^{-4} \frac{H^5 K_r^3}{\alpha \mu^3 \Gamma^3} W_p \quad (2.16)$$

There are two figures to show the accuracy of the attrition model. Figure 2.12 is the theoretical and experimental values of abraded volume for all substances that used in the experiment of Gahn and Mersmann (1999). Figure 2.11 shows the brittle fracture ($E/H < 100$).

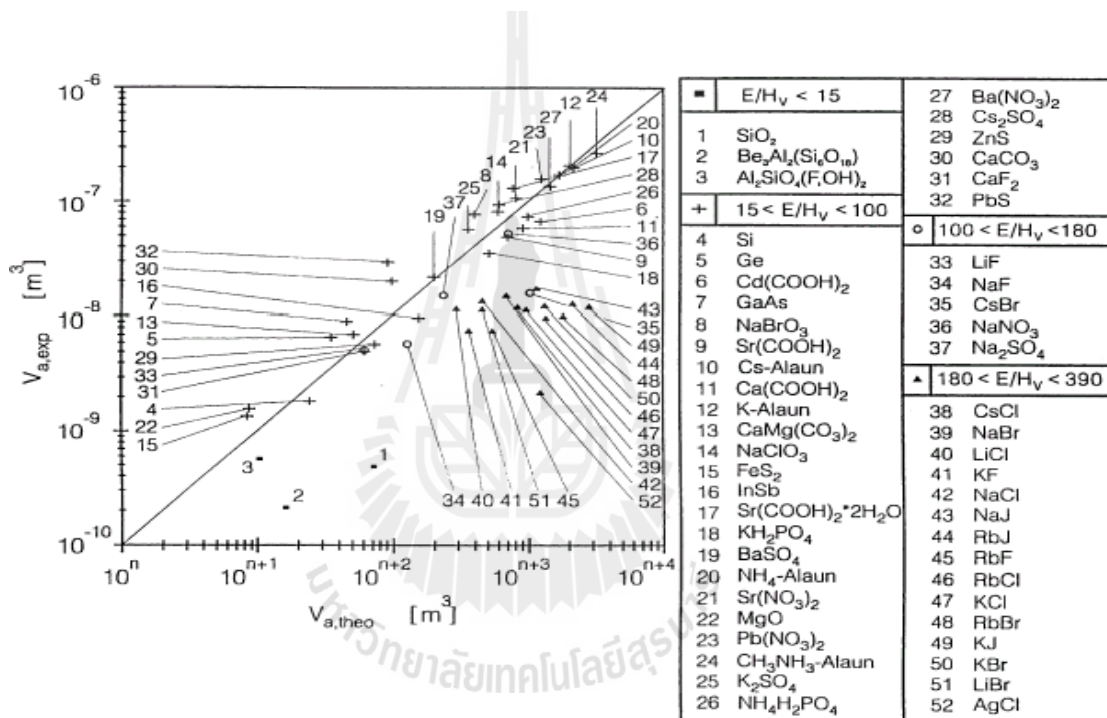


Figure 2.12 Theoretical and experimental values of abraded volumes. (Gahn and Mersmann, 1999a)

As can be seen in the Figure 2.10, we can separate the substances into four groups. There is only one group which this model can estimate the correct values of abraded volumes. They are the brittle solid which have the ratio of E/H_v less

than 100. So, the models which Gahn and Mersmann (1999a) proposed are accurate for brittle substances as can be seen in Figure 2.13.

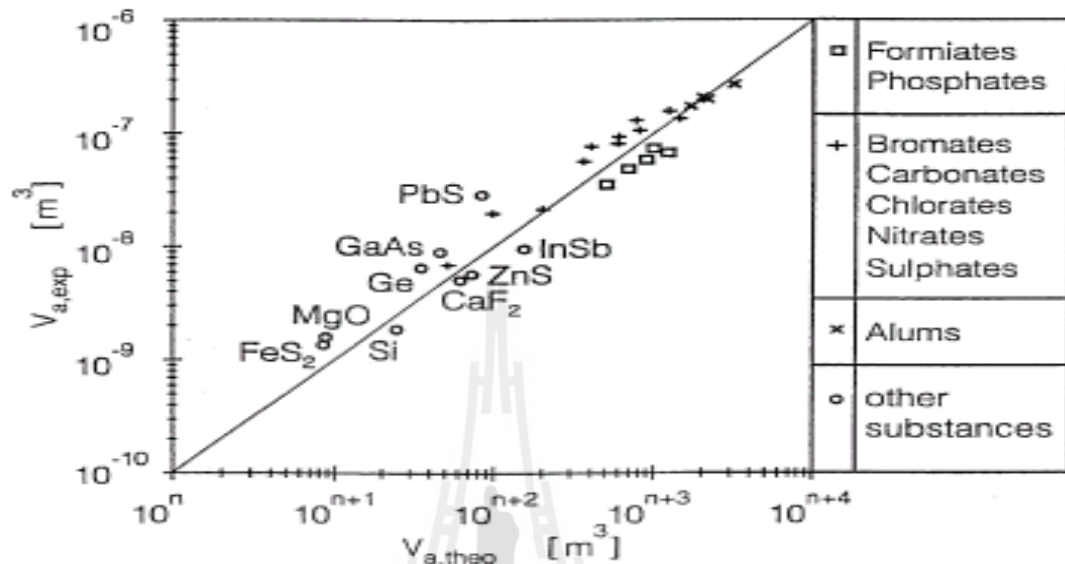


Figure 2.13 Theoretical and experimental values of abraded volumes. The substances meet the requirement for the brittle fracture. (Gahn and Mersmann, 1999a)

Briesen (2007) improved the predictive capabilities of the attrition model according to Gahn and Mersmann (1997, 1999a, 1999b) by dropping some of the assumptions and by making an extended derivation of the attrition model. There are three extensions to improve the model:

1. The force acting to the contact surface is assumed to be any direction that is not perpendicular to the symmetric axis of the contact surface.
2. The polar angles have the effect on strain energy distribution the same as the radial coordinate.
3. The breakage plane is along the constant energy line.

He obtained a new attrition constant which is compared to the attrition constant from Gahn and Mersmann in Figure 2.14. His results show the extended model is better than the original one.

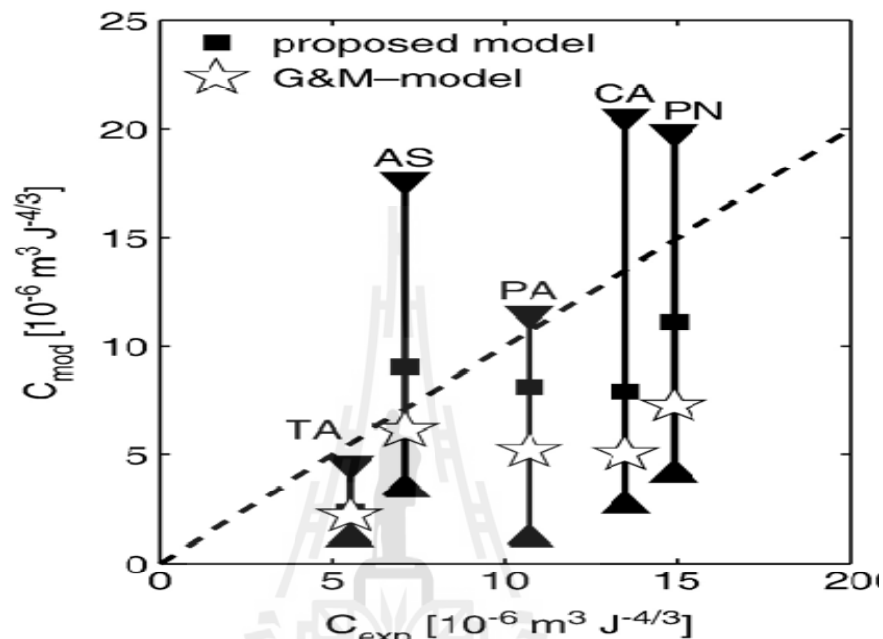


Figure 2.14 Comparison of experimental results with the prediction of the original model by Gahn and Mersmann (with original, non-tuned material properties) and the proposed extended model. (Briesen, 2007)

2.3.3 Yokota et al. model

Yokota et al. (1999) proposed an empirical rate equation of contact nucleation caused by collision of crystals with an impeller. They assumed the contact nucleation rate is a function of collision energy and collision frequency. The target efficiency model was used to develop the contact nucleation rate equation and the definition of the target efficiency is

$$\eta = \frac{(\text{effective contact frequency})}{(\text{ideal contact frequency})} = \frac{\omega_{\text{eff}}(d_p)}{\omega_{\text{id}}(d_p)} \quad (2.17)$$

where $\omega_{\text{id}}(d_p)$ is the ideal collision frequency per blade. By assuming a homogeneous suspension of particles, the ideal collision frequency per blade can be calculated from the following equation

$$\omega_{\text{id}}(d_p) = (\text{volume sweeping rate with a blade}) \times (\text{particle number density})$$

$$\omega_{\text{id}}(d_p) = pD_b^2 u (n_s / V_c) \quad (2.18)$$

where p is the number of impeller blades, D_b is the size of the blade, u is the tip speed, n_s is the number of seed crystals used to commence contact nucleation, and V_c is the tank volume.

The obtained rate equation of contact nucleation is

$$J_{c-i} = k' \cdot p \cdot n_s \cdot d_p^N \cdot u^{N+1} \cdot D_b^{-4} \quad (2.19)$$

where k' is the coefficient, p is the impeller blade number, n_s is the crystal number, d_p is the crystal size, u is the tip speed of an impeller, and D_b is the impeller blade size. This equation is successful to determine the contact nucleation rate of potassium alum where the unknown parameter (N) was equal to 3.

2.3.4 Gharidi and Zhang model

Gharidi and Zhang (2002) proposed a theoretical model of chipping for particulate solids. They used indentation fracture mechanics approach and impact damage analysis to develop the model. They defined a dimensionless attrition propensity parameter in the form:

$$\eta = \frac{\rho v^2 l H}{K_c^2} \quad (2.20)$$

where ρ is the particle density, v is the impact velocity, l is a characteristic particle size, H is the hardness and K_c is the fracture toughness.

The fractional loss from a particle is derived as

$$\xi = \alpha \eta = \alpha \frac{\rho v^2 l H}{K_c^2} \quad (2.21)$$

where α is the proportionality factor

They used a single particle impact testing to check the accuracy of the model. The ionic single crystals of MgO, NaCl, and KCl were used as model materials which have a semi-brittle failure mode. They studied the dependence of the fractional loss on material properties, impact velocity, and particle size and influence of rigidity of target materials on attrition rate. Their results show the trend of the experimental data agrees with the predictions of the mechanistic model of impact attrition. There are some mistakes in this paper. The values of the proportionality factor should depend only on the experimental condition because the material properties are in the propensity parameter. But the experimental results show that the

proportionality factor still depend on material properties so it not fair to conclude that the fractional loss per impact is proportional to propensity parameter.

2.4 Case study of attrition experiment

Several investigators studied the behavior of attrition in the crystallization processes. They found that there are a lot of causes which influence attrition in a crystallizer. This section explains some important results of the attrition behavior. For example, the repeated impact of crystal, the collision of crystal with crystallizer parts and crystal-crystal contact, the impact energy and the shape of crystal, and the crystal properties such as crystal hardness and type of crystal.

2.4.1 The effect of repeated impacts of individual crystals

The work of Biscans (2004) attempted to understand the mechanism of attrition in suspension crystallizers with analysis of repeated impact events of individual crystals. Figure 2.15 shows the results which were an example of data obtained from sodium glutamate, at an impact velocity of 7.00 ms^{-1} on a steel target. From the figure it can be seen that two mechanisms occurred. In the first period, the mass of parent crystal decreased slowly because the amount of material loss was very small. When the number of impact increased to reach some values, the parent crystal broke. So, the mass of crystal in the figure rapidly decreased. The reason for these mechanisms was explained by the effect of repeated impact. At a small number of impact, the crystal absorbed the stress inside and loss of mass was from critical areas such as corners and edges. When the number of impact increased, the accumulation of stress in crystal increased also. Then the breakage occurred with the crystal, if the stress accumulation is high enough.

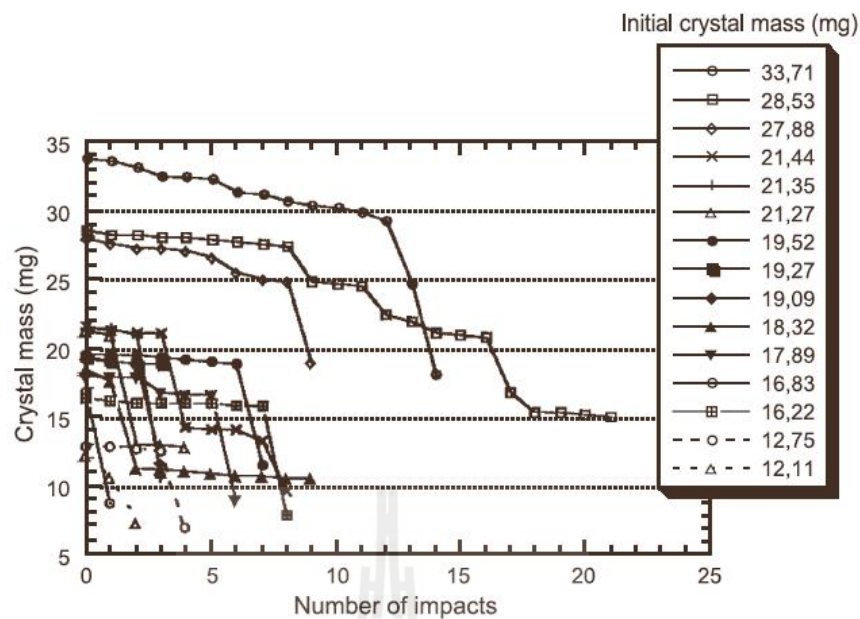


Figure 2.15 Influence of the number of impacts on the attrition of sodium glutamate crystals at an impact velocity of 7 ms^{-1} . (Biscans, 2004)

2.4.2 The effect of crystal-wall or crystal-stirrer impact

Biscans et al. (1996) proposed the study of attrition due to the impact between crystal and crystallizer parts. Their results can be discussed in two ways, crystal size distribution and evolution of crystal shape. Figure 2.16 shows the crystal size distribution before and after the impact occurs. After the crystal contact with the wall or impeller the mean size of the crystal decreased. Thus, the attrition can occur when the crystal contacts with the part of crystallizer or impeller. The attrition has an effect on the crystal size distribution. If we observe the shape of the crystal in Figure 2.17, after the impact the shape of crystal changed. The mass of crystal at the edges and corners are lost from parent crystal. These results confirmed that the contact between crystal and crystallizer parts or impeller effect to attrition rate.

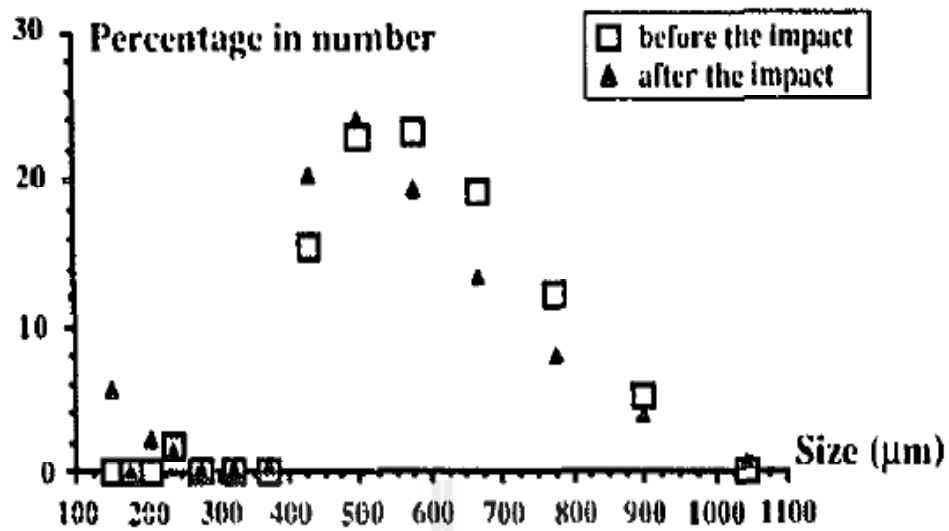


Figure 2.16 Comparison between the size distribution (in number) of the NaCl crystals before and after the impact (pressure 2 bars, inject-target distance 8 cm). (Biscans et al., 1996)

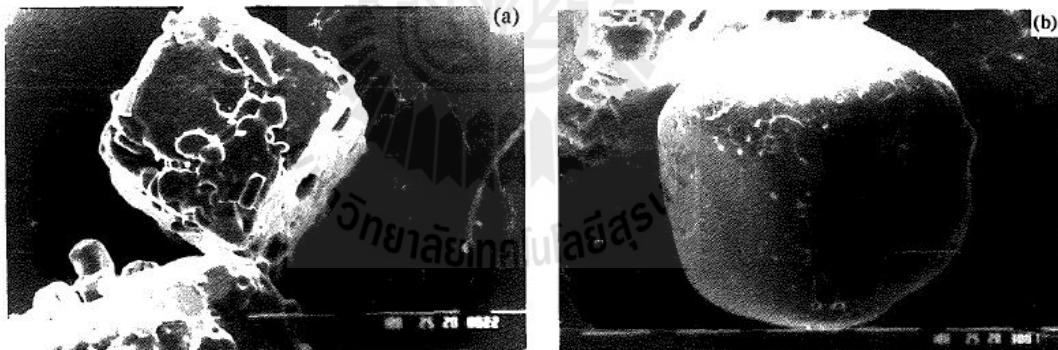


Figure 2.17 Picture of examples of NaCl crystals before the impact (a) and after the impact (b) (pressure 2 bars, inject-target distance 8 cm). (Biscans et al., 1996)

2.4.3 The effect of impact energy and shape of crystal

Gahn, Krey, and Mersmann (1996) studied the volume and mass of attrition fragments produced by a single impact. They calculated the impact energy of crystal-impeller contacts according to the Ploss and Mersmann (1989) equation.

$$E_p = \frac{1}{2}mv^2\eta_{geo}\eta_T \quad (2.22)$$

where m is the mass of the colliding crystal, v is the impact velocity, η_{geo} is the probability that the crystal is on a streamline moving towards the impeller, and η_T is the target efficiency.

From their results, it was found that the attrition fragment is proportional to impact energy as can be seen in Figure 2.18 and Figure 2.19. Both the volume of attrition fragments and mass of attrition fragments increased when the impact energy increased. The results in the paper are different from the results from Biscans (2004) who studied the effect of repeated impact of individual crystals. Biscans (2004) found that when the number of impact increased, the crystal will finally break. In this paper, they found when the number of impact increased, the attrition rate decreased because the shape of the crystal changed to a rounded shape and this had resistance to attrition. The differences of these two papers may be from the magnitude of the impact in the experiment is not equal. Biscans (2004) used the higher value of impact energy so the crystal can be easy to break when the numbers of impacts increase.

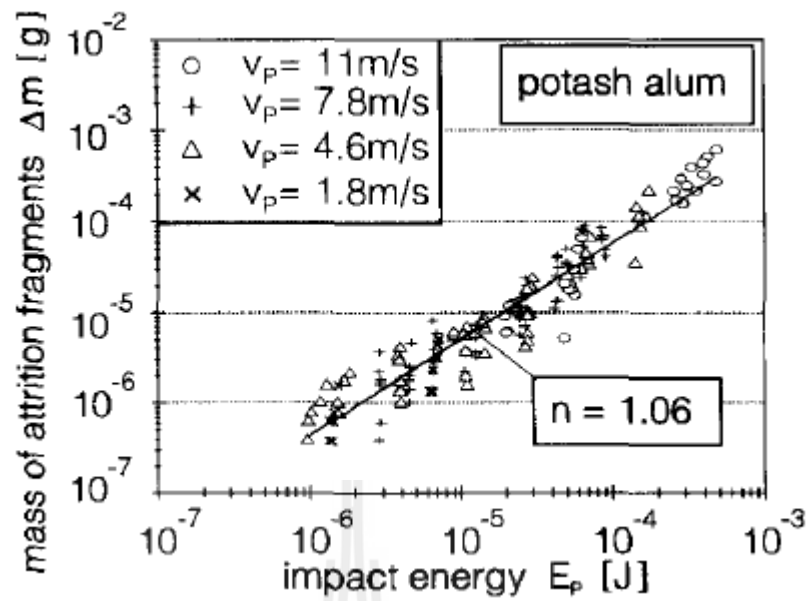


Figure 2.18 Mass of attrition fragments as a function of impact energy. (Gahn et al., 1996)

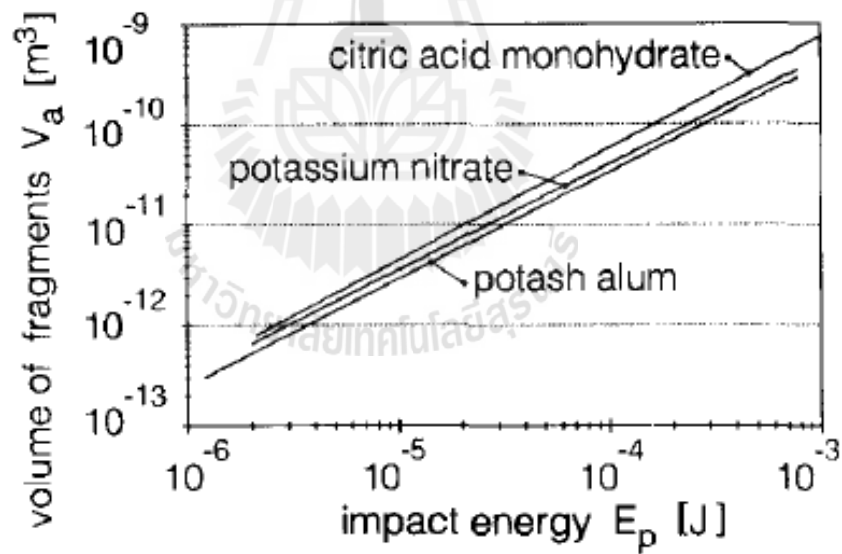


Figure 2.19 Volume of fragments as a function of impact energy. (Gahn et al., 1996)

2.4.4 Mechanical properties of the crystal

The mechanical properties of the particle are very important because several models use them to predict the attrition behavior of the particle. This section

will explain two mechanical properties that are used in many attrition models. They are Young's modulus and Vickers hardness.

2.4.4.1 Young's modulus

The Young modulus (E) has the units of N/m^2 . The Young modulus of a single crystal can be obtained by performing a compression test. The compression test will apply a given load on the object and analyze its deformation. The size of the object must be large enough to apply the force on it. The characteristic dimension of the crystals used in this test was around 3 or 4 mm. The example of the determination of the NaCl crystal's Young modulus is shown in Figure 2.20. An elastic deformation is observed at the starting region, then, the slope changes because the strain increases and the crystal shows the plastic deformation. If the crystal breakage occurs after the elastic deformation, it means the plastic deformation is not important. From Figure 2.20 the Young modulus of NaCl crystal is 25.0 GPa.

2.4.4.2 Vickers hardness

The resistance of the solid to local plastic deformation can be predicted from the hardness of the solid. The Vickers hardness test uses a Vickers pyramid as an indentation apparatus. The objective of this technique is to consider the fracture surface and the work of indentation after the test. The fracture surface will form after indentation by the Vickers pyramid. Dividing the load applied by the area of indentation formed, the hardness is obtained with a unit of pressure (N/m^2). For the small crystal, it is not possible to use the Vickers hardness test to measure the hardness of the crystal because the size of the crystal is less than the characteristic dimension. The microhardness test was used for these crystals because it concerns a

weak load (5×10^{-3} to 2 kg). The indentation geometry is a pyramidal type, with a square base having an angle of 136° at the top as shown in Figure 2.21.

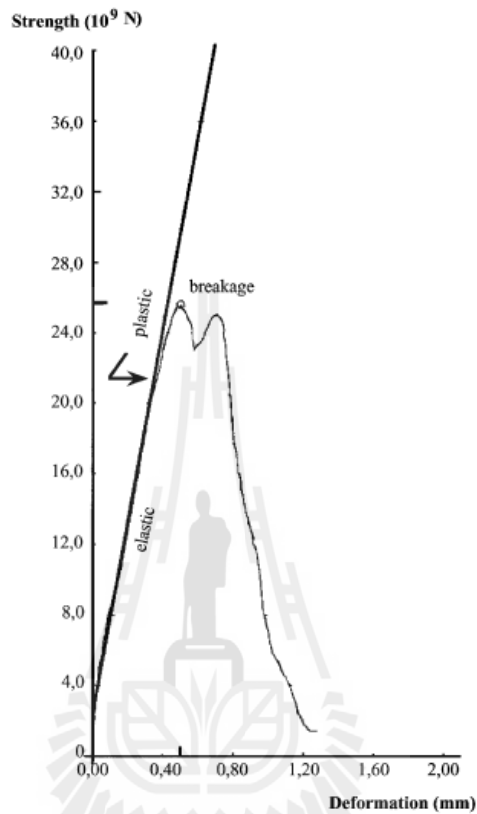


Figure 2.20 Compression profile obtained for NaCl single crystal. (Marrot and Biscans, 2001)

The equation for the lateral surface of the pyramidal print made on the crystals is

$$S = \frac{d^2}{2 \sin \alpha / 2} \quad (2.23)$$

This feature of the surface can be measured by observation under a microscope.

The Vickers hardness, H_v can be calculated from the following equation. The hardness is a function of the load and the depth of penetration.

$$H_v = 1.854 \frac{F}{d^2} \quad (2.24)$$

The indentation can be performed at different positions on the surface of the crystal. The crystal that is used to measure the hardness should have a smooth surface. The example of Vickers hardness for NaCl crystal at different size and different positions of the indenter are shown in Table 2.2.

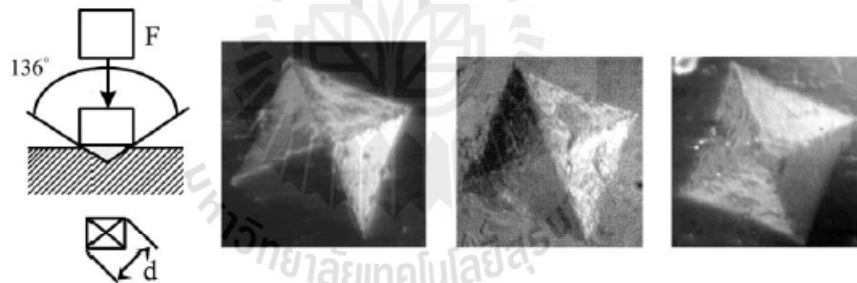


Figure 2.21 Geometry of the indentation in the Vickers test and obtained pattern on a single crystal surface with 1 N load. (Marrot and Biscans, 2001)

Table 2.2 Hardness values for NaCl crystals (Marrot and Biscans, 2001)

Position of the indenter						
Crystal size (μm)	200	200	1000	1000	2000	2000
$H_v(\times 10^{-6} \text{ Pa})$	168	172	165	171	169	174

CHAPTER III

RESEARCH PROCEDURE

3.1 Instrumentation

The main equipment used in this research are a crystallizer, a Coulter Multisizer 3 particle sizer/counter, a Malvern Mastersizer S particle sizer, a wireless rotary torque transducer, and a scanning electron microscope. The details of these pieces of equipment are described below.

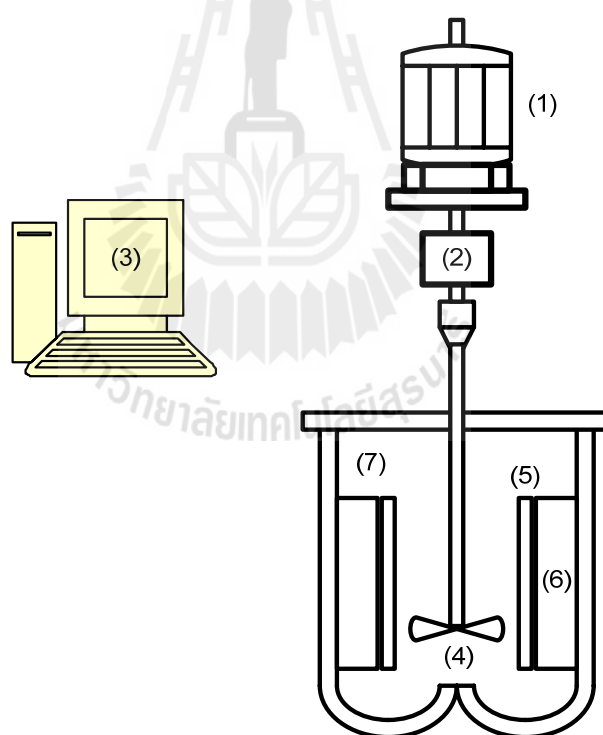
3.1.1 The crystallizer

There are two scales of crystallizer used in this study, 500 mL and 2000 mL. The crystallizers are made from Borosilicate glass. Details of the geometry of the crystallizers are shown in Table 3.1. Figure 3.1 shows a schematic diagram of the experimental set-up. It consists of a batch crystallizer equipped with four vertical baffles, a draft tube, and an up-flow impeller connected to a wireless rotary torque transducer and a variable speed overhead stirrer. The two crystallizers are geometrically similar based on the ratio of the draft tube diameter to crystallizer diameter, the ratio of impeller diameter to crystallizer diameter, and the ratio of off-bottom clearance to crystallizer diameter.

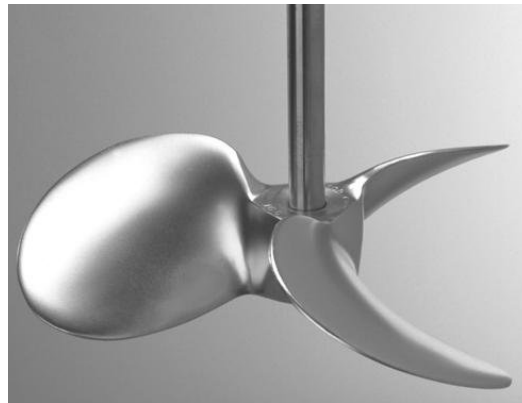
There are two types of the blades in this study. They are a marine propeller and a 45° pitch blade impeller as shown in Figure 3.2. To study the effect of impeller material, we selected a marine propeller as the standard condition, so the marine propellers are made from stainless steel and resin.

Table 3.1 Dimensions of the crystallizers

	Small scale	Large scale
Diameter (mm)	90	150
Diameter of draft tube (mm)	64 and 75	110
Diameter of impeller (mm)	50	85
Off-bottom clearance (mm)	10 and 20	15

**Figure 3.1** Schematic diagram of a crystallizer used in the study and experimental set-up

Key: (1) motor, (2) wireless rotary torque transducer, (3) data recording, (4) impeller, (5) draft tube, (6) baffles, and (7) crystallizer.



a) marine propeller



b) pitch blade impeller

Figure 3.2 The types of the impeller in the study.

3.1.2 Multisizer 3 COULTER COUNTER®

This equipment is used for the measurement of the size distribution of the attrition fragments and also to count the number of the attrition fragments. Figure 3.3 shows a schematic illustration of the Coulter Principle applied in the Multisizer 3, and the basic set-up of the electrical sensing zone technique. The Coulter Counter measures the number based size distribution of the particles suspended in a suitable

electrolyte. The particles will be forced to pass through the orifice of the aperture tube. When the particles pass through the sensing zone, it will change the aperture resistance and generate the voltage pulses (Garside et al., 2002). The Coulter Principle states that the amplitude of the voltage pulse is directly proportional to the volume of the particle that produced it (Beckman Coulter Inc., 2000 - 2011). The Multisizer 3 COULTER COUNTER® is shown in Figure 3.4.

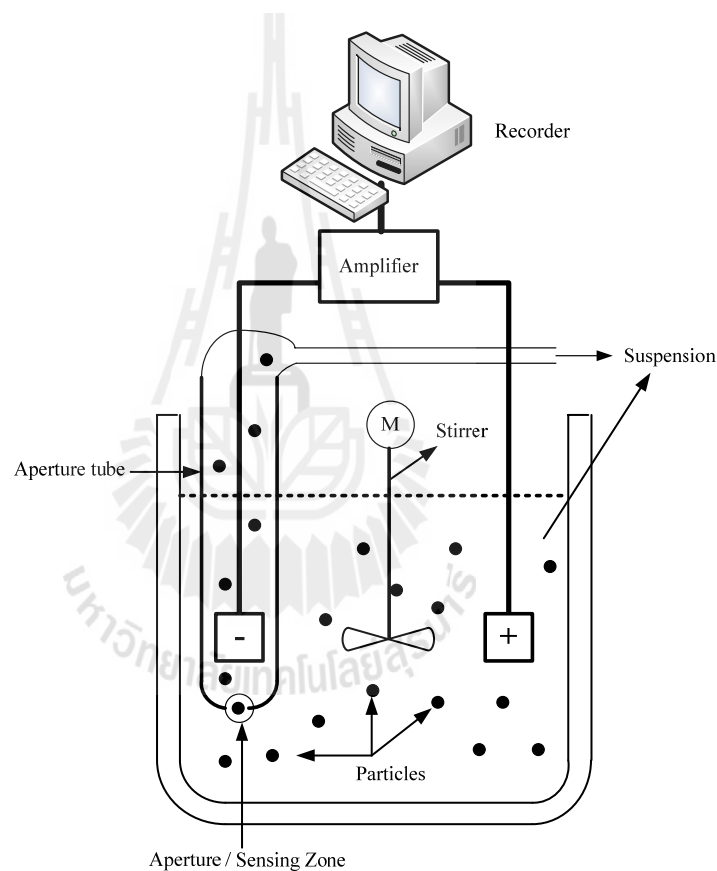


Figure 3.3 Diagrammatic illustration of the Coulter Principle applied in the Multisizer 3 and electrical sensing zone technique. (Adapted from Garside et al., 2002 and Malvern Instruments Ltd., 2012)



Figure 3.4 Multisizer 3 COULTER COUNTER®. (Beckman Coulter Inc., 2000 - 2011)

3.1.3 Malvern Mastersizer S

In this study, we used the small volume stirred cell of the Malvern Mastersizer S to measure the particle size distribution of the attrition fragments. The small cell stirs the cell contents with a magnetic bead operated from an external magnet rotated by the unit. It is controlled by a knob to adjust the stirrer speed. Figure 3.5 shows the Malvern Mastersizer S and its accessories. The Malvern Mastersizer S was also used to infer the counts of the attrition fragments using the combination of the volume based particle size distribution and the suspension density measurement. The method is described in section 3.3.1.1.

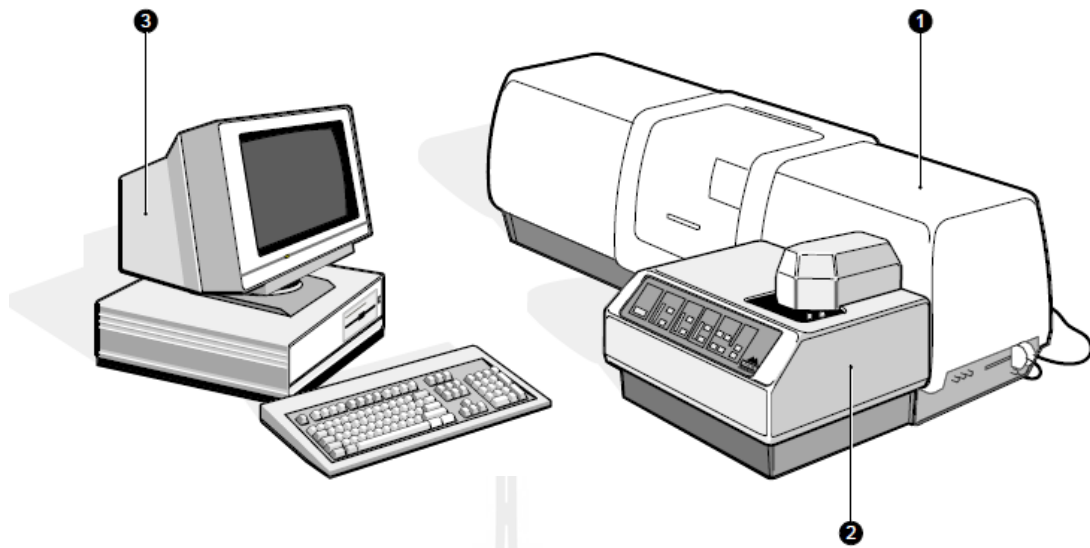


Figure 3.5 The Malvern Mastersizer S and its accessories Key: (1) the optical unit, (2) one or more sample preparation accessories, and (3) a computer system. (Malvern Instruments Ltd. 1995, 1997)

3.1.4 Wireless Rotary Torque Transducer

To measure the power input into the crystallizer a torque transducer was used to measure the torque in the shaft, and then the power was calculated from the torque. Figure 3.6 shows the schematic diagram of the rotary torque transducer and wireless force indicator. The connection between the motor and the torque transducer is shown in Figure 3.1. We can measure the torque in the crystallizer in real time mode and the results can be recorded by the computer.

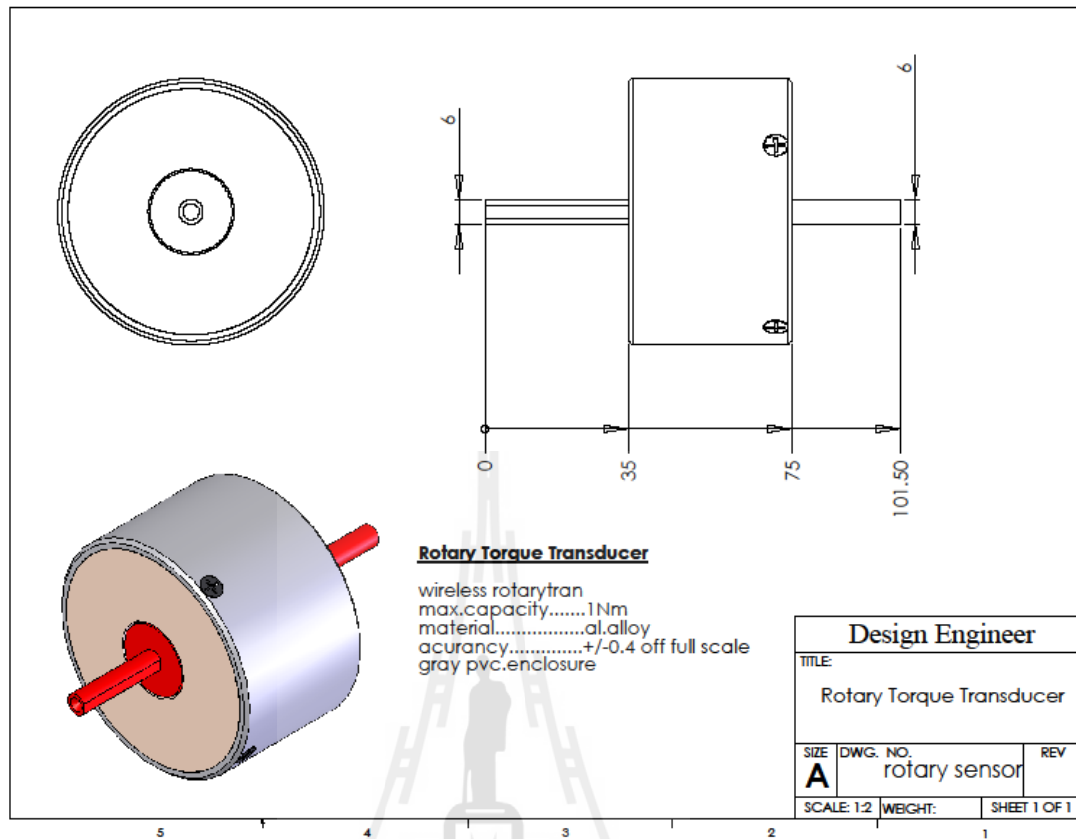


Figure 3.6 Rotary torque transducer and wireless force indicator.

3.1.5 Scanning Electron Microscope (SEM)

The parent crystals and attrition fragments are observed by the SEM model JCM-5000 NeoScope. When we measured the size distribution of the attrition fragments by the Coulter Counter and the Malvern Mastersizer, we also checked the shape of the attrition fragments again by SEM.

3.2 Materials

3.2.1 Sucrose

The sucrose in this study is refined sugar (commercial grade (~99.8%)) from Mitr Phol, Thailand. There are three size ranges of parent crystal, 300 – 425, 425 – 600, and 600 - 850 μm , which were prepared by sieving with ASTM sieves. An example of a parent crystal of sucrose is shown in Figure 3.7. There are some fragments on the surface of parent crystal so it is necessary to wash the crystal with saturated solution before the attrition experiment to avoid the initial breeding mechanism by add the crystals in the clean saturated solution for three times.

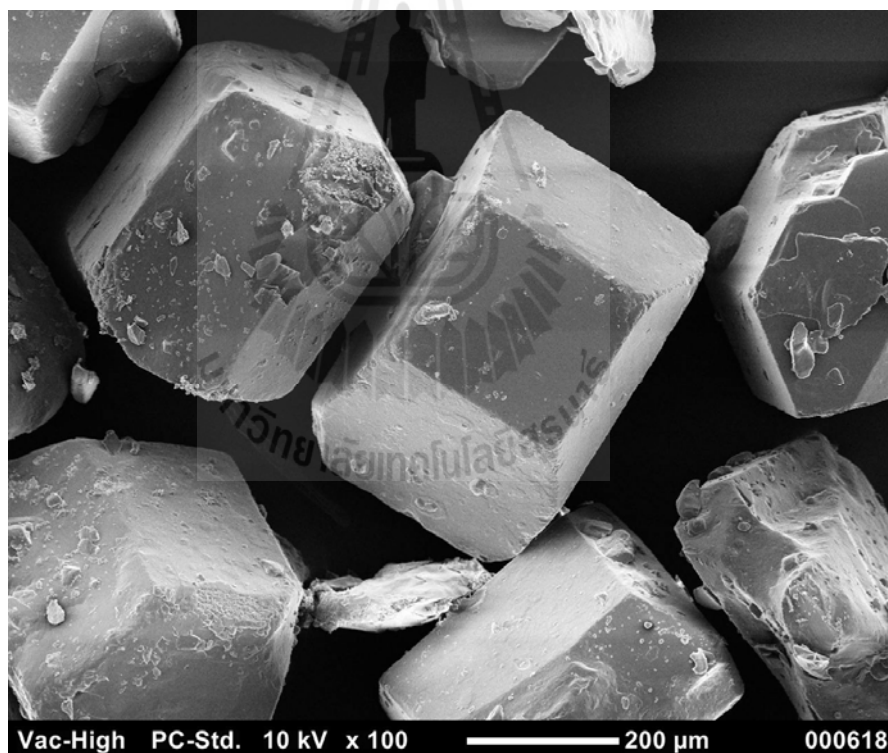


Figure 3.7 SEM micrograph of a sucrose parent crystal size range 300 - 425 μm .

3.2.2 Sodium Chloride

The sodium chloride (NaCl) in this study is refined salt from Thai Refined Salt Co., Ltd. It has a maximum moisture content equal to 0.15%. Salt crystals were sieved into three size ranges, 150 – 300, 300 – 425, and 425 – 600 μm using ASTM sieves. A picture of a typical parent crystal is shown in Figure 3.8. The edges and corners of the parent crystals are quite sharp so they are useful for a study of the attrition. They were washed by a slightly supersaturated solution to remove surface impurities and fine particles (to avoid initial breeding).

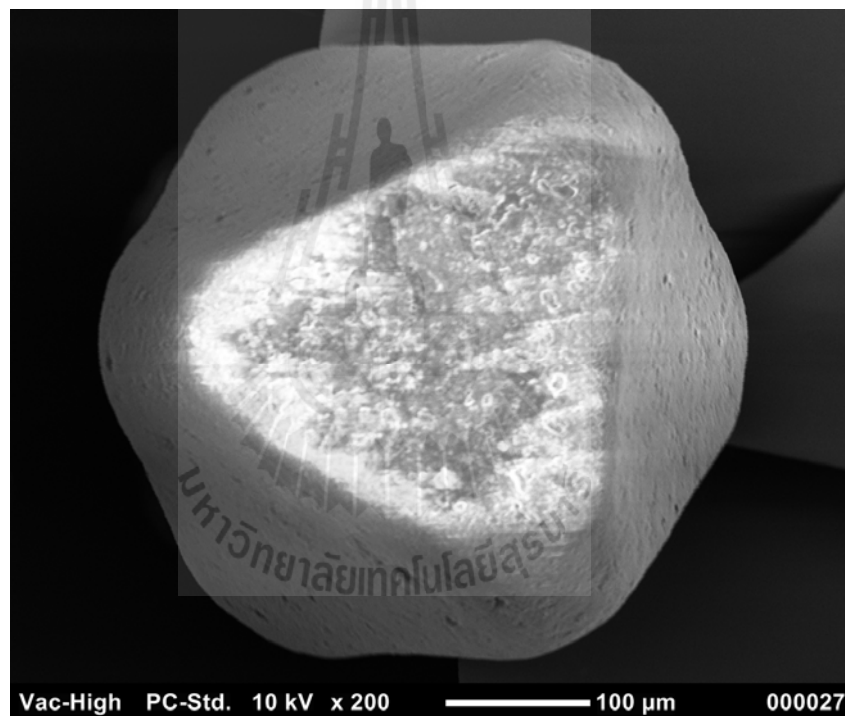


Figure 3.8 SEM micrograph of a NaCl parent crystal size range 300 - 425 μm .

3.2.3 Cellulose Acetate Membrane

For preparation of the clean electrolyte solution, we need to remove all impurities and parent crystals from the solution. For this, cellulose acetate membranes of pore size 0.45 μm and a vacuum pump were used to filter the electrolyte solution.

3.2.4 Methanol

The methanol used in this study is commercial grade methanol from The Shell Company of Thailand Limited. It has 99% purity. The methanol was used for preparation of electrolyte solutions, saturated solutions, and supersaturated solutions of the solutes.

3.2.5 Lithium Chloride

Lithium Chloride was used for the preparation of the electrolyte solution for the study of sucrose attrition using the Coulter Counter. The electrolyte solution was 5% LiCl in methanol. After we prepared the electrolyte solution, we used the electrolyte solution for preparation of saturated solutions of sucrose.

3.2.6 Deionized water (DI water)

DI water was used to vary the viscosity and density of the solution; by changing the solvent composition (the ratio of DI water to methanol, for example) the solubility of sucrose and sodium chloride in the solution can be varied, thus varying viscosity and density. The DI water for the experiments was produced from a MembraPure Aquinity unit at SUT.

3.3 Experimental Methods

3.3.1 Determination of significant parameters on attrition rate

We separated sources of parameters into three groups, crystallizer geometry and operating conditions, crystal properties, and solution and suspension properties.

The parameter from crystallizer geometry and operating conditions

1. Diameter of the impeller (mm)
2. Diameter of the draft tube (mm)
3. Impeller clearance (mm)
4. Impeller speed (rpm)
5. Type of material used in the blade
6. Diameter of the crystallizer (mm)

The parameter from crystal properties

1. Average size of the parent crystals (μm)
2. Density of the parent crystals (g/mL)
3. Type of parent crystals (sucrose and NaCl)

The parameters from solution and suspension properties

1. Supersaturation (-)
2. Viscosity of the solution (cP)
3. Density of the solution (kg/m^3)
4. Suspension density (kg/m^3)

In order to minimize crystal growth or dissolution during the experiment, the crystals were suspended in slightly supersaturated solution (2°C sub-

cooling). A small supersaturation was used because it is very difficult to create an exactly saturated solution (because the temperature control cannot be exact throughout the experiment); since growth is a much slower process than dissolution, having a small supersaturation is the safest option.

Presently, there are many methods to determine the particle size distribution, but in this study two methods are used. The first method uses the Malvern Mastersizer S and the second one uses the Multisizer 3 Coulter Counter.

3.3.1.1 Determination of attrition fragment by Malvern

Mastersizer S (Sucrose is the model material)

All experiments in this study were performed in a 500 mL batch crystallizer equipped with four vertical baffles, draft tube, and an upflow impeller connected to a variable speed overhead mixer. A schematic figure of the crystallizer is shown in Fig. 3.1. Experiments were performed via a partial factorial design, with standard conditions (low value : high value) for the experiments being:

Crystallizer geometry and operating conditions

- Diameter of draft tube = 64 : 75 mm
- Diameter of impeller = 50 mm
- Impeller clearance = 10 : 20 mm
- Type of blade = *marine type propeller* : 45° pitch blade impeller
- Material of blade = *stainless steel* : resin
- Impeller speed = 800 : 1000 : 1200 rpm

Crystal properties

- Size range of parent crystals (L) = 300 – 425 : 425 – 600 : 600 – 850 μm

- Type of parent crystals = *sucrose*

Suspension properties

- Parent crystal suspension density (M_T) = *10* : 15 g of crystal/100 mL
- Saturated solution (25 °C, sucrose in *100% MeOH* : 90% MeOH : 80% MeOH)
- Reynolds Number = 14,400 : 36,700 : *43,900*

The conditions for the standard case (all variables at the base level in the factorial design) are indicated by the use of italics. Other conditions were also studied where extra points appeared necessary for model fitting.

When a sampling time was reached the impeller speed was lowered to 200 rpm, which is low enough that the parent crystals (which had sizes in the order of hundreds of micrometers) settled out while attrition fragments (which were of the order of 1 – 5 micrometers) remained suspended. 20 mL of suspension was sampled using a pipette for analysis of the suspension density by determination of the weight of particles left after filtration through a 0.45 μm filter. Samples were also taken for particle sizing, which was performed with a Malvern Mastersizer S with a 300 mm lens and a beam length of 14.3 mm.

3.3.1.2 Determination of attrition fragment by Multisizer 3 Coulter

Counter (Sodium Chloride is the model material)

In this case, we need an electrolyte solution for the measurement using the Multisizer 3 Coulter Counter. The electrolyte solution is a mixture of 80% methanol and 20% water saturated with NaCl at 27°C and subcooled to 25°C. A water bath was used to control the temperature of the crystallizer. Experiments were performed via a partial factorial design, with standard conditions (low value : high value) for the experiments being:

Crystallizer geometry and operating conditions

- Diameter of draft tube = *64 : 75 mm*
- Diameter of impeller = *50 mm*
- Impeller clearance = *10 : 20 mm*
- Type of blade = *marine type propeller : 45° pitch blade impeller*
- Material of blade = *stainless steel : resin*
- Impeller speed = *800 : 1000 : 1200 rpm*

Crystal properties

- Size range of parent crystals (L) = *150 – 300 : 300 – 425 : 425 – 600 μm*
- Type of parent crystals = *NaCl*

Suspension properties

- Parent crystal suspension density (M_T) = *2.5 : 5 : 10 g of crystal/100 mL*
- Slightly supersaturated solution (*2°C sub-cooling*).

The standard conditions are indicated by the use of italics. Other conditions were also studied where extra points appeared necessary for model fitting. 50 g of the parent crystals and 500 mL of slightly supersaturated

solution were added in the crystallizer at 25°C and agitation begun. After 5 minutes, the agitation was stopped. The whole suspension in the crystallizer was poured through 75 μm and 38 μm sieves (using wet-sieving) to separate the parent crystals and attrition fragments.

The Multizer 3 Coulter Counter is better than the Malvern Mastersizer S for a study of the attrition rate. This is because directly measuring counts (as done via the zone sensing method in the Coulter Counter) gives a more accurate answer for the number of particles than inferring this value from a light scattering measurement. The sample of suspension was diluted with a slightly supersaturated solution. The resulting suspension was analyzed using the Beckman Coulter Multisizer 3 with a 50 μm aperture tube. The number based distributions were converted to total number of attrition fragment per unit volume. This experiment was repeated using the same procedure as above for 15 minute and 30 minute samples for the standard condition. The background counts of particles (the clean electrolyte solution at 0 minute) were also measured using the Beckman Coulter Multisizer 3.

3.3.2 Determination of the attrition fragment size distribution and number per unit volume

The size distribution of attrition fragments and parent crystals was studied by several investigators who were interested in the behavior of attrition in crystallizers. If we compare the size distribution before and after impact in the crystallizer, we can predict whether attrition occurs in the crystallizer. We can also predict the mechanism of the attrition, because if the breakage mechanism occurs the size of fragment will bigger than the fragment from an abrasion mechanism.

3.3.2.1 Malvern Mastersizer S

The result from the Malvern Mastersizer S is a volume based PSD. The volume based PSDs found were log-normal (See Figure), indicating that the number based PSDs were also log-normal. The conversion to the number of attrition fragments could then be calculated from the Malvern data and the suspension density via the equations (Allen, 1997)

$$\ln(\mu_{gN}) = \ln(\mu_{gV}) - 3(\ln(\sigma_g))^2 \quad (3.1)$$

$$\overline{L}_{3,0} = \sqrt[3]{\exp(3 \ln \mu_{gN} + 4.5 \ln^2 \sigma_g)} \quad (3.2)$$

$$N_T = \frac{V_T}{\frac{\pi}{6} \overline{L}_{3,0}^3} \quad (3.3)$$

3.3.2.2 Multisizer 3 Coulter Counter

The result from the Multisizer 3 Coulter Counter is a number based PSD so we can convert to total number of attrition fragment per unit volume directly. The results should be checked with another method to confirm the accuracy of the measurement. We used an SEM to observe the shape of attrition fragments and we also compare the result from the Multisizer 3 Coulter Counter with Malvern Mastersizer S. After separation of parent crystals from the attrition fragments, the suspension was filtered by a 0.45 μm cellulose acetate membrane to separate the attrition fragments and the slightly supersaturated solution. We then collected the attrition fragments from the membrane to observe by SEM.

The parameters varied in the study are parent crystal size (L_p), off-bottom impeller clearance (C_{OB}), impeller-draft tube clearance ($D_D - D_I$), impeller speed (N), impeller type (-), impeller material (-), and suspension density (M_T). Sufficient measurements to characterize the attrition rate and other variables required for the dimensionless group correlation of the attrition in the system were measured. Experiments were replicated at least three times at all conditions in order to estimate uncertainty of the measurements. An example of the time progression of the number-based and volume-based particle size distribution for a single replicate is shown in Figure 3.9. The particle size distribution at 5 and 15 minutes have the same mode at 1.7 micron for volume-based distribution but at 15 minutes produced more attrition fragments therefore a higher peak is shown.

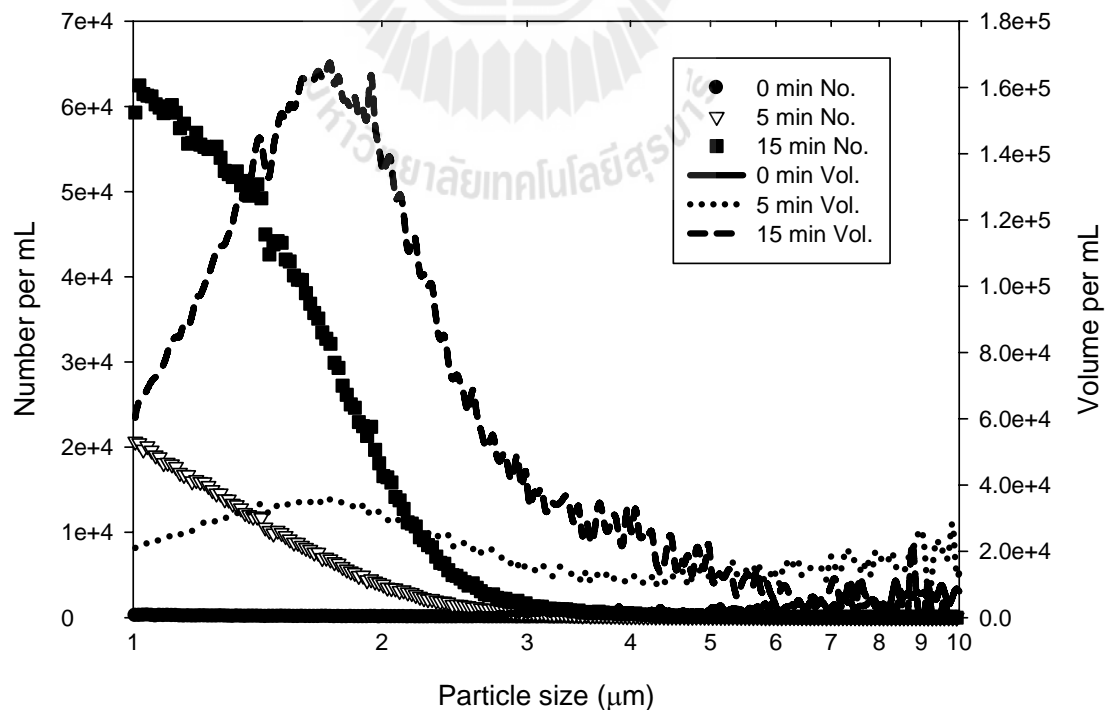


Figure 3.9 Changes in the number-based and volume-based particle size distributions for a sample taken from the 500 mL batch crystallizer (slightly supersaturated solution of NaCl in 80% methanol; 300-425 μm NaCl parent crystals; suspension density 0.1 g/mL; stainless steel marine upflow impeller; impeller speed 1000 rpm; crystallizer diameter 90 mm; draft tube diameter 64 mm; impeller diameter 50 mm; off-bottom clearance 10 mm).

3.3.3 Determination of attrition rate

For constant conditions for a slightly supersaturated solution, the number of counts increases linearly with time for a short period of time (ca 20 min) after the commencement of attrition and then the number of counts plateaus due to reduced attrition as the edges of the parent crystals become rounded. We can calculate the attrition rate from the slope of the relationship between number of attrition fragment per unit volume and time as show in Figure 3.11.

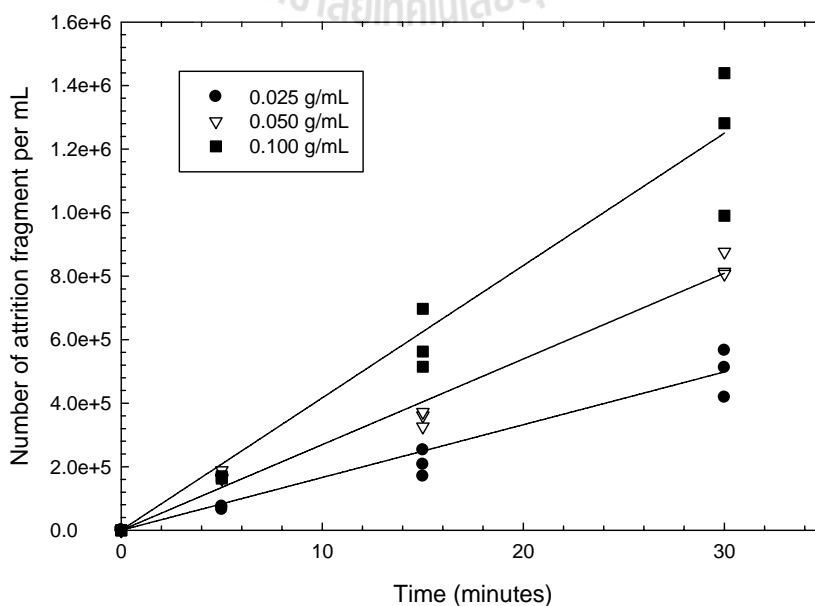


Figure 3.10 Increase in number counts with respect to time for a sample taken from the 500 mL batch crystallizer (slightly supersaturated solution of NaCl in 80% methanol; 300-425 μm NaCl parent crystals; suspension density 0.025, 0.050, and 0.100 g/mL; stainless steel marine upflow impeller; impeller speed 1000 rpm; crystallizer diameter 90 mm; draft tube diameter 64 mm; impeller diameter 50 mm; off-bottom clearance 10 mm).

The results from the particle counts at small times can be used to estimate the attrition rate of ‘well-shaped’ (i.e. growing) crystals under similar conditions. In an industrial crystallizer, the parent crystals in the supersaturated solution are growing after the attrition mechanism occurs, and hence the parent crystals will be well-shaped.

3.3.4 Scale-up crystallizer study

To apply the information in this research to industrial crystallization, we have to study the effect of scale-up. The experiments were carried out in two geometrically similar crystallizers with diameters of 80 and 145 mm (Figure 3.11). The crystallizers featured a hemispherical base, four baffles and a draft tube. Agitation was with stainless steel marine impeller pumping downward and driven by a variable speed motor. The crystallizer dimensions and characteristics are given in Table 3.2. The scale up factor for the design of the large scale crystallizer is about 2.

Commercial sugar crystals were used for the experiments. Three size ranges of parent crystals were sieved, using ASTM sieves. They are 250 – 355, 355 –

450, and 450 – 560 μm . Then the parent crystals were washed using a saturated solution of sucrose in methanol to separate the small particles from the parent crystals.

The experimental conditions for the current study vary two parameters, parent crystal size and impeller speed (1400, 1700 and 2000 rpm). The suspension density of parent crystal was 10% weight per volume, which corresponds to a reasonable value for a crystallizer, obtained by mixing 37.5 g of parent crystals and 350 mL of saturated solution for the small scale and mixing 200 g of parent crystal and 1875 mL of saturated solution for the large scale. The operating temperature was 20 °C. The experimental condition for the large scale was calculated from the constant tip speed criteria (Geisler, 1993). Therefore the impeller speed for the large scale which compares to the small scale crystallizer at 1700 rpm was 850 rpm.

After stirring for 5 min, the suspension was discharged and filtered by 160 μm sieves to separate the parent crystals out from the attrition fragments. Then the whole suspension was filtered under vacuum using a cellulose acetate membrane with a pore size of 0.45 μm to collect the attrition fragments. After drying in a hood overnight, the mass of attrition fragments was measured to obtain the attrition fragment suspension density. The experiments were also performed for particle sizing, which was carried out by a Malvern-Mastersizer 2000 (Hydro S). The attrition fragment concentrations are quite low so the suspensions were kept at 20 °C overnight to concentrate the suspension and took the sample at the bottom of the bottle before measuring with the Malvern-Mastersizer 2000. So the concentration was in the right range for measurement.

The particle size distributions based on the volume of the attrition fragments varied from approximately 0.3 – 100 μm and the volume based PSD was

log-normal indicating that the number based PSD was also log-normal (See Appendix B). The conversion to the number of attrition fragments could then be calculated from the Malvern data and the suspension density via the equation 3.1 to 3.3 (Allen, 1997 and Randolph and Larson, 1988). Equation 3.1 in section 3.3.2.1 is used for calculating the geometric mean of the number distribution from the volume distribution. Then the volume-number mean size of attrition fragments based on number distribution which is used for calculating the total number per unit volume can be determined from Equation 3.2. The total volume concentration of attrition fragments (V_T) and the volume-number mean size of attrition fragments will be used to calculate the total number of attrition fragments per unit volume by Equation 3.3. The attrition rate was calculated by dividing the total number of attrition fragments per unit volume with the experimental time.

Table 3.2 General dimensions and characteristics of crystallizer.

Dimensions and characteristics	Large scale (2000 mL)	Small scale (375 mL)
Crystallizer diameter (D_T , mm)	145	80
Draft tube diameter (D_D , mm)	100	57
Impeller diameter (D_I , mm)	50	25
Draft tube height (H_D , mm)	75	45
Liquid height (H_T , mm)	145	80
Draft tube clearance (C_D , mm)	35	17.5

Baffles width (B, mm)	12	7
Impeller clearance (C_{OB} , mm)	27	15

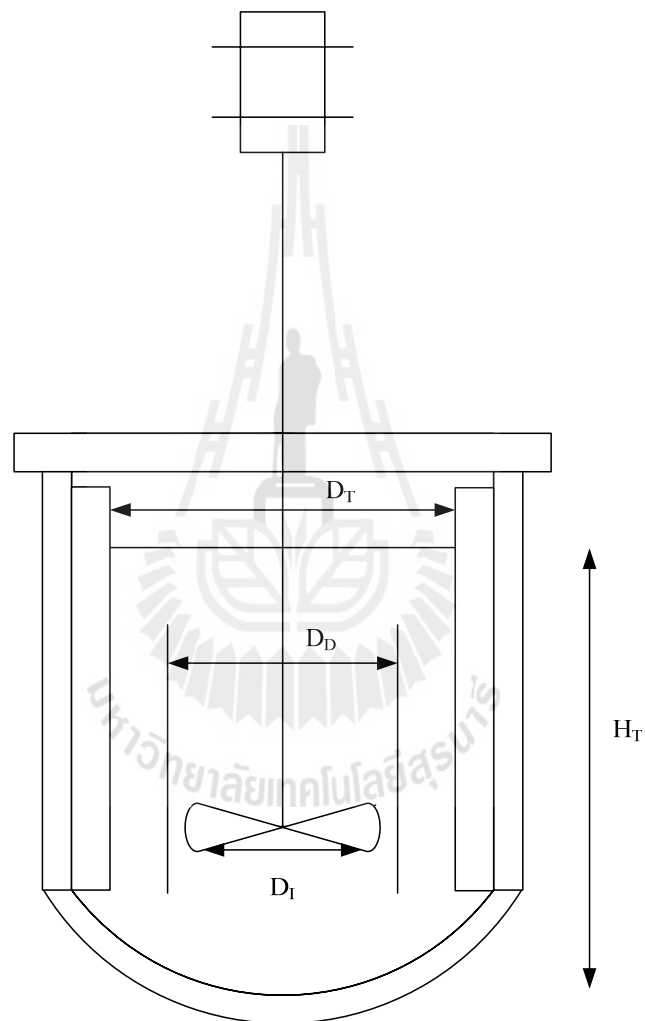


Figure 3.11 Schematic diagram of the crystallizer for scale up study.

3.3.5 Determination of power input in the crystallizer and suspension properties

For each condition, we measured the torque of the impeller to calculate the power input. The schematic diagram of the torque measurement is shown in Figure 3.1. The torque measurement used a wireless rotary torque transducer with a maximum capacity range 0.5 N-m and has a digital monitor connected to computer. We can measure the torque inside the crystallizer in real time mode. The power input of each condition was calculated from the torque and impeller speed. We measured the torque of the impeller using a wireless torque transducer. Then the calculations were based on the equation below.

$$Power = Torque \times 2\pi \times n \quad (3.4)$$

where n is a rotational speed (revolutions per second). The unit of torque is Newton-meter (N.m) and the unit of power is Watt (W).

There are two suspension properties which we have to measure, the suspension viscosity and density. For the viscosity, we used a capillary tube viscometer, type Cannon-Fenske, which is routine for transparent liquids. The viscometer is a no. 25, Cannon-Fenske tube ($C = 0.00220225 \text{ mm}^2/\text{s}$) and the kinematic viscosity range is from 0.5 to 2 mm^2/s . The equation for the calculation of kinematic viscosity is

$$\nu = C * t \quad (3.5)$$

where ν = kinematic viscosity, mm^2/s

C = Calibration constant of the viscometer, $(\text{mm}^2/\text{s})/\text{s}$

t = Mean flow time, s

The dynamic viscosity can be calculated from

$$\eta = \nu * \rho * 10^{-3} \quad (3.6)$$

where η = dynamic viscosity, mPa.s

ρ = density, kg/m³, at the same temperature used for the determination of the kinematic viscosity

ν = kinematic viscosity, mm²/s

The solution density is measured using a density bottle of volume 50.898 cm³. The density was calculated from the equation below.

$$\rho = m / V \quad (3.7)$$

where ρ = density, kg/m³

m = mass of suspension, kg

V = volume of suspension, m³

3.4 Data analysis method and empirical modeling procedure

3.4.1 Determination of dimensionless groups

A method called dimensional analysis along with Buckingham's Pi Theorem is used to identify the dimensionless groups in this study. The first step of dimensional analysis is to identify all independent parameters for the study. The second step is to determine the number of basic dimensions involved. The next step is

to determine the number of dimensionless groups. Buckingham's Pi Theorem states that if there are n variables in a problem and these variables contain m primary dimensions (for example M, L, T) the equation relating all the variables will have $(n-m)$ dimensionless groups. There are 12 variables ($n = 12$) in this work. They are attrition rate (B), number of parent crystal per volume ($\#_p/V$), impeller speed (N), power input (P), diameter of impeller (D_I), density of solution (ρ_f), viscosity of solution (μ_f), suspension density (M_T), density of crystal (ρ_c), parent crystal size (L_P), draft tube diameter (D_D), and off-bottom clearance (C_{OB}). The number of primary dimensions is 4 ($m = 4$, number, mass, length, and time) so we will get 8 dimensionless groups as follows

1. Attrition number (N_{Att})

$$N_{Att} = \frac{B}{(\#_p/V) \cdot N} \quad (3.8)$$

2. Power number (N_P)

$$N_P = \frac{P}{N^3 D_I^5 \rho_f} \quad (3.9)$$

3. Reynolds number (N_{Re})

$$N_{Re} = \frac{D_I^2 N \rho_f}{\mu_f} \quad (3.10)$$

4. Suspension density and fluid density ratio (N_{SF})

$$N_{SF} = \frac{M_T}{\rho_f} \quad (3.11)$$

5. Crystal density and fluid density ratio (N_{CF})

$$N_{CF} = \frac{\rho_C}{\rho_f} \quad (3.12)$$

6. Parent crystal size and impeller diameter ratio (N_{LP})

$$N_{LP} = \frac{L_P}{D_I} \quad (3.13)$$

7. Draft tube impeller clearance and impeller diameter ratio (N_{DT})

$$N_{DT} = \frac{(D_D - D_I)}{D_I} \quad (3.14)$$

8. Off-bottom clearance and impeller diameter ratio (N_{OB})

$$N_{OB} = \frac{C_{OB}}{D_I} \quad (3.15)$$

From the dimensionless groups above, we can reduce the number of dimensionless groups by multiplying or dividing two dimensionless groups. In this study, we divided equation 3.11 by 3.12 and we get the new dimensionless group below.

9. Suspension density and crystal density ratio (N_{MT})

$$N_{M_T} = \frac{M_T}{\rho_C} \quad (3.16)$$

3.4.2 Determination of the empirical model

A simple power law model was chosen initially as the function between the output dimensionless group (N_{Att}) and the other groups. If this was found not to fit the data adequately then it is possible to find a new empirical function to fit the data using the same dimensionless groups.

$$N_{Att} = f(N_p, N_{Re}, N_{M_T}, N_{L_p}, N_{DT}, N_{OB}) \quad (3.17)$$

$$N_{Att} = aN_p^b N_{Re}^c N_{M_T}^d N_{L_p}^e N_{DT}^f N_{OB}^g \quad (3.18)$$

where a, b, c, d, e, f, and g are the parameters from curve fitting.

From a dimensional analysis of the variables expected to be significant in attrition it is expected that the following dimensionless groups should reflect the mechanism best; the Impeller Reynolds number (N_{Re}), which is varied in the current study by variations in impeller speed; the Power Number (N_p); the parent crystal size and impeller diameter ratio (N_{L_p}); the off-bottom clearance and impeller diameter ratio (N_{OB}); the impeller-draft tube clearance and impeller diameter ratio (N_{DT}); and the ratio of suspension density to crystal density (N_{MT}). The rate of attrition is characterized by the attrition number (N_{Att}), which is original (to the best knowledge of the authors). The experimental data will be fitted by a simple power law model to

get an empirical engineering model for the attrition number as shown in equation 3.18.



CHAPTER IV

RESULTS AND DISCUSSION

In this chapter, there are two main parts. The first section shows the experimental results, for example, the attrition fragment size distribution, SEM photographs of attrition fragments, number of attrition fragment per unit volume versus time, and attrition rate. From the information in the first part, we will know which are the significant parameters affecting attrition rate. Thus, we can select the suitable parameters for the empirical engineering model. The second part is the data analysis and modeling. In this part we show the dimensionless groups as a function of the significant parameters and the empirical engineering model for crystal attrition.

4.1 Attrition of sucrose crystal in a mixed-suspension crystallizer

The current section describes attrition of sucrose crystals in a small scale mixed suspension crystallizer, varying the following parameters: impeller diameter; draft tube diameter; impeller clearance; impeller speed; blade type; blade material; parent crystal size; suspension density; solution viscosity; and solution density. In all experiments it was found that the attrition fragments had a finite particle size distribution (PSD), and in particular had relatively wide PSDs. The fragments typically had geometric mean sizes in the order of 5 μm , and geometric standard

deviations of approximately 0.8-0.9. The initial rate of generation of attrition fragments was far higher than a latter rate of 'steady' attrition. This initial rate is presumably higher due to the sharp edges on the particles at the start of the experiment; after the edges becomes rounded the rate of attrition drops off significantly, but then stays at a constant rate for the remainder of the batch run. The most parameters varied during the study had a strong effect on the attrition rate, and some parameters also had a significant effect on the PSD of the attrition fragments.

4.1.1 Parent crystal and attrition fragment size distribution

In each experiment the number of attrition fragments was measured as a function of time, based on the output from the Malvern Mastersizer S, the measured suspension density of fragments, and equations (3.1) – (3.3). The PSD of the attrition fragments was essentially constant with respect to time during the experiments indicating that the attrition only occurred to the parent crystals added to the vessel (not occurring again to fragments) and that the mechanism was maintained throughout the process. Average sizes over time and in triplicate experiments did vary slightly but randomly, and values were taken as averages of the nine PSDs; triplicate experiments over three time periods. The example of attrition fragment size distribution is shown in Figure 4.1. The number of attrition fragments vs. time is shown in Figure 4.2.

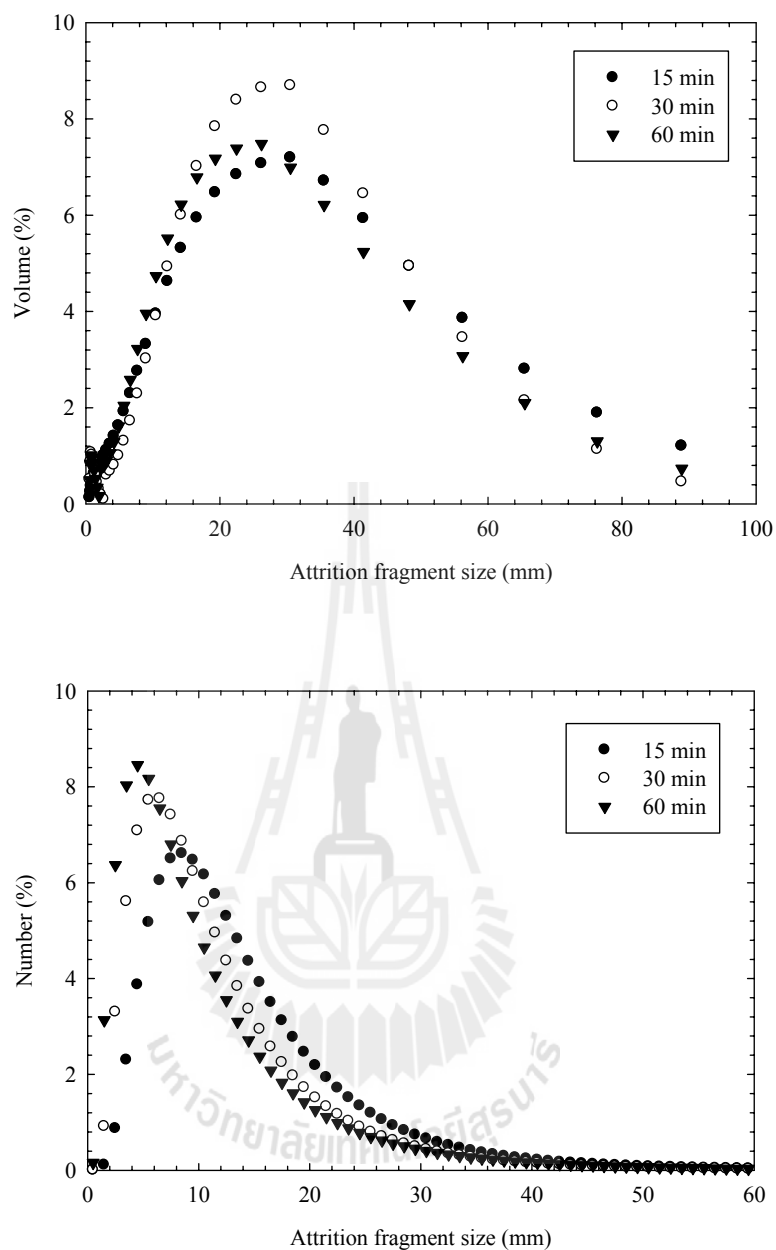


Figure 4.1 Changes in the volume-based and number-based particle size distribution for a sample taken from the 500 mL batch crystallizer. (Saturated solution of sucrose in methanol; 425 - 600 μm NaCl parent crystals; suspension density 0.1 g/mL; stainless steel marine upflow impeller; impeller speed 1200 rpm; crystallizer diameter 90 mm; draft tube diameter 64 mm; impeller diameter 50 mm; off-bottom clearance 10 mm)

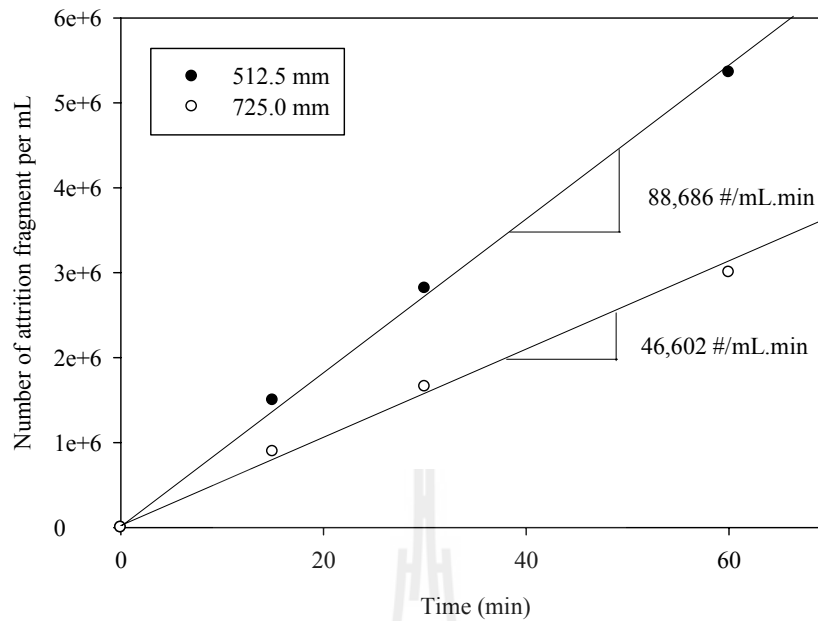


Figure 4.2 Number of attrition fragments as a function of time for calculation of attrition rate. (Saturated solution of sucrose in methanol; 425 – 600 and 600 - 850 μm NaCl parent crystals; suspension density 0.1 g/mL; stainless steel marine upflow impeller; impeller speed 1000 rpm; crystallizer diameter 90 mm; draft tube diameter 64 mm; impeller diameter 50 mm; off-bottom clearance 10 mm)

Although the size of the fragments produced is constant during an experiment under a particular set of conditions, it varies strongly depending on the condition being investigated, which makes the system more difficult to analyze in terms of the attrition rate. For a particular volume rate of production of attrition fragments the number rate of attrition varies strongly with the size of the fragments produced. Figure 4.3 shows the average size of fragments at standard conditions in the crystallizer as the impeller speed is increased from 800 to 1200 rpm. Higher agitation rates (and therefore higher power inputs) clearly produce larger attrition fragments.

Figure 4.4 shows how the suspension density of the attrition fragments (on the basis of volume fragments per suspension volume) increases over the course of an experiment, for the conditions shown in Figure 4.3. Although the increase in the suspension density at 1200 rpm occurs at a higher rate than at the lower stirrer speeds, the average particle size (and also the value of $L_{3,0}$ for the fragments) is also much higher. These effects balance each other out to some extent when the number rate of attrition is calculated from the data.

After analyzing data from the Malvern Mastersizer S, we observed the parent crystal and attrition fragments with SEM photograph to confirm their shape and size. The SEM photographs of the attrition fragments and parent crystals are shown in Figure 4.5 and Figure 4.6 respectively. The size of parent crystal did not change very much. It only lost mass from the surface, edges and corners. This result confirms that the mechanism of secondary nucleation occurring in the system is attrition, because if breakage occurs the parent crystal size will reduce significantly, and the size of fragments will be larger than 50 μm . However, Figure 4.6 shows that the size of the attrition fragments is very small, around 1 to 10 μm .

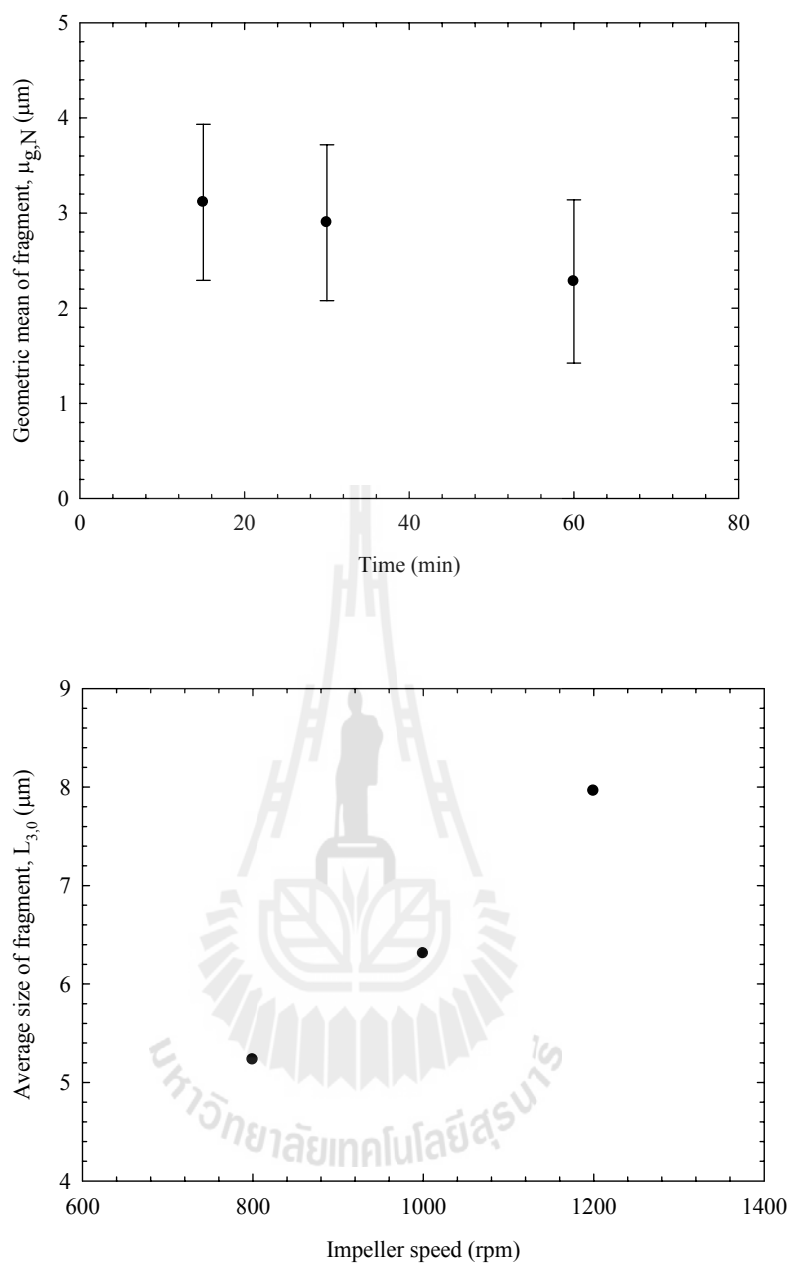


Figure 4.3 Attrition fragment geometric mean versus time and average size as a function of impeller speed. (Saturated solution of sucrose in methanol; 425 – 600 μm NaCl parent crystals; suspension density 0.1 g/mL; stainless steel marine upflow impeller; impeller speed 800, 1000, 1200 rpm; crystallizer diameter 90 mm; draft tube diameter 64 mm; impeller diameter 50 mm; off-bottom clearance 10 mm)

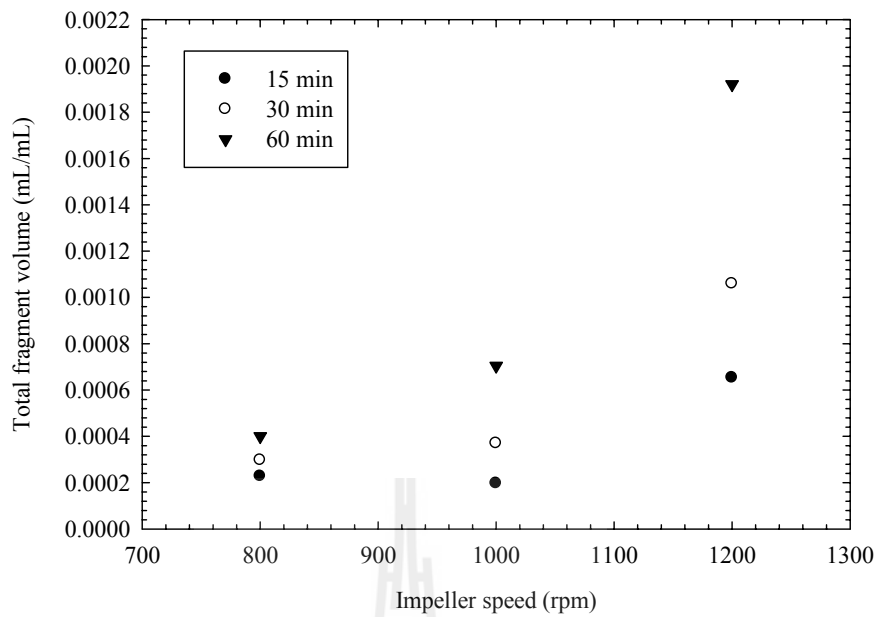
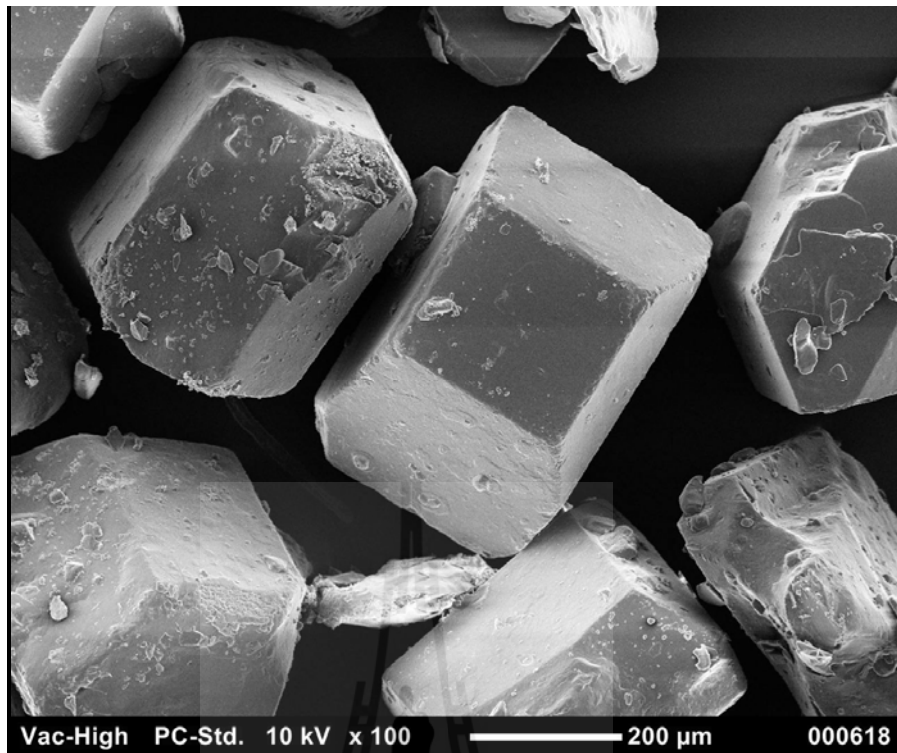
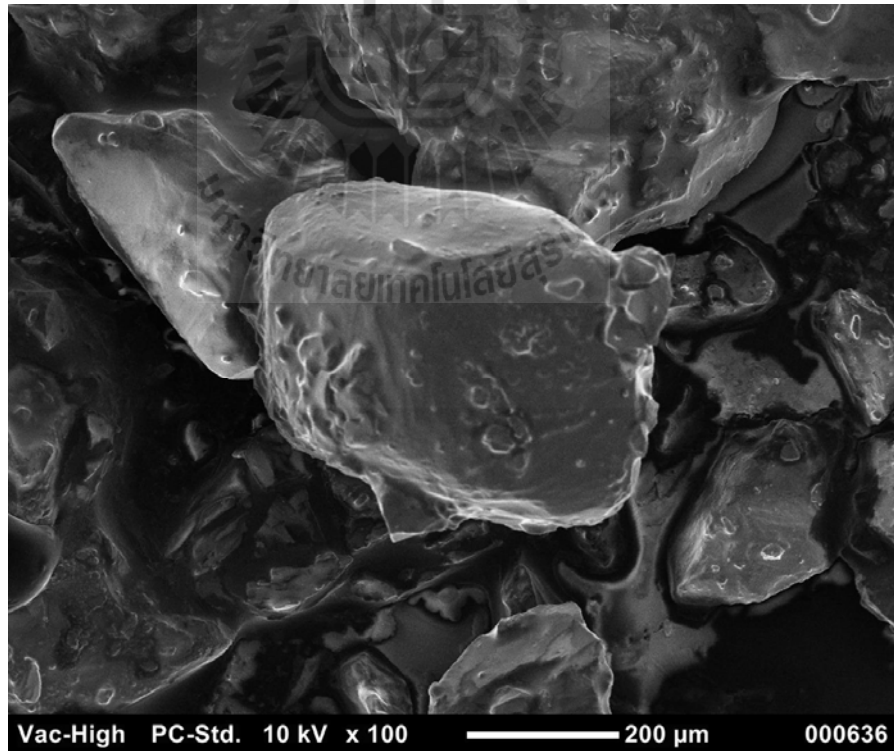


Figure 4.4 Rate of increase in fragment volume per mL suspension. (Saturated solution of sucrose in methanol; 425 – 600 μm NaCl parent crystals; suspension density 0.1 g/mL; stainless steel marine upflow impeller; impeller speed 800, 1000, 1200 rpm; crystallizer diameter 90 mm; draft tube diameter 64 mm; impeller diameter 50 mm; off-bottom clearance 10 mm)



a) Parent crystals before the experiment



b) Parent crystals after the experiment

Figure 4.5 Parent crystals of sucrose; size range 300 – 425 μm.

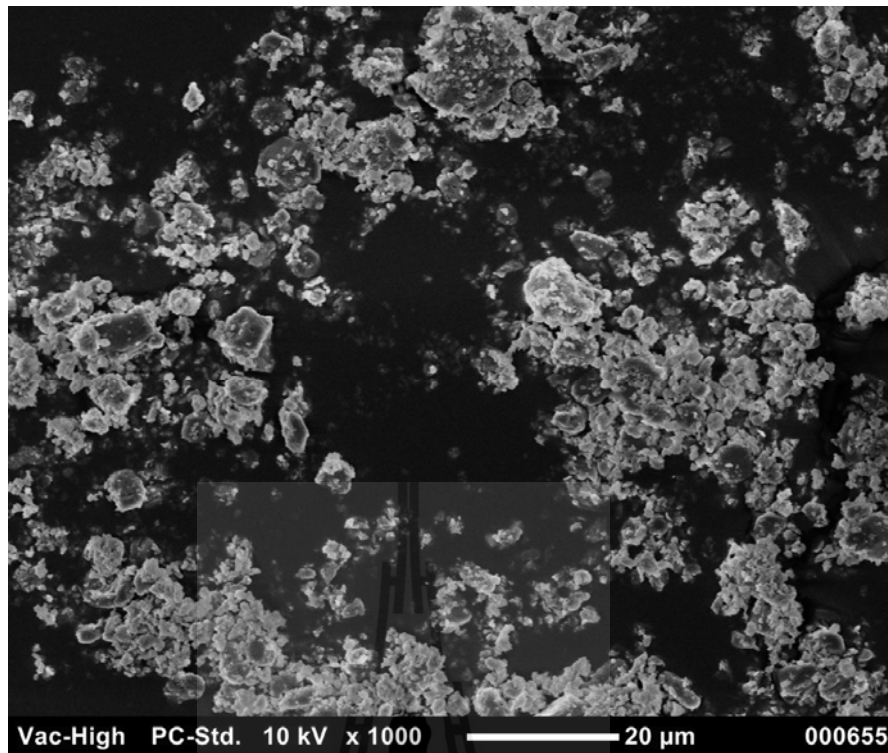


Figure 4.6 Attrition fragment of sucrose for a sample taken from the 500 mL batch crystallizer. (Saturated solution of sucrose in methanol; 300-425 μm parent crystals; suspension density 0.1 g/mL; stainless steel marine upflow impeller; impeller speed 1000 rpm; crystallizer diameter 90 mm; draft tube diameter 64 mm; impeller diameter 50 mm; off-bottom clearance 10 mm)

4.1.2 Effect of impeller speed on attrition rate

The effect of the impeller speed on the attrition rate (at standard conditions) is shown in Figure 4.7. It is clear that the increased volume rate of production of the attrition fragments more than compensates for the increased size of the attrition fragments at higher speeds, and thus the number based attrition rate increases as the impeller speed increases.

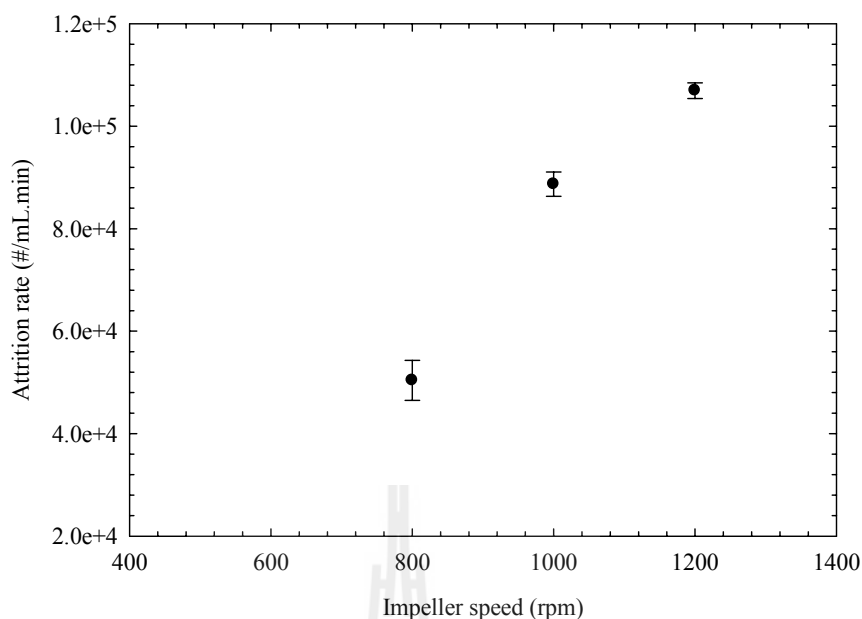


Figure 4.7 Attrition rate as a function of impeller speed at standard conditions.

(Saturated solution of sucrose in methanol; 425 - 600 μm parent crystals; suspension density 0.1 g/mL; stainless steel marine upflow impeller; impeller speed 1000 rpm; crystallizer diameter 90 mm; draft tube diameter 64 mm; impeller diameter 50 mm; off-bottom clearance 10 mm)

4.1.3 Effect of parent crystal size on attrition rate

Figure 4.8 shows the attrition rate as a function of the size of the parent crystals used in the experiment. Although it is expected that the larger parent crystals are more likely to impact the impeller because they have more momentum than the small crystals, and therefore more likely to undergo attrition, it was found that smaller parent crystals resulted in higher attrition rates at a particular suspension density of parent crystals. This is due to the much larger *number* of the smaller parent crystals

compared to the larger parent crystals at a constant value of the suspension density (in this case 10%).

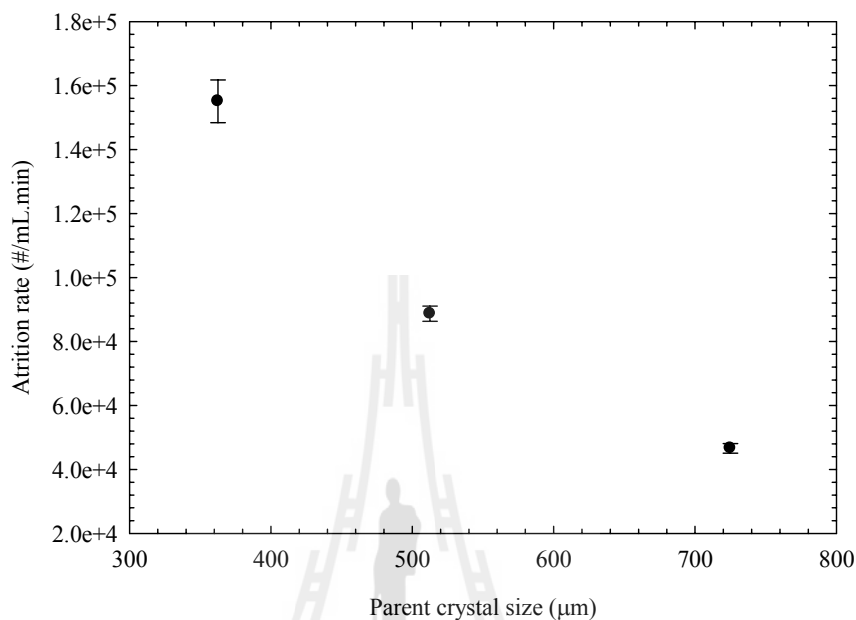


Figure 4.8 Attrition rate as a function of parent crystal size at standard conditions.

(Saturated solution of sucrose in methanol; 300 – 425, 425 – 600, 600 - 850 μm parent crystals; suspension density 0.1 g/mL; stainless steel marine upflow impeller; impeller speed 1000 rpm; crystallizer diameter 90 mm; draft tube diameter 64 mm; impeller diameter 50 mm; off-bottom clearance 10 mm)

4.1.4 Effect of suspension density on attrition rate

The attrition rate as a function of suspension density is shown in Figure 4.9. The increase in suspension density had a larger than anticipated effect on the rate of production of attrition fragments; much larger than the 50% increase anticipated from the relative magnitudes of the number of parent crystals. It is likely that this

increased effect is due to a much larger number of crystal-crystal interactions in the zone of the impeller.

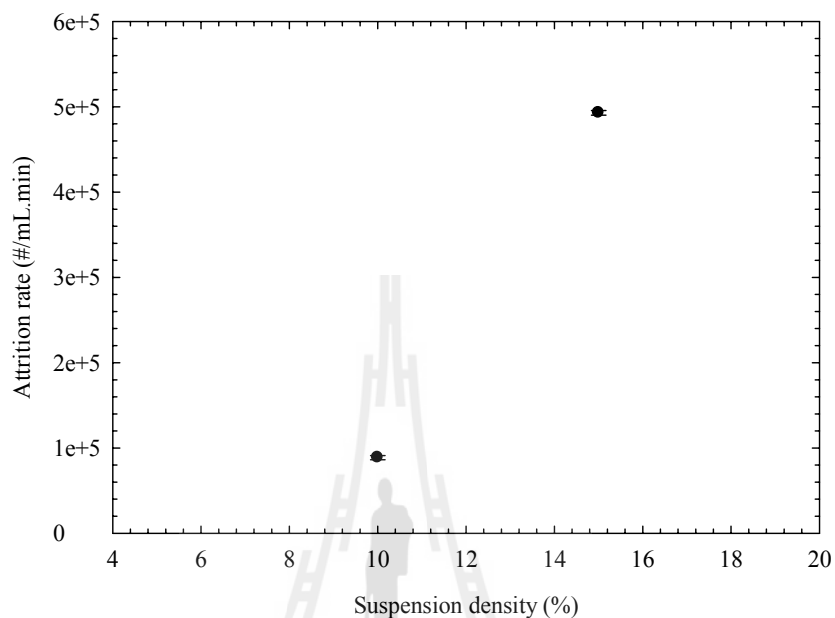


Figure 4.9 Attrition rate as a function of suspension density at standard conditions.

(Saturated solution of sucrose in methanol; 425 – 600 μm parent crystals; suspension density 0.1 and 0.15 g/mL; stainless steel marine upflow impeller; impeller speed 1000 rpm; crystallizer diameter 90 mm; draft tube diameter 64 mm; impeller diameter 50 mm; off-bottom clearance 10 mm)

4.1.5 Effect of impeller material on attrition rate

As anticipated, the material of construction of the impeller had a significant effect on the rate of fragment generation (Figure 4.10), although this effect may be difficult to include in a general model, as it seems unlikely to be entirely due to the differences in hardness of the two materials. The resin material gave smaller

average size of attrition fragment compared to stainless steel impeller so the number of attrition fragment is higher than the number from stainless steel material.

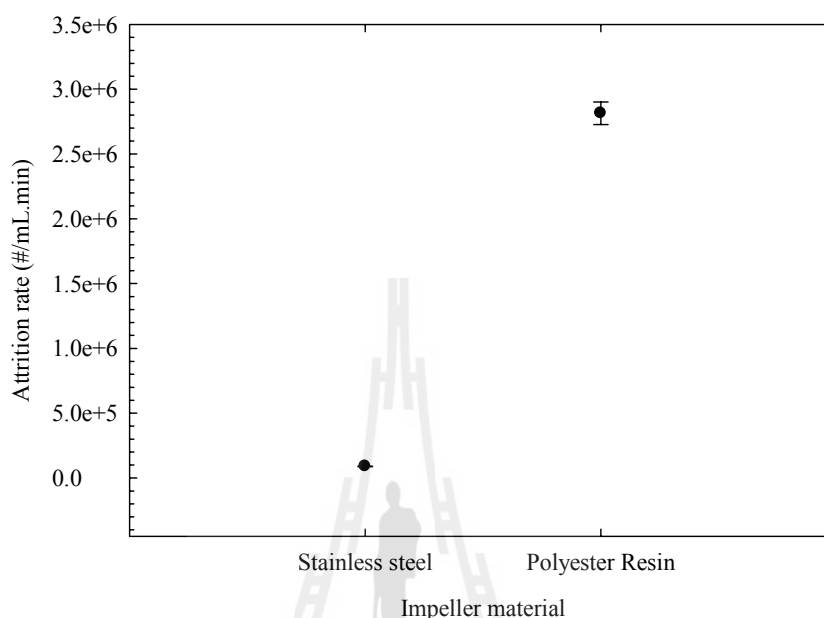


Figure 4.10 Attrition rate as a function of impeller material at standard conditions.

(Saturated solution of sucrose in methanol; 425 – 600 μm parent crystals; suspension density 0.1 g/mL; stainless steel and resin marine upflow impeller; impeller speed 1000 rpm; crystallizer diameter 90 mm; draft tube diameter 64 mm; impeller diameter 50 mm; off-bottom clearance 10 mm)

4.1.6 Effect of impeller type on attrition rate

Figure 4.11 and Figure 4.12 show the effect of the impeller speed on the attrition rate for a marine impeller and a pitch blade impeller respectively. In both cases the attrition rate increases strongly with the impeller speed, however the effect of the impeller speed is far more pronounced for the pitch blade impeller. The pitch

blade has 4 blades so it can contact with the parent crystals more than marine propeller. This characteristic also produces difficulty for an entirely general model for the system.

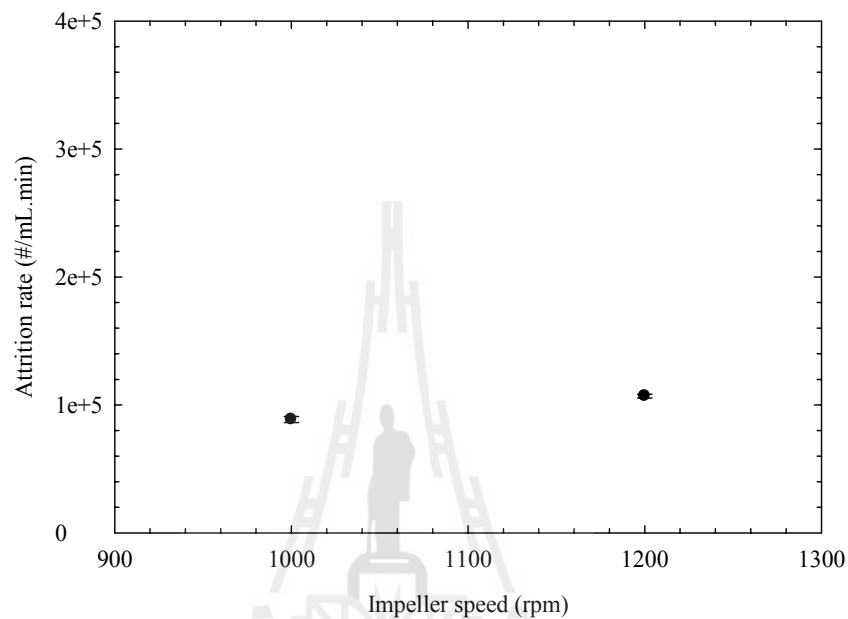


Figure 4.11 Attrition rate as a function of impeller speed for the marine impeller.

(Saturated solution of sucrose in methanol; 425 – 600 μm parent crystals; suspension density 0.1 g/mL; stainless steel marine upflow impeller; impeller speed 1000 and 1200 rpm; crystallizer diameter 90 mm; draft tube diameter 64 mm; impeller diameter 50 mm; off-bottom clearance 10 mm)

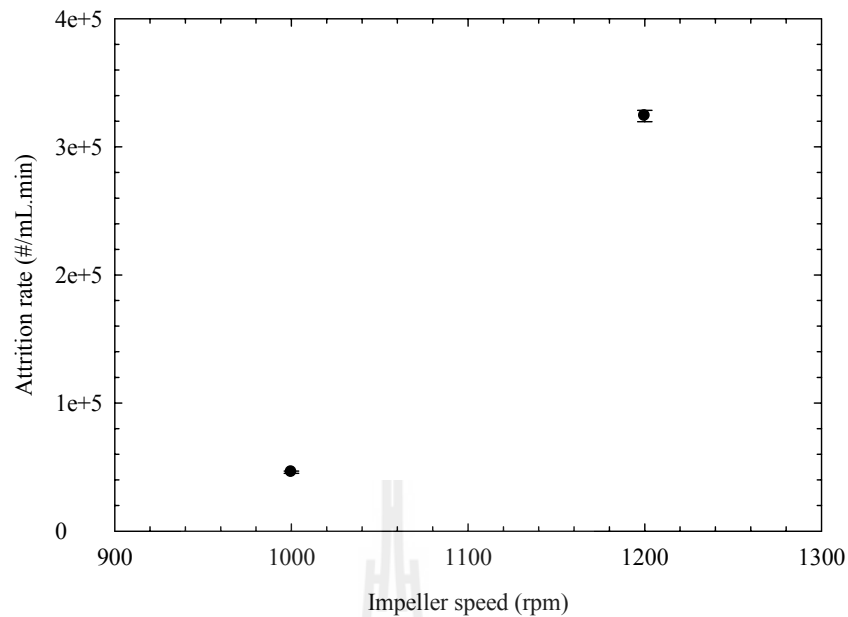


Figure 4.12 Attrition rate as a function of impeller speed for pitch blade impeller.

(Saturated solution of sucrose in methanol; 425 – 600 μm parent crystals; suspension density 0.1 g/mL; stainless steel pitch blade upflow impeller; impeller speed 1000 and 1200 rpm; crystallizer diameter 90 mm; draft tube diameter 64 mm; impeller diameter 50 mm; off-bottom clearance 10 mm)

4.1.7 Effect of impeller and draft tube clearance on attrition rate

Figure 4.13 shows the effect of the impeller and draft tube clearance on the attrition rate for the standard conditions. The attrition rate decreases strongly as the diameter of the draft tube increases with respect to the impeller diameter. This is presumably due to the added clearance between the impeller tip and the draft tube, allowing more parent crystals to avoid contact with the impeller.

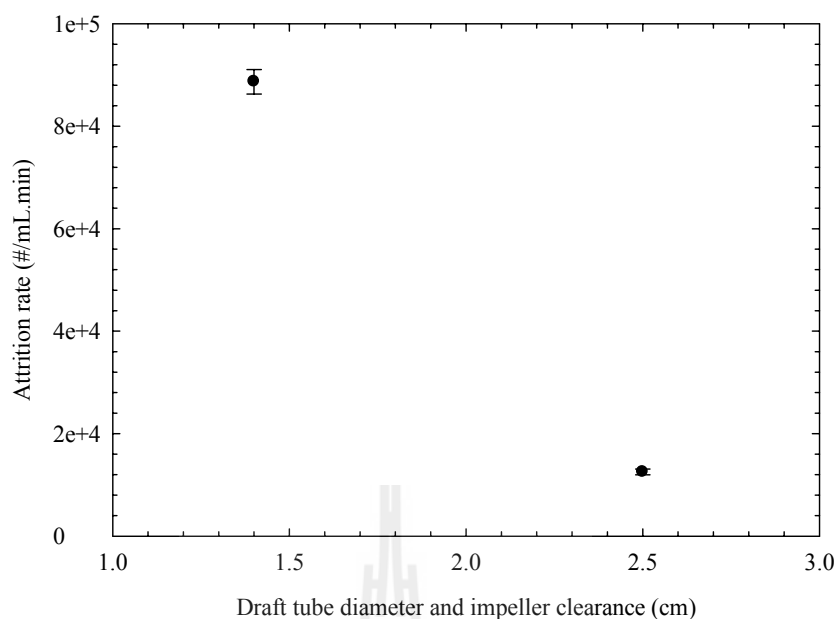


Figure 4.13 Attrition rate as a function of draft tube diameter and impeller clearance at standard conditions. (Saturated solution of sucrose in methanol; 425 – 600 μm parent crystals; suspension density 0.1 g/mL; stainless steel pitch blade upflow impeller; impeller speed 1000 rpm; crystallizer diameter 90 mm; draft tube diameter 64 and 75 mm; impeller diameter 50 mm; off-bottom clearance 10 mm)

4.1.8 Effect of off-bottom impeller clearance on attrition rate

Figure 4.14 shows the effect of the off-bottom impeller clearance. An increase in the off-bottom clearance for the impeller also greatly reduces the attrition rate, presumably also because increased clearance allows for a greater proportion of parent crystals to escape contact with the impeller.

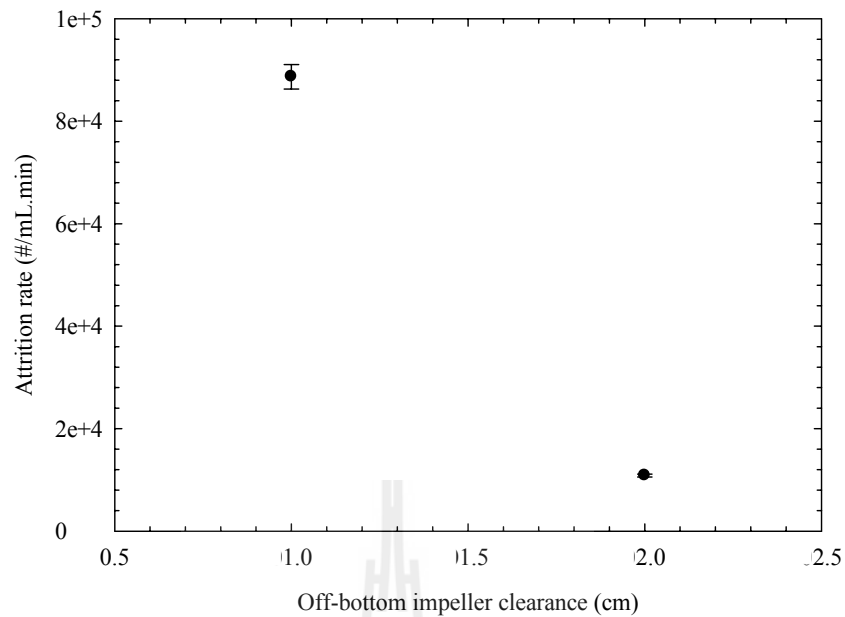


Figure 4.14 Attrition rate as a function of off-bottom impeller clearance at standard conditions. (Saturated solution of sucrose in methanol; 425 – 600 μm parent crystals; suspension density 0.1 g/mL; stainless steel pitch blade upflow impeller; impeller speed 1000 rpm; crystallizer diameter 90 mm; draft tube diameter 64 mm; impeller diameter 50 mm; off-bottom clearance 10 and 20 mm)

Although increased clearance between the impeller and the wall of the draft tube, and increased clearance between the impeller and the crystallizer vessel wall (at the base of the crystallizer) improves the performance of the crystallizer with respect to attrition, it is not possible to allow these parameters to take on any value. These parameters will also have a strong effect on the efficiency of mixing in the crystallizer, and also on the ability of the impeller to fully suspend the particles in the vessel. There is almost certainly a trade-off between improved design with respect to attrition, and improved design with respect to solution and suspension flow within the

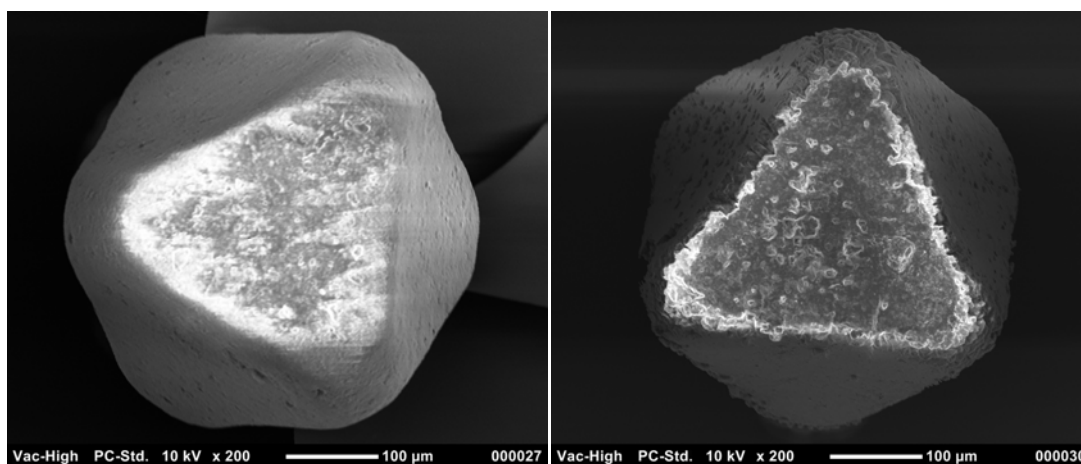
crystallizer. CFD studies are likely to enable a better understanding of this trade-off, and overall optimum values for clearance and draft tube diameter.

4.2 Attrition of Sodium Chloride crystals in mixed suspension crystallizers

Similar to previous section (sucrose results), in this section the results of NaCl crystal attrition experiments will be presented. Firstly, parent crystal and attrition fragment size distribution will be shown. Secondly, the effect of parameters affecting attrition rates will be presented; the experimental condition (for instance the impeller speed) and suspension properties; the geometry of the crystallizer (off-bottom clearances, draft tube diameter, impeller material, and impeller type), and the properties of the crystals.

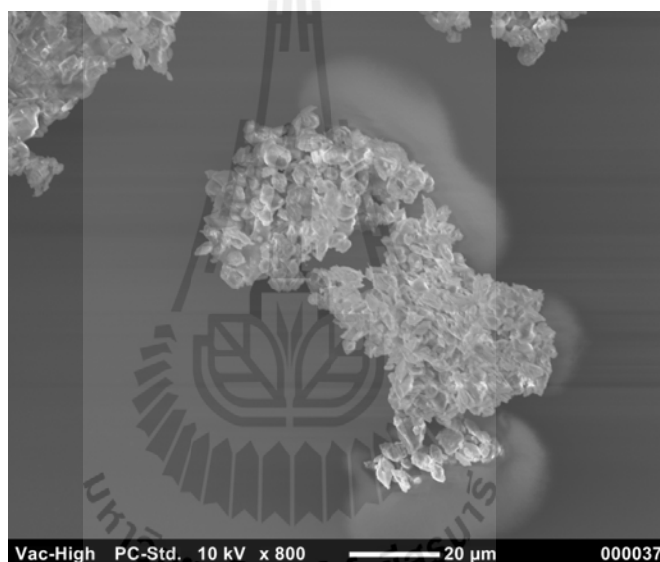
4.2.1 Parent crystal and attrition fragment size distribution

Figure 4.15 shows the SEM photographs of parent crystals and attrition fragments from NaCl experiments. If we consider the parent crystal, we will see the loss of mass of the parent crystal from edges, corner and surfaces. The sizes of parent crystals are quite similar before and after the experiment. Therefore the main mechanism of the secondary nucleation is attrition. The size of attrition fragment is around 1 to 10 micrometers which confirms that the mechanism occurs in the crystallizer is attrition more than fragmentation or breakage. If breakage occurs the size of the parent crystal will be decrease significantly or the parent crystal will disappear and the size of attrition fragment will be very large (larger than 50 μm).



a) Before

b) After



c) Attrition fragments

Figure 4.15 SEM photographs of parent crystals before and after the experiment and attrition fragments. (Slightly supersaturated solution of NaCl in 80% methanol; 300 - 425 μm NaCl parent crystals; suspension density 0.1 g/mL; stainless steel marine upflow impeller; impeller speed 1000 rpm; crystallizer diameter 90 mm; draft tube diameter 64 mm; impeller diameter 50 mm; off-bottom clearance 10 mm)

4.2.2 The effect of impeller speed on attrition rate

The effect of the impeller speed on the attrition rate is shown in Figure 4.16. As the impeller speed increase the attrition rate increase. This is because at higher impeller speeds it makes more sweeps of impeller region per second therefore the parent crystals are more likely to contact with the impeller blade. The attrition fragments were produced from contact between parent crystals and crystallizer parts or other crystals. So if we have more contacts at higher impeller speeds, we will get higher attrition rates. After 1000 rpm, the result shows attrition rate stops increasing may be because extra turbulence helps the particles avoid contact with the impeller or the source of attrition fragment (parent crystal edges or corners) is already used so the parent crystals are rounded. If we increase the impeller speed, it does not increase the attrition rate.

4.2.3 The effect of parent crystal size on attrition rate

The effect of parent crystal size is shown in Figure 4.17. The attrition rate sharply decreases as the parent crystal size increases from the 150-300 μm particles to the 300-425 μm particles, and then sharply increases again as the parent particle increase up to 425-600 μm . The reason for the initial decrease is due to the decreasing number of parent crystals as the average particle size is increased at constant suspension density. As the parent crystal size increases further the number of parent crystals continues to decrease, hence the increase in the attrition rate must be due to higher numbers of impeller crystal contacts (perhaps the larger crystals do not follow fluid streamlines as well as the smaller crystals and hence have a higher probability of colliding with an impeller blade rather than passing around it with the

fluid streamlines. It may also be due to the increased momentum of the contacts when the parent crystals are larger.

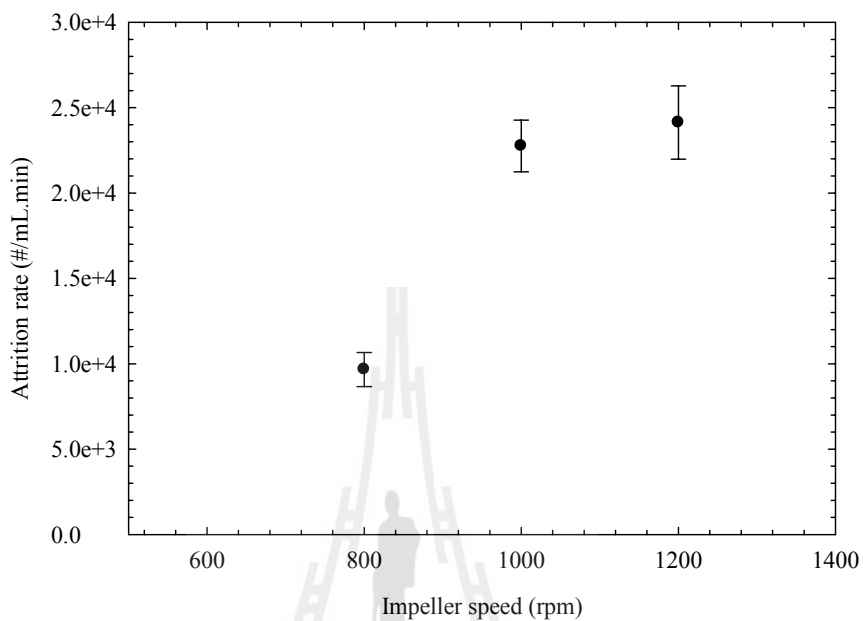


Figure 4.16 The attrition rate as a function of impeller speed. (Slightly supersaturated solution of NaCl in 80% methanol; 300-425 μm NaCl parent crystals; suspension density 0.10 g/mL; stainless steel marine upflow impeller; impeller speed 800, 1000, 1200 rpm; crystallizer diameter 90 mm; draft tube diameter 64 mm; impeller diameter 50 mm; off-bottom clearance 10 mm)

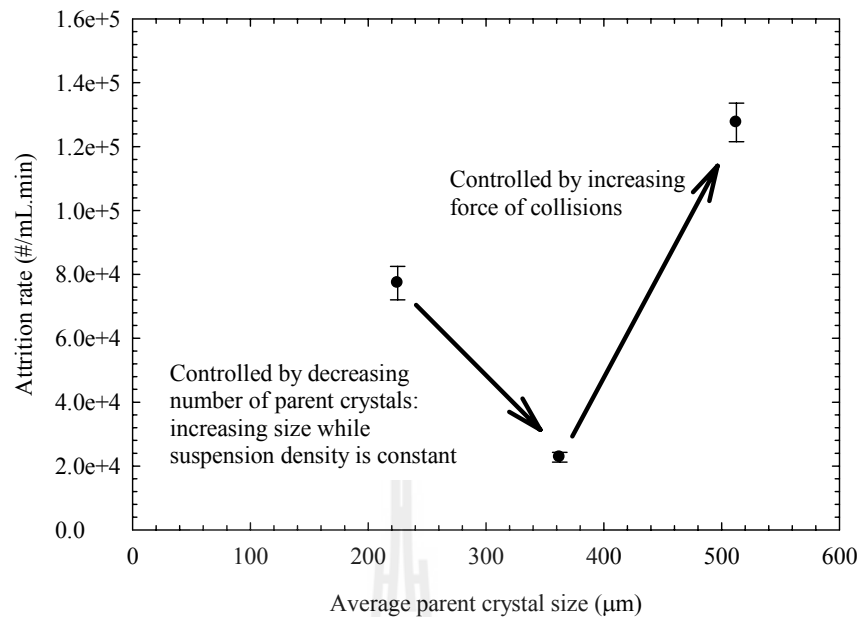


Figure 4.17 The attrition rate as a function of parent crystal size. (Slightly supersaturated solution of NaCl in 80% methanol; 150 – 300, 300-425, 425 - 600 μm NaCl parent crystals; suspension density 0.10 g/mL; stainless steel marine upflow impeller; impeller speed 1000 rpm; crystallizer diameter 90 mm; draft tube diameter 64 mm; impeller diameter 50 mm; off-bottom clearance 10 mm)

4.2.4 The effect of suspension density on attrition rate

Figure 4.18 shows the attrition rate as a function of the suspension density used in the experiment. When the suspension density increases (at constant levels of the other variables) the number of crystals in the system rises proportionally. The attrition rate increases because there are a higher number of contacts between parent crystals and the impeller or other crystallizer parts. These results agree with other investigators because the most models for secondary nucleation are consisted of suspension density (Grootscholten et al., 1982, Ottents et al., 1972, Ottens and De

Jong, 1973, Ó Meadhra et al., 1996, van Der Heijden et al., 1994, and Reeves and Hill, 2012).

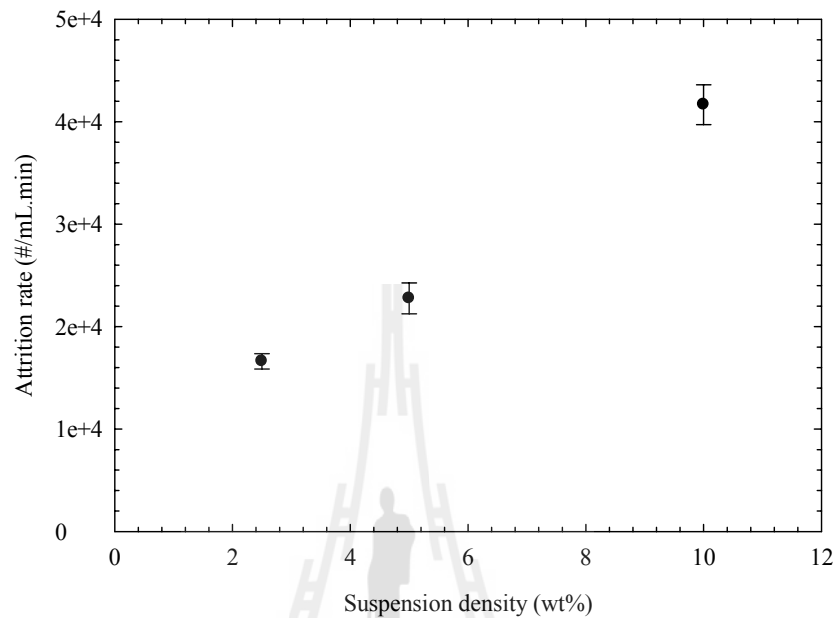


Figure 4.18 The attrition rate as a function of suspension density. (Slightly supersaturated solution of NaCl in 80% methanol; 300-425 μm NaCl parent crystals; suspension density 0.05, 0.10, and 0.15 g/mL; stainless steel marine upflow impeller; impeller speed 1000 rpm; crystallizer diameter 90 mm; draft tube diameter 64 mm; impeller diameter 50 mm; off-bottom clearance 10 mm)

4.2.5 The effect of draft tube impeller clearance on attrition rate

Figure 4.19 shows the effect of impeller-draft tube clearance on the attrition rate. The attrition rate decreases strongly as the impeller-draft tube clearance increases. This is due to the added clearance between the impeller tip and the draft tube, allowing more parent crystals to avoid contact with the impeller.

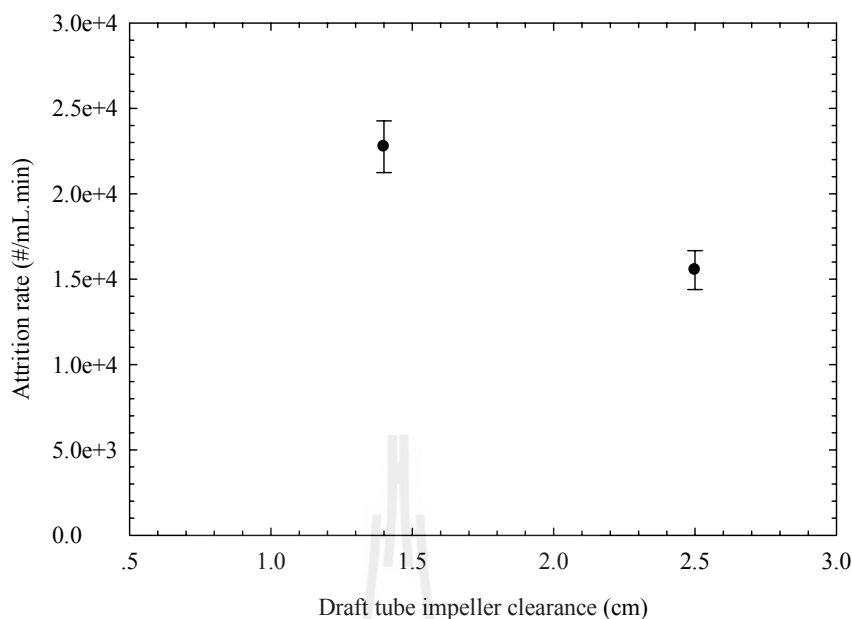


Figure 4.19 The attrition rate as a function of draft tube impeller clearance. (Slightly supersaturated solution of NaCl in 80% methanol; 300-425 μm NaCl parent crystals; suspension density 0.10 g/mL; stainless steel marine upflow impeller; impeller speed 1000 rpm; crystallizer diameter 90 mm; draft tube diameter 64 and 75 mm; impeller diameter 50 mm; off-bottom clearance 10 mm)

4.2.6 The effect of impeller type on attrition rate

The effect of impeller type is shown in Figure 4.20. Pitch blade impellers and marine propellers were chosen for the study. The result shows there is no significant effect of impeller type on attrition rate. The type of impeller has the effect on attrition rate in some literature (Ottens and De Jong, 1973). The attrition fragments are generated from contact between parent crystals and crystallizer parts so it means that the pitch blade impeller has a smaller contact area between crystal and

impeller than marine propeller, but marine and pitch blade impellers also have different flow patterns, so the flow pattern for marine propeller should force the particle to contact with impeller more than pitch blade. In this study the effect of the impeller type is very small so we will neglect this parameter from the model.

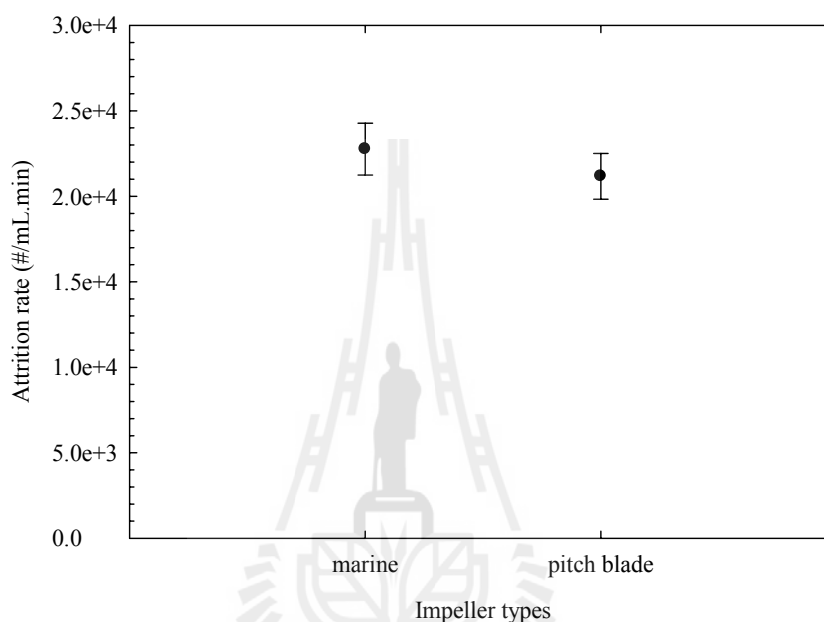


Figure 4.20 The attrition rate as a function of impeller type. (Slightly supersaturated solution of NaCl in 80% methanol; 300-425 μm NaCl parent crystals; suspension density 0.10 g/mL; stainless steel marine upflow impeller and pitch blade; impeller speed 1000 rpm; crystallizer diameter 90 mm; draft tube diameter 64 mm; impeller diameter 50 mm; off-bottom clearance 10 mm)

4.2.7 The effect of impeller material on attrition rate

Figure 4.21 is the effect of the impeller material on the attrition rate of NaCl crystals. The impeller made from resin gives a slightly higher average attrition

rate (22,821 #/mL.min) than stainless steel impeller (22,756 #/mL.min) but the standard errors are in the same region. In any case, it is difficult to include the material of impeller in an empirical model and the results show there is no significant effect so we will not add this parameter in the model.

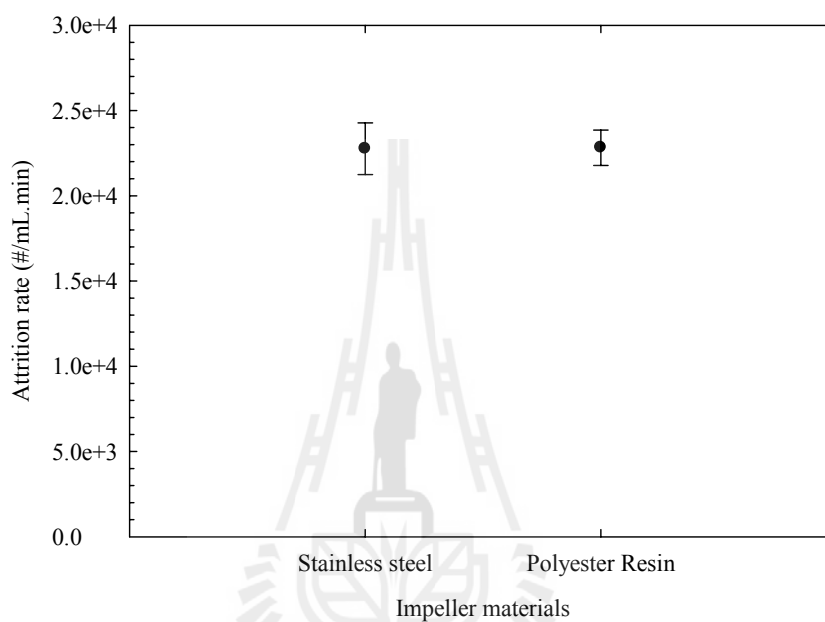


Figure 4.21 The attrition rate as a function of impeller material. (Slightly supersaturated solution of NaCl in 80% methanol; 300-425 μm NaCl parent crystals; suspension density 0.10 g/mL; stainless steel and resin marine upflow impeller; impeller speed 1000 rpm; crystallizer diameter 90 mm; draft tube diameter 64 mm; impeller diameter 50 mm; off-bottom clearance 10 mm)

4.2.8 The effect of off-bottom clearance on attrition rate

Figure 4.22 shows the effect of the off-bottom clearance on attrition rate of NaCl but from the figure there is no significant effect of off-bottom clearance

so we will not include this parameter in the attrition model. The reason that there is no effect of off-bottom clearance and impeller diameter ratio is the source of contact is the impeller if we move the impeller up or down in the draft tube it does not matter to the attrition rate and this result confirms that the suspension in the crystallizer is very good. In this study, the crystallizer is very small so it is difficult to vary this parameter more than two points.

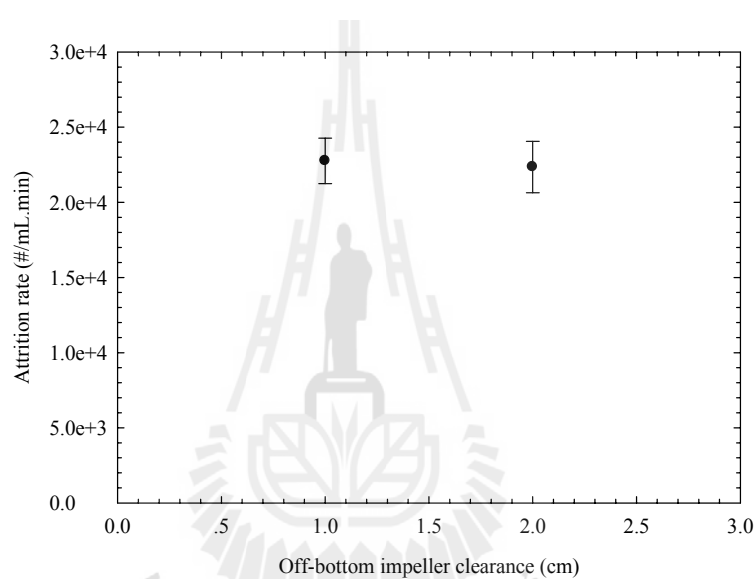


Figure 4.22 The attrition rate as a function of off-bottom clearance. (Slightly supersaturated solution of NaCl in 80% methanol; 300-425 μm NaCl parent crystals; suspension density 0.10 g/mL; stainless steel marine upflow impeller; impeller speed 1000 rpm; crystallizer diameter 90 mm; draft tube diameter 64 mm; impeller diameter 50 mm; off-bottom clearance 10 and 20 mm)

4.3 The effect of scale-up on attrition rate

This section is the study of scale-up effect on attrition rate, however we used a slightly different system in the study because this part of experiment was performed in Germany and we cannot find the same crystallizer that we used in Thailand. The details of the experimental method and condition are in section 3.3.4. The results of this study are divided into two parts. They are the effect of parent crystal size for the small scale crystallizer and the effect of parent crystal size for large scale crystallizer.

4.3.1 The effect of parent crystal size for small scale crystallizer

From Figure 4.23 the particle size distributions based on the volume of the attrition fragments varied from approximately 0.3 – 100 μm but higher parent crystal sizes show more than one peak. This effect makes the explanation of attrition fragment size distribution more complicated. If the larger attrition fragments and the small fragments agglomerate, there will be a loss of the small fragments in the system.

However, the first peaks of all distributions are in the same range so when the distribution was fitted by log-normal 3 parameters the mean size of attrition fragments are the same. Therefore, the size of parent crystals appears to have no effect on the size of attrition fragment based on number. The second peak of which the size is around 50 μm when the distribution is converted into a number distribution is negligible. The equation of log-normal 3 parameters for curve fitting is shown below.

$$y = a \exp \left[-0.5 \left(\frac{\ln x - \ln x_{g,V}}{\ln \sigma_g} \right)^2 \right] \quad (4.1)$$

where a is the constant, $x_{g,v}$ is the geometric mean of volume distribution, and σ_g is the geometric standard deviation

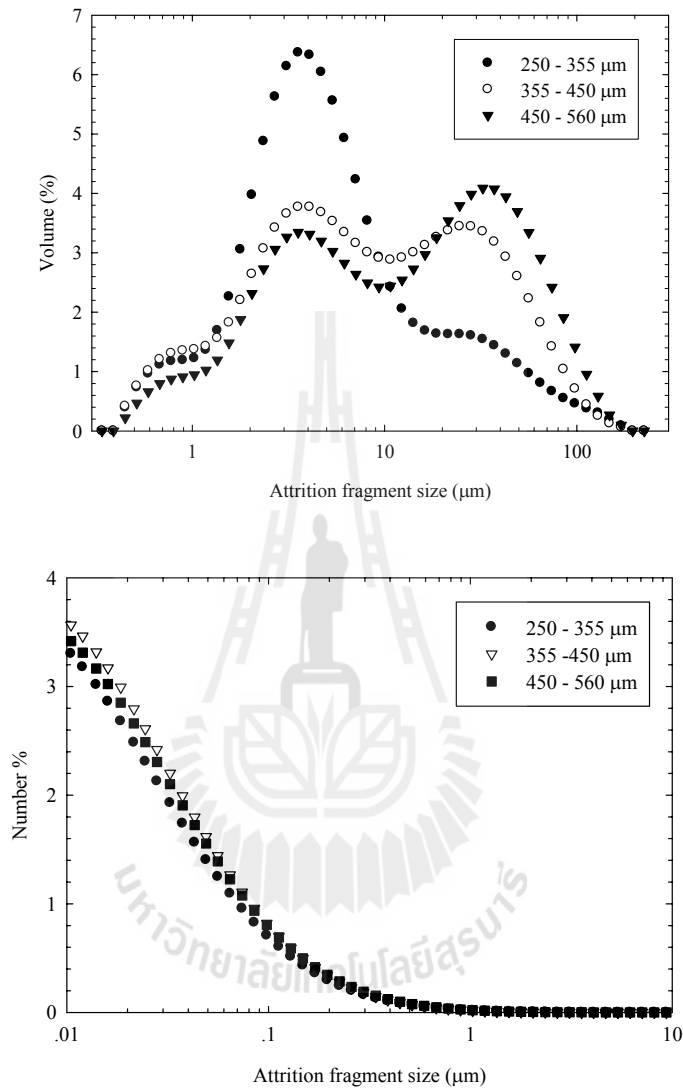


Figure 4.23 Attrition fragment size distribution for different the parent crystal size.

(Saturated solution of sucrose in methanol; 250 – 355, 355 – 450, 450 - 600 μm parent crystals; suspension density 0.1 g/mL; stainless steel marine impeller; impeller speed 1700 rpm; crystallizer diameter 80 mm; draft tube diameter 57 mm; impeller diameter 25 mm; off-bottom clearance 15 mm)

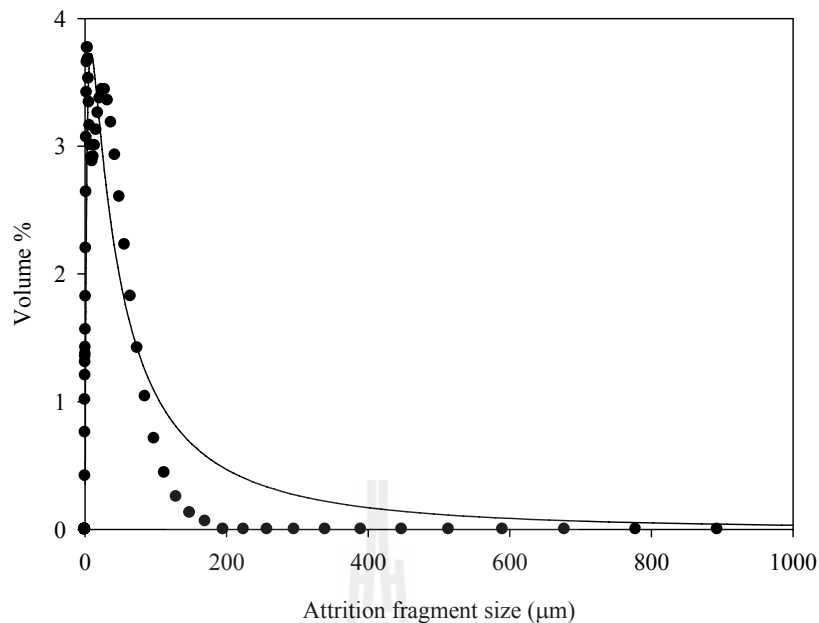


Figure 4.24 Illustration of log-normal 3 parameters fitting for volume distribution.

(Saturated solution of sucrose in methanol; 355 – 450 µm parent crystals; suspension density 0.1 g/mL; stainless steel marine impeller; impeller speed 1700 rpm; crystallizer diameter 80 mm; draft tube diameter 57 mm; impeller diameter 25 mm; off-bottom clearance 15 mm)

Figure 4.25 and Figure 4.26 show the normalized volume concentration and attrition rate, respectively. The calculation was normalized by parent crystal number because the experiments were performed with the same mass of parent crystals. The trends of both curves are quite similar. This confirms the size of the parent crystals has no effect on the size (based on number) of the attrition fragments. The normalized attrition rate increases with the parent crystal size because the mass of the individual crystals of bigger sizes is higher than the small parent crystals so they can produce higher numbers of attrition fragments.

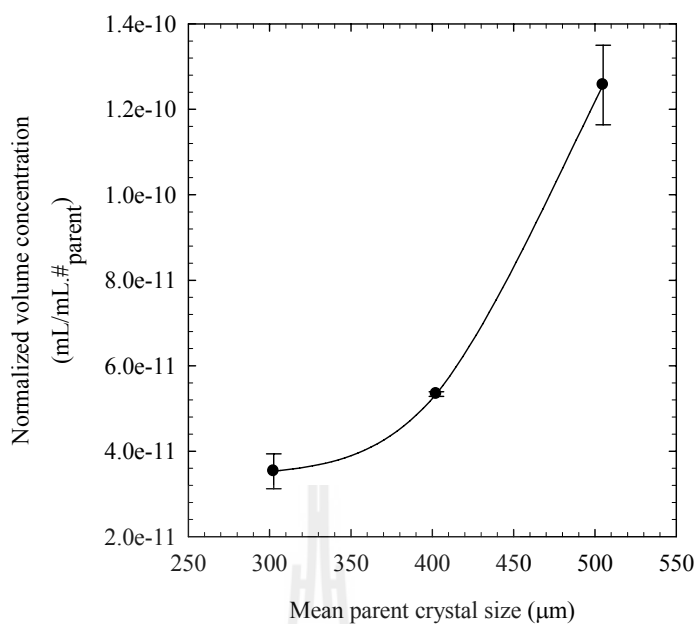


Figure 4.25 Normalized volume concentrations of attrition fragments as a function of parent crystal size for the small scale crystallizer. (Saturated solution of sucrose in methanol; 250 – 355, 355 – 450, 450 - 600 μm parent crystals; suspension density 0.1 g/mL; stainless steel marine impeller; impeller speed 1700 rpm; crystallizer diameter 80 mm; draft tube diameter 57 mm; impeller diameter 25 mm; off-bottom clearance 15 mm)

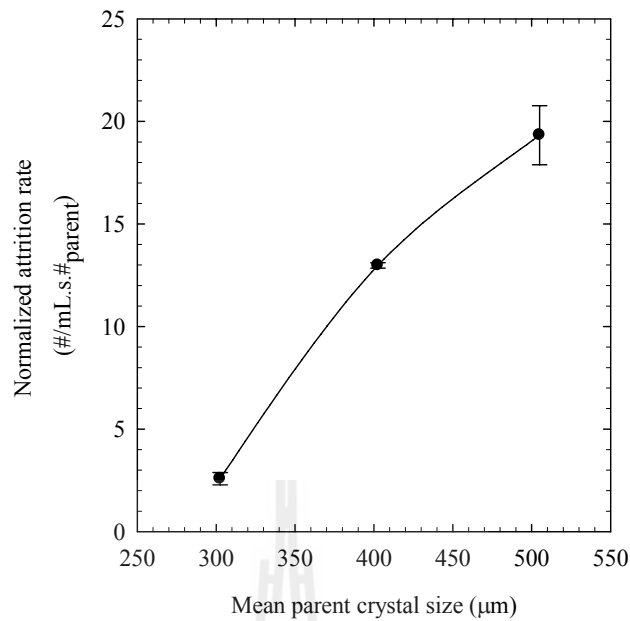


Figure 4.26 Normalized attrition rate per seed crystal as a function of parent crystal size for the small scale crystallizer. (Saturated solution of sucrose in methanol; 250 – 355, 355 – 450, 450 - 600 μm parent crystals; suspension density 0.1 g/mL; stainless steel marine impeller; impeller speed 1700 rpm; crystallizer diameter 80 mm; draft tube diameter 57 mm; impeller diameter 25 mm; off-bottom clearance 15 mm)

4.3.2 The effect of parent crystal size in case of the large scale crystallizer

Figure 4.27 shows the attrition fragment size distribution from the large scale crystallizer. The same size distributions of attrition fragments are produced. The small scale shows a different size distribution because there are two peaks for larger parent crystal sizes (Figure 4.23). The size distributions of attrition fragments show different trends which could be caused by agglomeration.

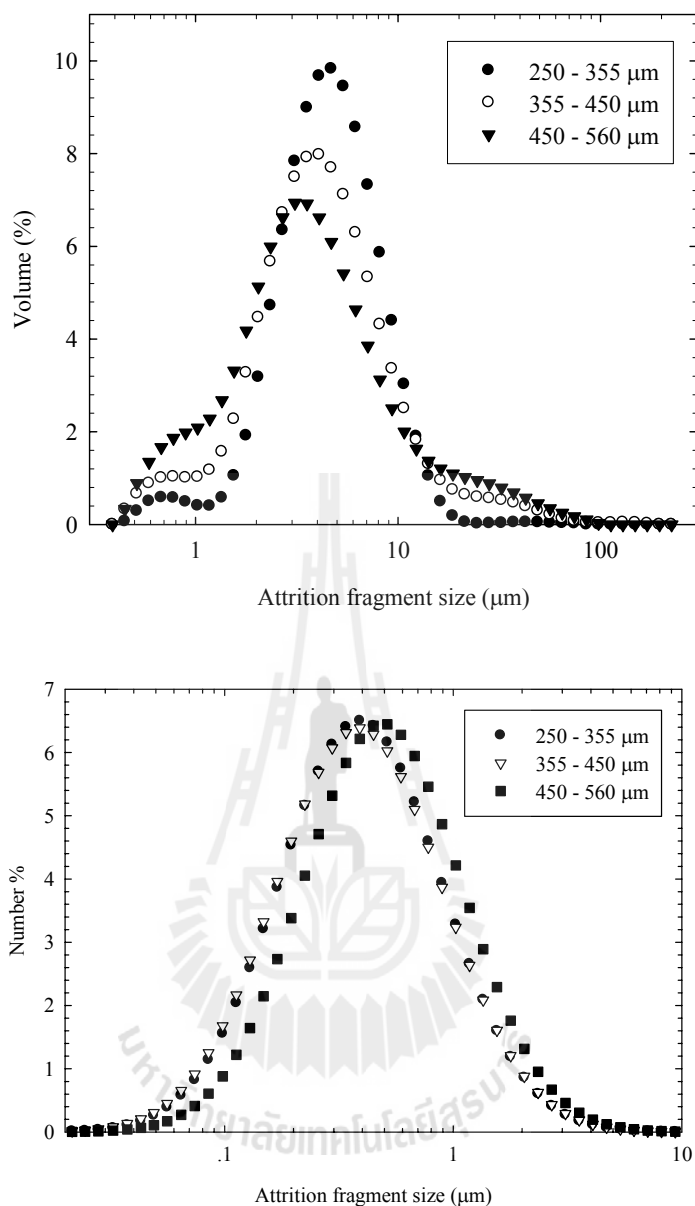


Figure 4.27 Size distribution of the attrition fragments for the large scale crystallizer.

(Saturated solution of sucrose in methanol; 250 – 355, 355 – 450, 450 - 600 μm parent crystals; suspension density 0.1 g/mL; stainless steel marine impeller; impeller speed 850 rpm; crystallizer diameter 100 mm; draft tube diameter 57 mm; impeller diameter 50 mm; off-bottom clearance 27 mm)

Figure 4.28 and 4.29 show the normalized volume concentration and attrition rate as a function of mean parent crystal size for large scale crystallizer, respectively. The calculation was normalized by parent crystal number because the experiments were performed with the same mass of parent crystals the same as small scale crystallizer. The trends of both curves are increase with parent crystal size increase. The normalized attrition rate increases with the parent crystal size because the mass of the individual crystals of bigger sizes is higher than the small parent crystals so they can produce higher numbers of attrition fragments.

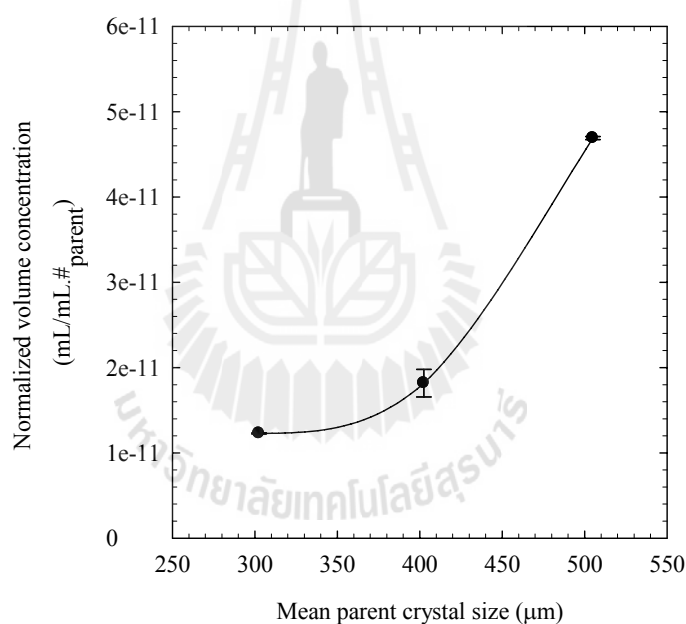


Figure 4.28 Normalized volume concentrations as a function of parent crystal size for the large scale crystallizer. (Saturated solution of sucrose in methanol; 250 – 355, 355 – 450, 450 - 600 μm parent crystals; suspension density 0.1 g/mL; stainless steel marine impeller; impeller speed 850 rpm; crystallizer diameter 100 mm; draft tube diameter 57 mm; impeller diameter 50 mm; off-bottom clearance 27 mm)

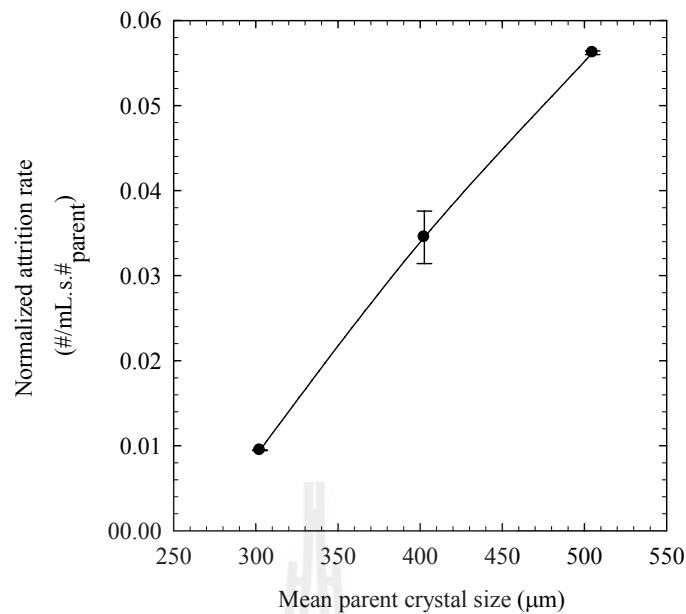


Figure 4.29 Normalized attrition rate as a function of parent crystal size for the large scale crystallizer. (Saturated solution of sucrose in methanol; 250 – 355, 355 – 450, 450 - 600 μm parent crystals; suspension density 0.1 g/mL; stainless steel marine impeller; impeller speed 850 rpm; crystallizer diameter 100 mm; draft tube diameter 57 mm; impeller diameter 50 mm; off-bottom clearance 27 mm)

The results of large and small scale show in principle the same results but are different in magnitude. The large scale has an attrition rate lower than that in the small scale. This is because the same sizes of parent crystals in the larger crystallizer have a reduced chance to hit the impeller or crystallizer parts. From the work of Vauck and Müller (1969), the volume flow rate inside the crystallizer can be calculated to compare the different phenomena between small scale and large scale. For this work the volume flow rate of small scale is 10,625 mL/min and the volume flow rate of large scale is 42,500 mL/min. When multiplied with the volume flow rate

of the experimental time per suspension volume, the result gives the chance of a parent crystal to hit the impeller which can be compared to the circulation time. The numbers of the volume flow rate multiplied by the experimental time per suspension volume ratio for small and large scale are 141.67 and 106.25, respectively. These non-dimension numbers of small and large scale show normalized volume flow rates with the experimental time and volume of the suspension. Thus, this data confirms the results of the attrition rates from both scales.

4.4 A study of power input and solution properties

The power input and solution properties are very important in this work because we need them to develop the empirical engineering model. The power input of each condition was calculated from the torque and impeller speed. The following results are the effect of varied parameters in this study on the torque. An example of a torque measurement result is shown in Figure 4.30.

4.4.1 Torque measurement for NaCl system

4.4.1.1 Effect of impeller speed

It is clear that when we increased the impeller speed the torque will increase. Figure 4.31 shows three results of three suspension properties, all of them show similar trends when impeller speed increase the torque increase.

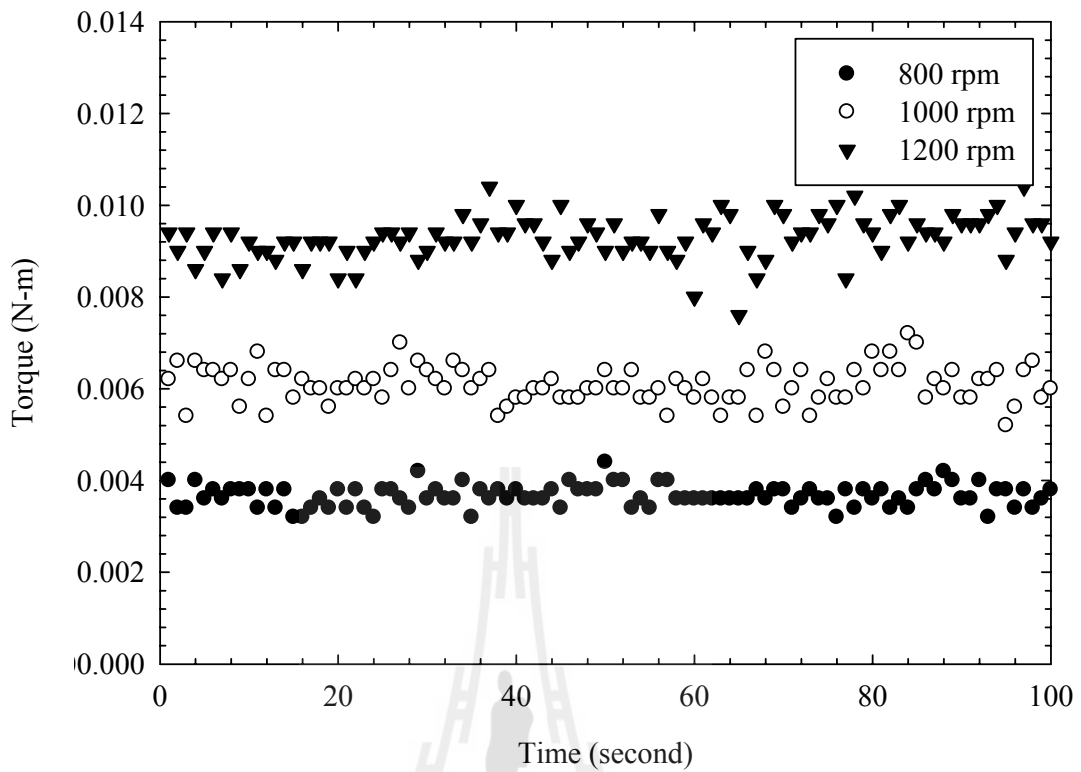


Figure 4.30 The relationship between torque and time for a standard condition.

(Slightly supersaturated solution of NaCl in 80% methanol; 300-425 μm NaCl parent crystals; suspension density 0.050 g/mL; stainless steel marine upflow impeller; impeller speed 800, 1000, 1200 rpm; crystallizer diameter 90 mm; draft tube diameter 64 mm; impeller diameter 50 mm; off-bottom clearance 10 mm)

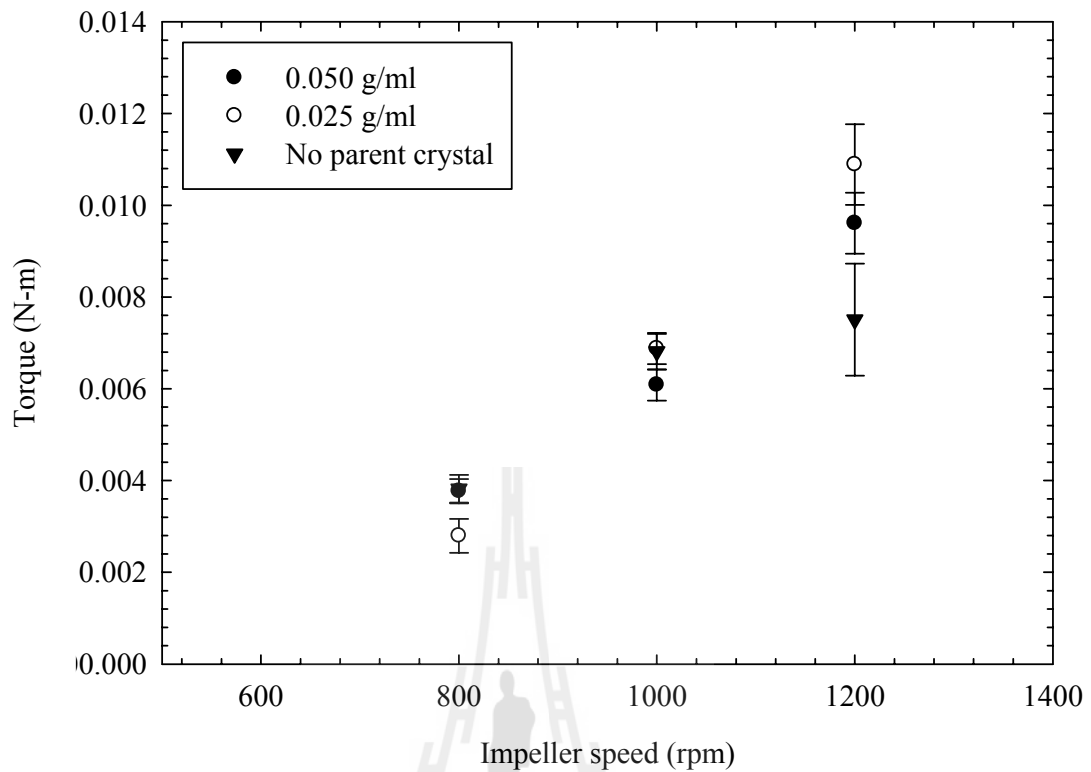


Figure 4.31 The effect of impeller speed on torque. (Slightly supersaturated solution of NaCl in 80% methanol; 300-425 μm NaCl parent crystals; suspension density 0, 0.025, 0.050 g/mL; stainless steel marine upflow impeller; impeller speed 800, 1000, 1200 rpm; crystallizer diameter 90 mm; draft tube diameter 64 mm; impeller diameter 50 mm; off-bottom clearance 10 mm)

4.4.1.2 Effect of suspension density

Interestingly, the relationship between torque and suspension density shows no significant change when we increased the suspension density. The reason that it shows the same result for torque is the values of suspension density in this work is too low to see any large effect on the torque measured in the experiments.

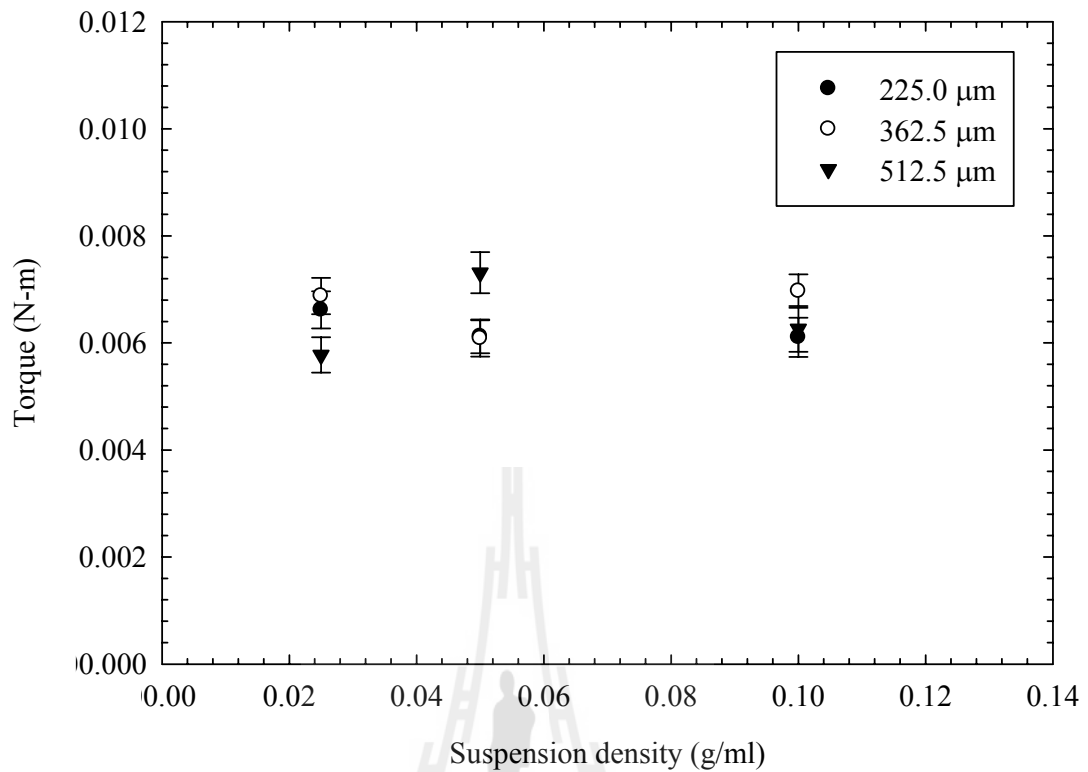


Figure 4.32 The effect of suspension density on torque. (Slightly supersaturated solution of NaCl in 80% methanol; 150-300, 300-425, and 425-600 μm NaCl parent crystals; suspension density 0.025, 0.050, and 0.100 g/mL; stainless steel marine upflow impeller; impeller speed 1000 rpm; crystallizer diameter 90 mm; draft tube diameter 64 mm; impeller diameter 50 mm; off-bottom clearance 10 mm)

4.4.1.3 Effect of parent crystal size

The result for effect of parent crystal size is the same with the effect of suspension density. The reason is the same; the amount of parent crystals in this work is not enough for changing the torque.

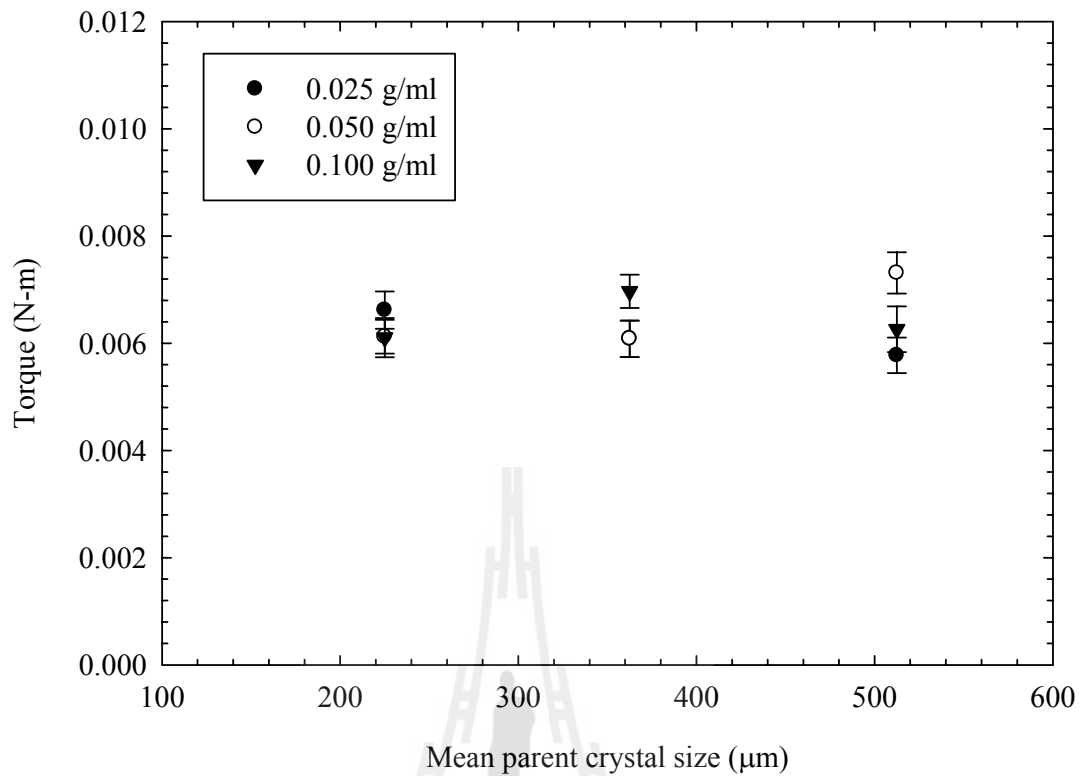


Figure 4.33 The effect of mean parent crystal size on torque. (Slightly supersaturated solution of NaCl in 80% methanol; 150-300, 300-425, and 425-600 μm NaCl parent crystals; suspension density 0.025, 0.050, and 0.100 g/mL; stainless steel marine upflow impeller; impeller speed 1000 rpm; crystallizer diameter 90 mm; draft tube diameter 64 mm; impeller diameter 50 mm; off-bottom clearance 10 mm)

4.4.1.4 Effect of off-bottom impeller clearance

For the effect of off-bottom clearance, when we increase the off-bottom clearance the torque is decreasing. This means at high off-bottom clearance we use less energy in the system.

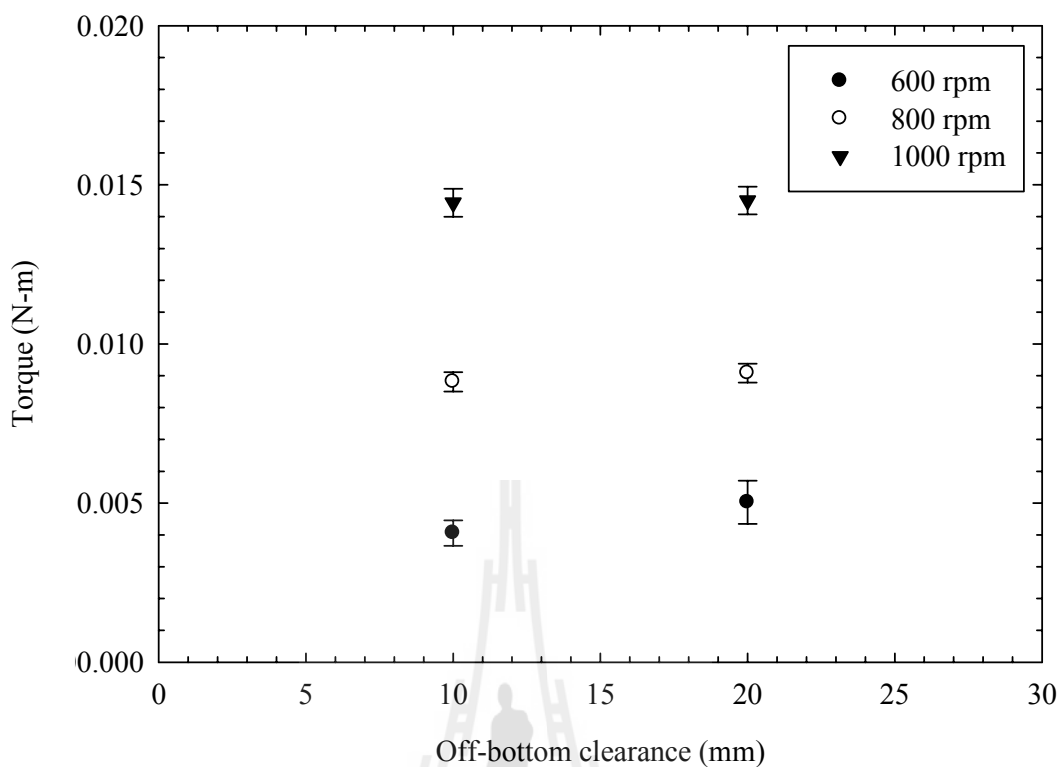


Figure 4.34 The effect of off-bottom impeller clearance on torque. (Slightly supersaturated solution of NaCl in 80% methanol; 300-425 μm NaCl parent crystals; suspension density 0.025 g/mL; stainless steel marine upflow impeller; impeller speed 800, 1000, and 1200 rpm; crystallizer diameter 90 mm; draft tube diameter 64 mm; impeller diameter 50 mm; off-bottom clearance 10 mm)

4.4.1.5 Effect of draft tube diameter

Similar results as the effect of off-bottom clearance are found for effect of the draft tube diameter and these results are similar to the effect of draft tube diameter on attrition rate too.

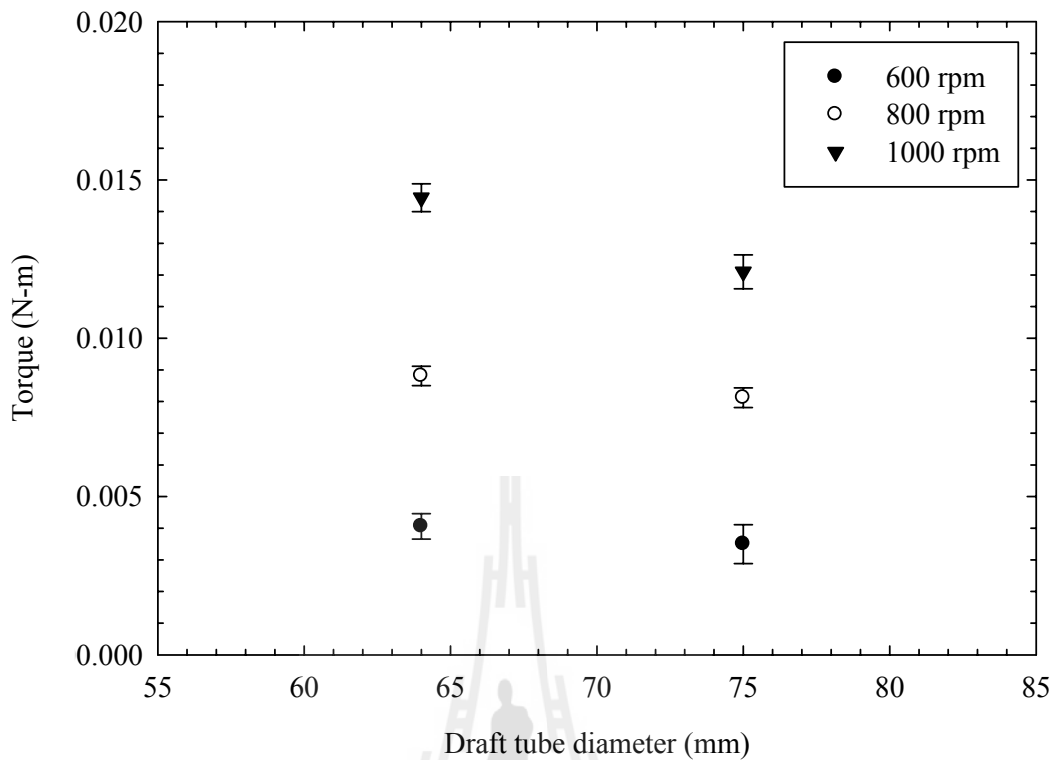


Figure 4.35 The effect of draft tube diameter on torque. (Slightly supersaturated solution of NaCl in 80% methanol; 300-425 μm NaCl parent crystals; suspension density 0.025 g/mL; stainless steel marine upflow impeller; impeller speed 800, 1000, and 1200 rpm; crystallizer diameter 90 mm; draft tube diameter 64 and 75 mm; impeller diameter 50 mm; off-bottom clearance 10 mm)

4.4.2 Torque measurement for sucrose system

4.4.2.1 Effect of impeller speed

Figure 4.36 shows three results of the impeller speed variation at different suspension densities. All torque measurements are increasing when the impeller speed is increased.

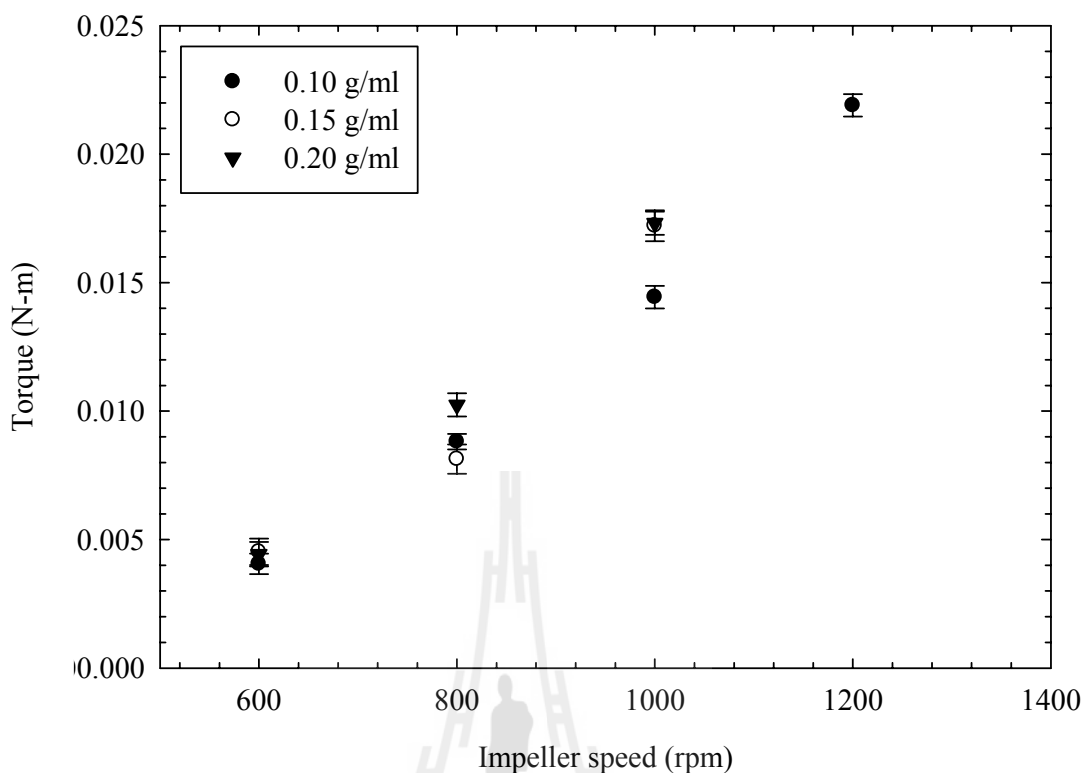


Figure 4.36 The effect of impeller speed on torque. (Saturated solution of sucrose in methanol; 425 – 600 μm sucrose parent crystals; suspension density 0.1, 0.15, 0.2 g/mL; stainless steel marine upflow impeller; impeller speed 800, 1000, 1200 rpm; crystallizer diameter 90 mm; draft tube diameter 64 mm; impeller diameter 50 mm; off-bottom clearance 10 mm)

4.4.2.2 Effect of suspension density

From Figure 4.37, the relationship between torque and suspension density shows no significant change when we increased the suspension density. The reason for similar values of torque is the varied values of suspension density in this work are too small so we cannot see the change of torque in the experiments.

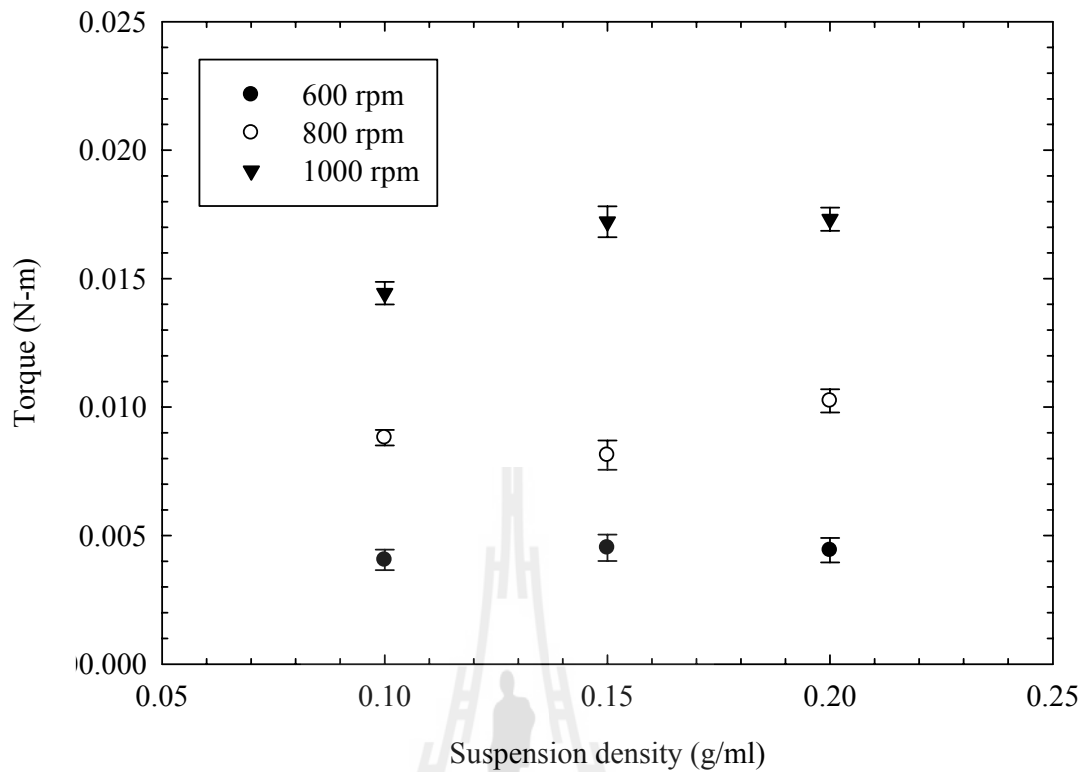


Figure 4.37 The effect of suspension density on torque. (Saturated solution of sucrose in methanol; 425 – 600 μm sucrose parent crystals; suspension density 0.1, 0.15, 0.2 g/mL; stainless steel marine upflow impeller; impeller speed 600, 800, and 1000 rpm; crystallizer diameter 90 mm; draft tube diameter 64 mm; impeller diameter 50 mm; off-bottom clearance 10 mm)

4.4.2.3 Effect of parent crystal size

From Figure 4.38, the results for the effect of parent crystal size are similar to the effect of suspension density and the reason should be the same too. The amount of parent crystals in this work is small so the crystals do not have a strong effect on the torque measurement.

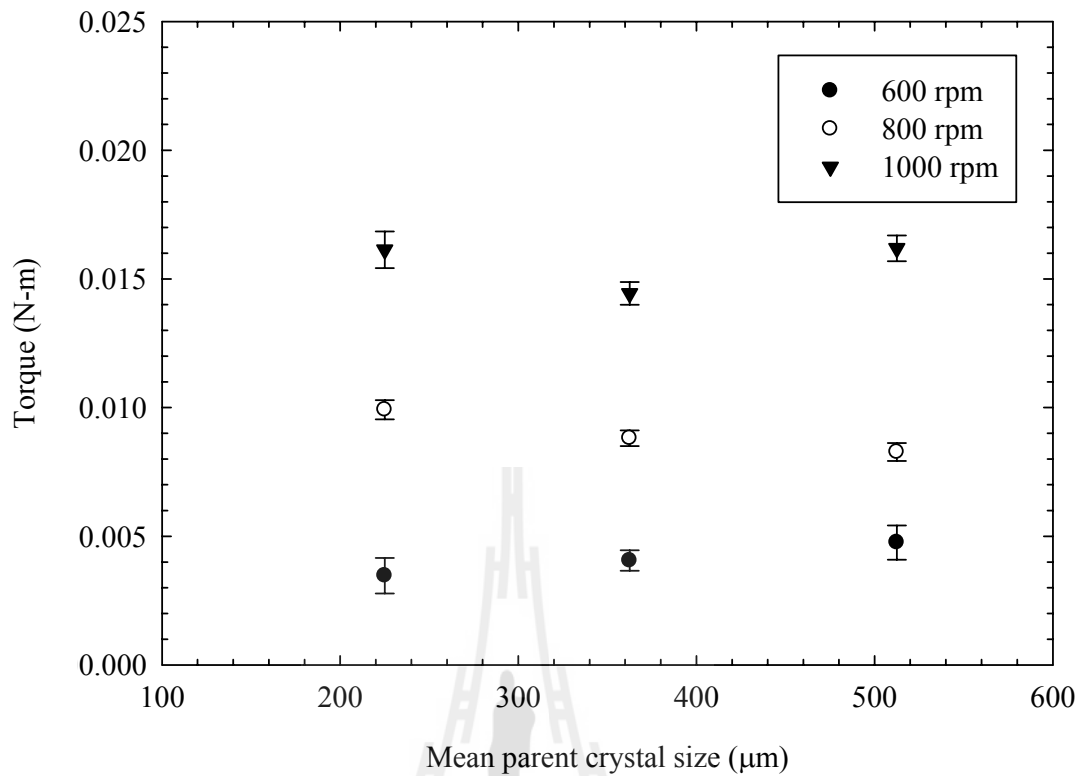


Figure 4.38 The effect of mean parent crystal size on torque. (Saturated solution of sucrose in methanol; 300 – 425, 425 – 600, 600 - 850 μm sucrose parent crystals; suspension density 0.1 g/mL; stainless steel marine upflow impeller; impeller speed 600, 800, and 1000 rpm; crystallizer diameter 90 mm; draft tube diameter 64 mm; impeller diameter 50 mm; off-bottom clearance 10 mm)

4.4.2.4 Effect of off-bottom impeller clearance

From Figure 4.39, the effect of off-bottom clearance on the torque. There is no change that can be observed. The condition in this work is not enough to see the different in the torque measurement.

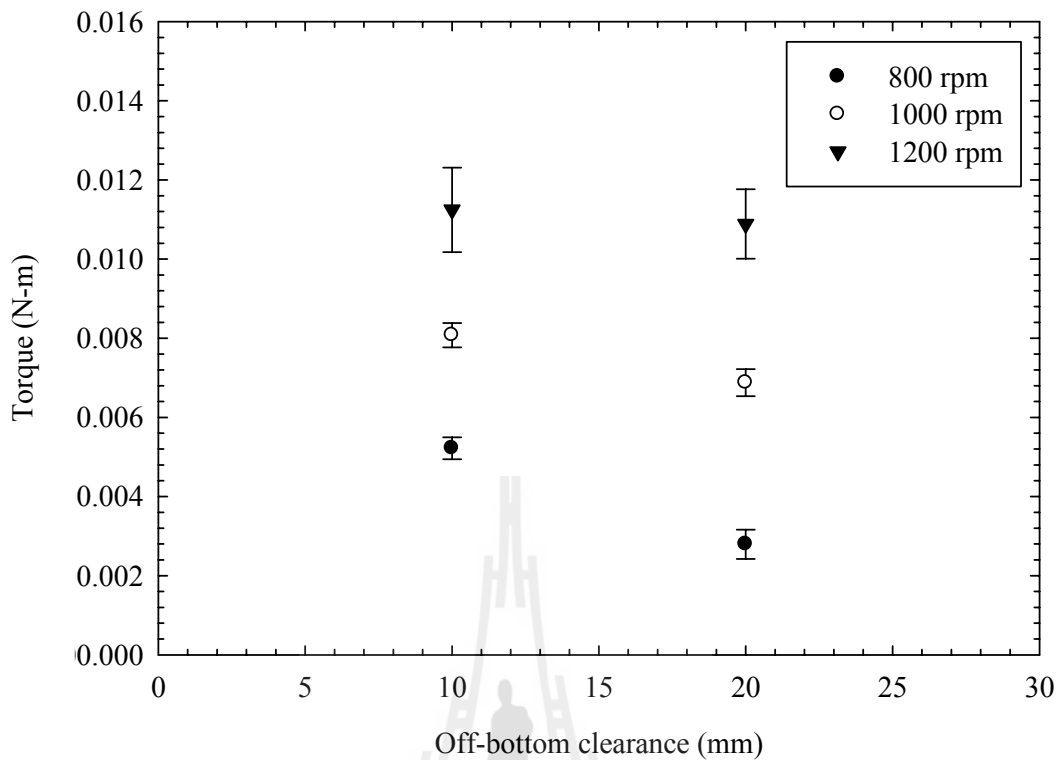


Figure 4.39 The effect of off-bottom impeller clearance on torque. (Saturated solution of sucrose in methanol; 425 - 600 μm sucrose parent crystals; suspension density 0.1 g/mL; stainless steel marine upflow impeller; impeller speed 600, 800, and 1000 rpm; crystallizer diameter 90 mm; draft tube diameter 64 mm; impeller diameter 50 mm; off-bottom clearance 10 and 20 mm)

4.4.2.5 Effect of draft tube diameter

From Figure 4.40, it shows decreasing torque when the draft tube diameter is increased. When we increased the diameter of the draft tube the clearance between impeller and draft tube are also increased so this requires less energy to move the impeller.

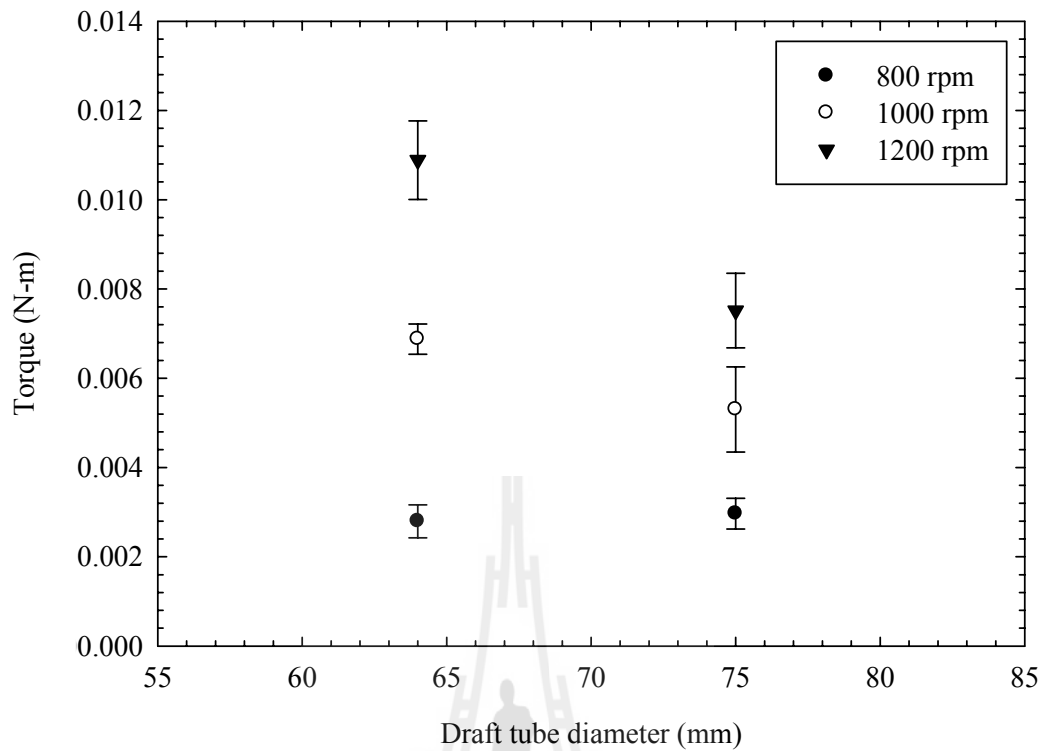


Figure 4.40 The effect of draft tube diameter on torque. (Saturated solution of sucrose in methanol; 425 - 600 μm sucrose parent crystals; suspension density 0.1 g/mL; stainless steel marine upflow impeller; impeller speed 600, 800, and 1000 rpm; crystallizer diameter 90 mm; draft tube diameter 64 and 75 mm; impeller diameter 50 mm; off-bottom clearance 10 mm)

4.4.3 Power input calculation results

We can calculate the power input by using equation 3.4. The results of power input are shown in Table 4.1 and 4.2.

Table 4.1 Power input and torque from NaCl experiment

Parameter	Torque (N-m)	Power input (Watt)
Impeller speed (rpm)		
800	0.0039	0.3267
1000	0.0064	0.6702
1200	0.0088	1.1058
Suspension density (g/ml)		
0.025	0.0064	0.6702
0.050	0.0064	0.6702
0.100	0.0065	0.6807
Parent crystal size (μm)		
150 – 300	0.0058	0.6074
300 – 425	0.0064	0.6702
425 - 600	0.0068	0.7121
Off-bottom clearance (mm)		
10	0.0064	0.6702
20	0.0075	0.7854
Draft tube diameter (mm)		
64	0.0064	0.6702
75	0.0035	0.3665

Table 4.2 Power input and torque from sucrose experiment

Parameter	Torque (N-m)	Power input (Watt)
Impeller speed (rpm)		
800	0.0088	0.7380
1000	0.0144	1.5117
1200	0.0219	2.7520
Suspension density (g/ml)		
0.10	0.0144	1.5117
0.15	0.0172	1.8028
0.20	0.0173	1.8130
Parent crystal size (μm)		
300 - 425	0.161	1.6897
425 - 600	0.0144	1.5117
600 - 850	0.0162	1.6954
Off-bottom clearance (mm)		
10	0.0144	1.5117
20	0.0091	1.5189
Draft tube diameter (mm)		
64	0.0144	1.5117
75	0.0081	1.2672

4.4.4 Solution properties

Determination of dimensionless groups such as power number and Reynolds number need the solution properties, for example, solution viscosity and solution density. In this research, there are no suspension properties available in the literature so we have to measure them in the laboratory. The method of measurement is shown in section 3.3.5. There are two solution properties, viscosity and density, that we need to measure. The results of viscosity and density are shown in Table 4.3.

Table 4.3 Viscosity and density of the solution in this work

Type of solution	Viscosity at 25°C (mPa.s)	Density at 25°C (kg/m ³)
Water (Korson et al., 1969)	0.8903	997.0751
Water (measured)	1.1276	996.0594
Slightly supersaturation (NaCl in methanol water)	1.5286	868.2214
Saturate solution (Sucrose in methanol)	0.9246	811.3867

4.5 Data analysis for modeling of crystal attrition

4.5.1 Dimensionless groups

4.5.1.1 Power number

Figure 4.41 shows the relationship between attrition number and power number for standard conditions, varying impeller speed (800, 1000, and 1200 rpm). As we expected, the high power number should give a high attrition rate because the attrition rate strongly depends on energy from the crystallizer unit to the parent crystals.

4.5.1.2 Reynolds number

Reynolds number is one of the most important parameters affecting attrition rates because it represents the hydrodynamic of the system, so high Reynolds number should give high attrition rate similar to the power number. Figure 4.42 presents the relationship between attrition number and Reynolds number but the maximum Reynolds number does not give the highest value of the attrition number. The reason is there is a maximum limit of attrition in this system because when the parent crystal undergoes attrition the surface will be rounded, so it can reduce the attrition rate.

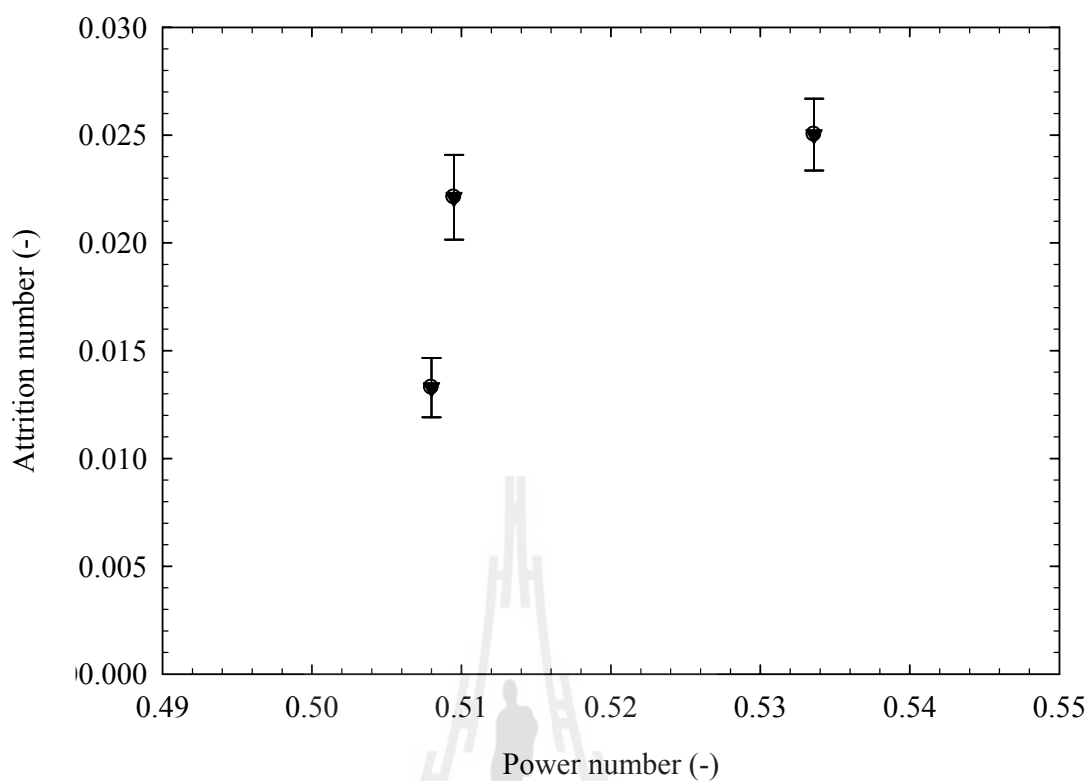


Figure 4.41 The attrition number as a function of power number. (Slightly supersaturated solution of NaCl in 80% methanol; 300-425 μm NaCl parent crystals; suspension density 0.10 g/mL; stainless steel marine upflow impeller; impeller speed 800, 1000, 1200 rpm; crystallizer diameter 90 mm; draft tube diameter 64 mm; impeller diameter 50 mm; off-bottom clearance 10 mm)

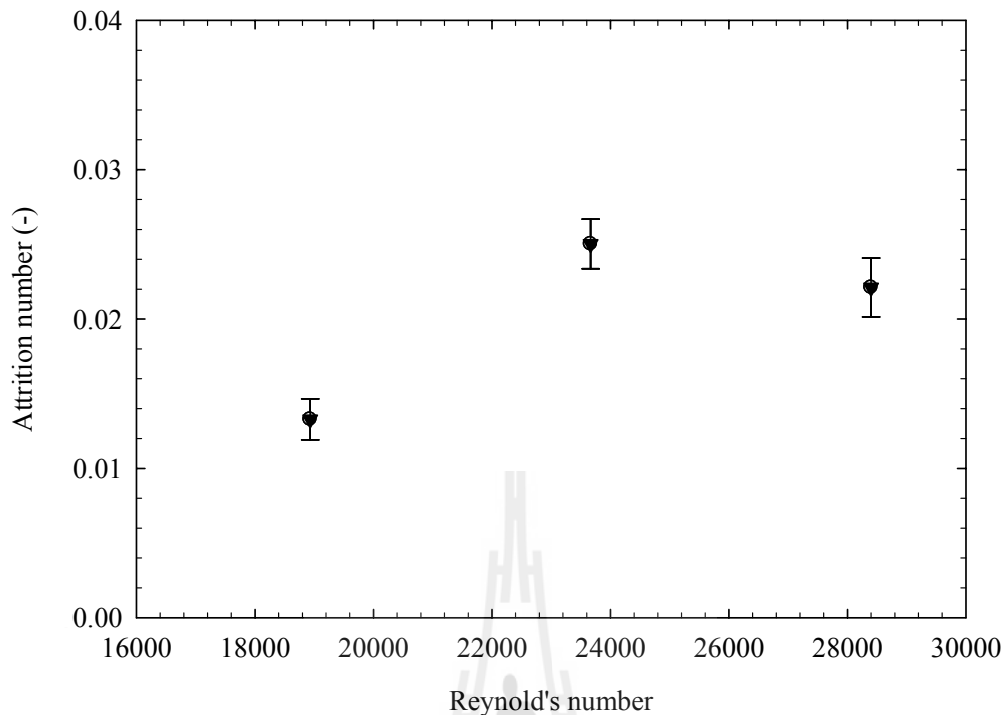


Figure 4.42 The attrition number as a function of Reynolds number. (Slightly supersaturated solution of NaCl in 80% methanol; 300-425 μm NaCl parent crystals; suspension density 0.10 g/mL; stainless steel marine upflow impeller; impeller speed 800, 1000, 1200 rpm; crystallizer diameter 90 mm; draft tube diameter 64 mm; impeller diameter 50 mm; off-bottom clearance 10 mm)

4.5.1.3 Parent crystal size and impeller diameter ratio

From Figure 4.43, the dimensionless group of attrition rate and parent crystal size is considered. As can be seen, if we focus on the parent crystal size, the large one has a higher attrition number compared to the small particle. This results show the effect of parent crystal size is very significant for attrition rate.

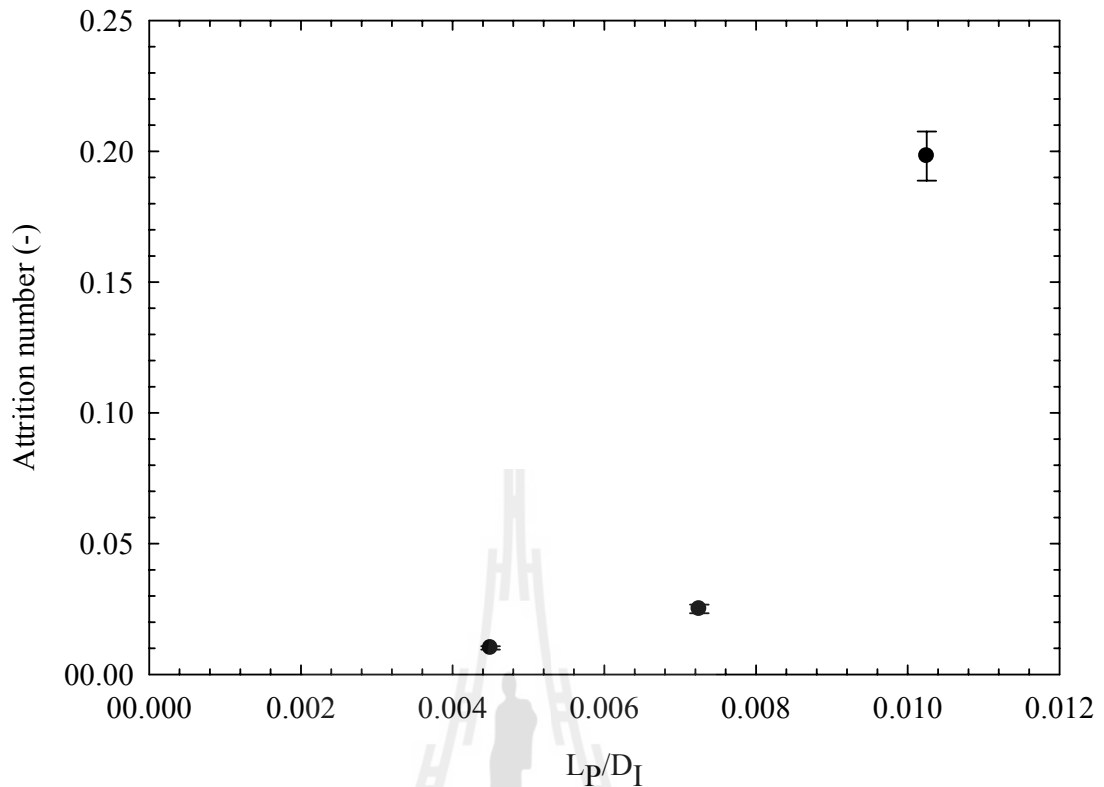


Figure 4.43 The attrition number as a function of parent crystal size and impeller diameter ratio. (Slightly supersaturated solution of NaCl in 80% methanol; 150 – 300, 300–425, 425 - 600 μm NaCl parent crystals; suspension density 0.10 g/mL; stainless steel marine upflow impeller; impeller speed 1000 rpm; crystallizer diameter 90 mm; draft tube diameter 64 mm; impeller diameter 50 mm; off-bottom clearance 10 mm)

4.5.1.4 Draft tube impeller clearance and impeller diameter ratio

Figure 4.44 shows the effect of impeller-draft tube clearance and impeller diameter ratio on the attrition number. The attrition number decreases strongly as the impeller-draft tube clearance and impeller diameter ratio increases.

This is due to the added clearance between the impeller tip and the draft tube, allowing more parent crystals to avoid contact with the impeller.

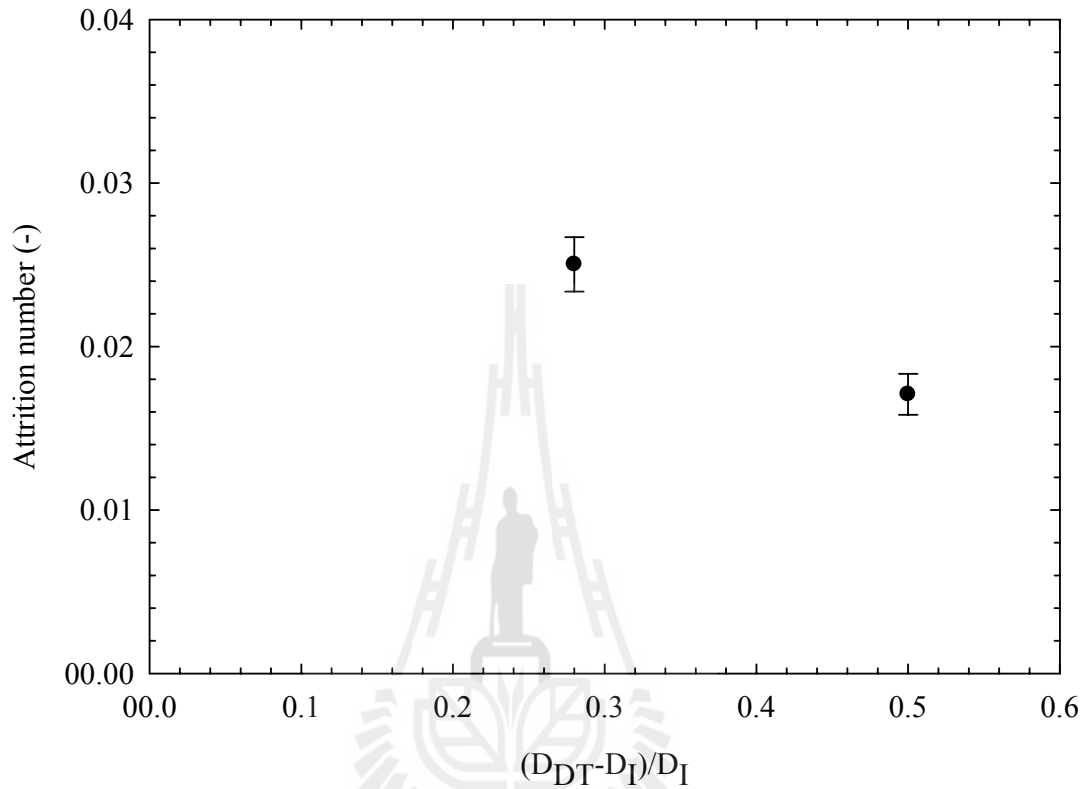


Figure 4.44 The attrition number as a function of draft tube impeller clearance and impeller diameter ratio. (Slightly supersaturated solution of NaCl in 80% methanol; 300-425 μm NaCl parent crystals; suspension density 0.10 g/mL; stainless steel marine upflow impeller; impeller speed 1000 rpm; crystallizer diameter 90 mm; draft tube diameter 64 and 75 mm; impeller diameter 50 mm; off-bottom clearance 10 mm)

4.5.1.5 Off-bottom clearance and impeller diameter ratio

From Figure 4.45, there is no significant difference between two values of off-bottom number, so this parameter will not be in the modeling of attrition rate in NaCl system.

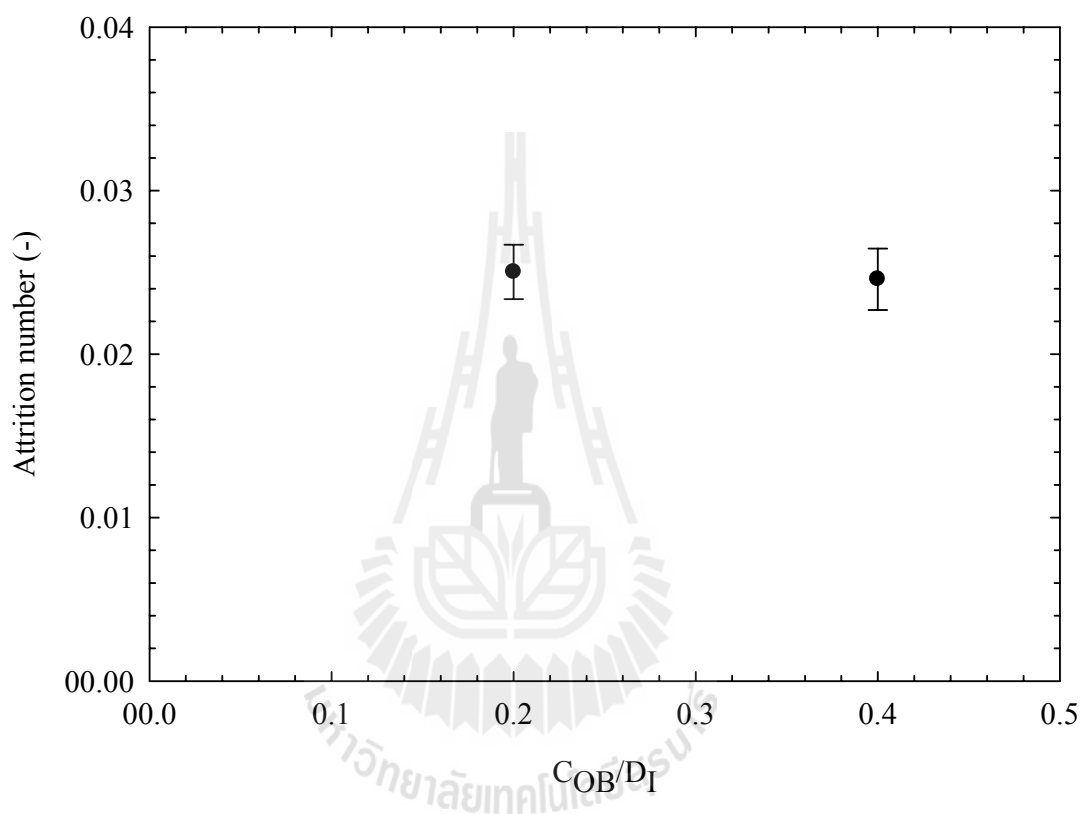


Figure 4.45 The attrition number as a function of off-bottom clearance and impeller diameter ratio. (Slightly supersaturated solution of NaCl in 80% methanol; 300-425 μm NaCl parent crystals; suspension density 0.10 g/mL; stainless steel marine upflow impeller; impeller speed 1000 rpm; crystallizer diameter 90 mm; draft tube diameter 64 mm; impeller diameter 50 mm; off-bottom clearance 10 and 20 mm)

4.5.1.6 Suspension density and crystal density ratio

For the dimensionless group of suspension density, it shows the attrition number decreases when the suspension density and crystal density ratio increases. In fact, the attrition number should be approximately the same because the calculation of attrition number is divided by number of parent crystals, but at the suspension density and crystal density ratio equal to 0.01 there is a higher attrition number. This is because the attrition rate is high compared to other conditions.

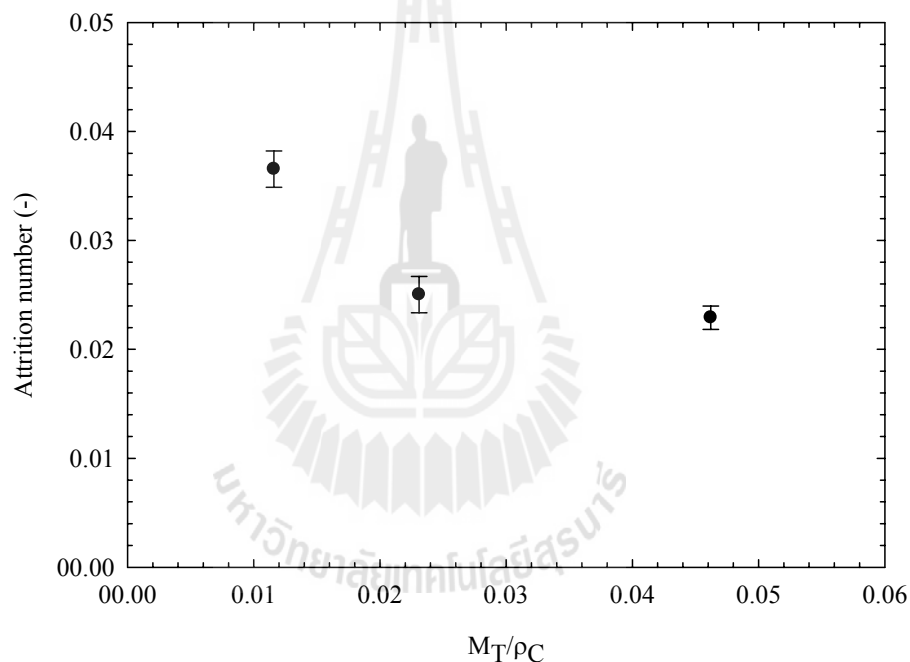


Figure 4.46 The attrition number as a function of suspension density and crystal density ratio. (Slightly supersaturated solution of NaCl in 80% methanol; 300-425 μm NaCl parent crystals; suspension density 0.05, 0.10, and 0.15 g/mL; stainless steel marine upflow impeller; impeller speed 1000 rpm; crystallizer diameter 90 mm; draft tube diameter 64 mm; impeller diameter 50 mm; off-bottom clearance 10 mm)

The following tables summarize the dimensionless groups of NaCl system and sucrose system (Table 4.4 and 4.5).

Table 4.4 Dimensionless groups for NaCl system.

Parameters	N_{Att}	N_P	N_{Re}	N_{MT}	N_{Lp}	N_{OB}	N_{DT}
Impeller speed							
800 rpm	0.0130	0.5080	18,933	0.023116	0.00725	0.2	0.28
1000 rpm	0.0250	0.5336	23,666	0.023116	0.00725	0.2	0.28
1200 rpm	0.0221	0.5095	28,399	0.023116	0.00725	0.2	0.28
Suspension density							
0.025 g/ml	0.0365	0.5336	23,666	0.011558	0.00725	0.2	0.28
0.050 g/ml	0.0250	0.5336	23,666	0.023116	0.00725	0.2	0.28
0.100 g/ml	0.0229	0.5419	23,666	0.046232	0.00725	0.2	0.28
Parent crystal size							
150 – 300 μm	0.0102	0.4835	23,666	0.023116	0.00450	0.2	0.28
300 – 425 μm	0.0250	0.5336	23,666	0.023116	0.00725	0.2	0.28
425 – 600 μm	0.1981	0.5669	23,666	0.023116	0.01025	0.2	0.28
Off-bottom clearance							
10 mm	0.0467	0.5336	23,666	0.023116	0.00725	0.2	0.28
20 mm	0.0331	0.6253	23,666	0.023116	0.00725	0.4	0.28
Draft tube diameter							
64 mm	0.0467	0.5336	23,666	0.023116	0.00725	0.2	0.28
75 mm	0.0321	0.2918	23,666	0.023116	0.00725	0.2	0.5

Table 4.5 Dimensionless groups for sucrose system.

Parameters	N_{Att}	N_P	N_{Re}	N_{MT}	N_{Lp}	N_{OB}	N_{DT}
Impeller speed							
800 rpm	0.1346	1.2279	29,252	0.063012	0.01025	0.2	0.28
1000 rpm	0.1895	1.2878	36,565	0.063012	0.01025	0.2	0.28
1200 rpm	0.1904	1.3567	43,878	0.063012	0.01025	0.2	0.28
Suspension density							
0.100 g/ml	0.1895	1.2878	36,565	0.063012	0.01025	0.2	0.28
0.150 g/ml	0.7018	1.5358	36,565	0.094518	0.01025	0.2	0.28
0.200 g/ml	0.1205	1.5444	36,565	0.126024	0.01025	0.2	0.28
Parent crystal size							
300 – 425 μm	1.1678	1.4394	36,565	0.063012	0.00725	0.2	0.28
425 – 600 μm	0.1895	1.2878	36,565	0.063012	0.01025	0.2	0.28
600 – 850 μm	0.2818	1.4443	36,565	0.063012	0.01450	0.2	0.28
Off-bottom clearance							
10 mm	0.1895	1.2878	36,565	0.063012	0.01025	0.2	0.28
20 mm	0.0232	1.2939	36,565	0.063012	0.01025	0.4	0.28
Draft tube diameter							
64 mm	0.1895	1.2878	36,565	0.063012	0.01025	0.2	0.28
75 mm	0.0267	1.0795	36,565	0.063012	0.01025	0.2	0.5

4.5.2 Empirical engineering model

Firstly, we analyzed attrition rate as a function of many parameters in the crystallization system which we separated into three groups (crystallizer geometry and operation condition, crystal properties, and solution and suspension properties). When we got the suitable parameter for modeling of empirical correlation, we reduced the parameter by dimensional analysis. We calculated the dimensionless groups by using Buckingham's Pi Theory. The next steps for modeling of empirical correlation are shown below.

4.5.2.1 Power law modeling of NaCl

From the previous section, we calculated the attrition number and other dimensionless groups from suitable parameters which had an effect on the attrition rate. Then, we fitted the power law model with the dimensionless groups to determine the empirical constants. Figure 4.47 shows the comparison of the results obtained by the empirical model with the experimental data (eight points). The empirical engineering model from curve fitting is

$$N_{Att} = 2.095 \times 10^7 N_P^{8.536} N_{Re}^{1.424} N_{MT}^{-0.4339} N_{Lp}^{4.222} N_{DT}^{8.080} \quad (4.2)$$

As can be seen in Figure 4.47, the empirical model fits the experimental results very well (for detail values of experimental data and empirical model see Table 4.6). The R-squared from the curve fitting is 0.9971. The root-mean-square deviation (RMSD) is 0.0034. Therefore the attrition rate or secondary nucleation rate can be calculated from this empirical model. In Figure 4.47, there is one point that deviate from the straight line. It is the estimated value of the attrition

number for 7.5 cm diameter of the draft tube which we use to compare with the 6.4 cm diameter of the draft tube (standard case). This shows the limitation of this empirical model because we have only two conditions for studying the effect of draft tube impeller clearance on the attrition rate, so the estimated value is not accurate. Therefore when we use simple power law model with all parameters it can make some mistakes in the empirical model but the overall standard error shows very good results.

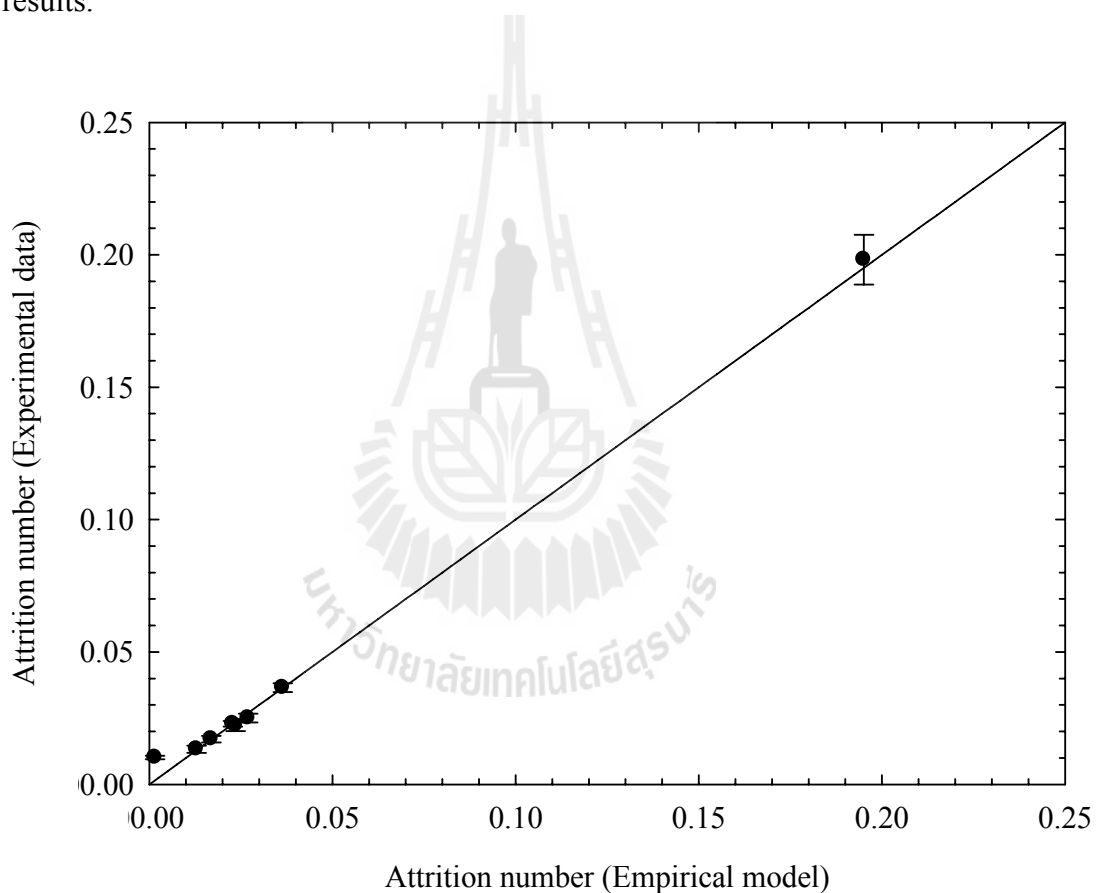


Figure 4.47 Comparison of experimental attrition number with the empirical attrition number estimated by power law model (for NaCl system).

Table 4.6 Attrition number from experiments and empirical model for NaCl system.

Parameters	$N_{Att, Exp.}$	$N_{Att, Eq.4.2}$	$N_{Att, Eq.4.4}$
Impeller speed (rpm)			
800	0.0130	0.0129	0.0131
1000	0.0250	0.0269	0.0248
1200	0.0221	0.0235	0.0220
Suspension density (g/ml)			
0.100	0.0365	0.0364	0.0360
0.150	0.0250	0.0269	0.0248
0.20	0.0229	0.0228	0.0228
Parent crystal size (μm)			
300 - 425	0.0102	0.0016	0.0099
425 - 600	0.0250	0.0269	0.0248
600 -850	0.1981	0.1950	0.1979
Off-bottom clearance (mm)			
10	0.0250	0.0269	0.0248
20	0.0331	0.0269	0.0248
Draft tube diameter (mm)			
64	0.0250	0.0269	0.0248
75	0.0171	0.0169	0.0171

4.5.2.2 Power law modeling of sucrose

Similar to previous section, we fitted the power law model with the dimensionless groups to determine the empirical constants. For the sucrose system

we have seven dimensionless groups. They are attrition number, power number, Reynolds number, suspension density number, parent crystal size number, draft tube number, and off-bottom clearance number. Figure 4.48 shows the comparison of the results obtained by the empirical model with the experimental data (eight points). The empirical engineering model from curve fitting is

$$N_{Att} = 4 \times 10^{-4} N_P^{10.2327} N_{Re}^{-1.5821} N_{MT}^{-1.0763} N_{Lp}^{-2.1264} N_{OB}^{-4.0728} N_{DT}^{-0.6119} \quad (4.3)$$

From Figure 4.48, the empirical model is fitted with experimental results very well. The R-square from the curve fitting is 0.9977 and the root-mean-square deviation (RMSD) is 0.0184.

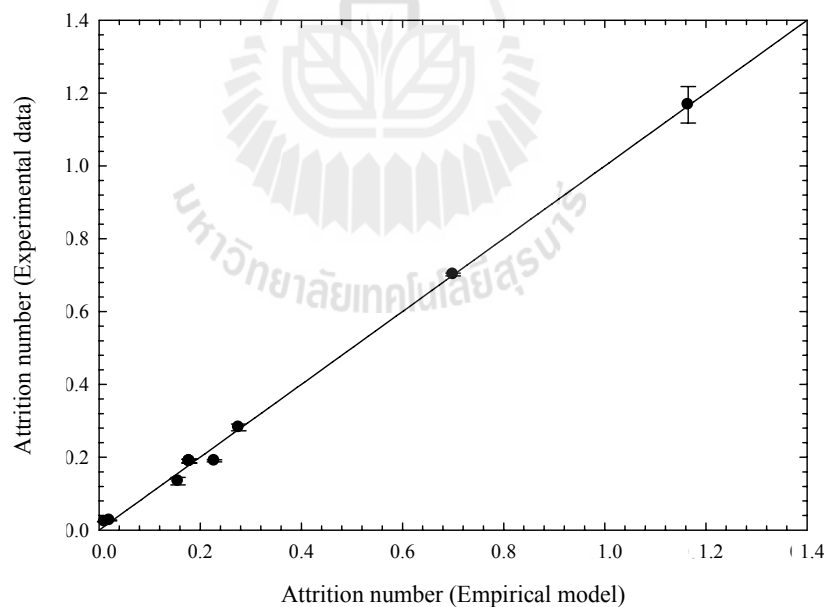


Figure 4.48 Comparison of experimental attrition number with the empirical attrition number estimated by power law model (for sucrose system).

Table 4.7 Attrition number from experiments and empirical model for sucrose.

Parameters	$N_{Att, Exp.}$	$N_{Att, Eq.4.3}$	$N_{Att, Eq.4.4}$
Impeller speed (rpm)			
800	0.1346	0.1561	0.1467
1000	0.1895	0.1785	0.1798
1200	0.1904	0.2281	0.2425
Suspension density (g/ml)			
0.100	0.1895	0.1785	0.1798
0.150	0.7018	0.6999	0.7006
Parent crystal size (μm)			
300 - 425	1.1678	1.1648	1.1663
425 - 600	0.1895	0.1785	0.1798
600 - 850	0.2818	0.2762	0.2711
Off-bottom clearance (mm)			
10	0.1895	0.1785	0.1798
20	0.0232	0.0111	0.0125
Draft tube diameter (mm)			
64	0.1895	0.1785	0.1798
75	0.0267	0.0206	0.0169

4.5.2.3 Power law modeling for both system (sucrose and NaCl)

From both system sucrose and NaCl, we can fit the data together to get the general empirical model. The dimensionless groups for curve fitting are attrition number, power number, Reynolds number, suspension density

number, parent crystal size number, draft tube number, and off-bottom clearance number. The empirical engineering model from curve fitting is

$$N_{Att} = 1.031 \times 10^{-5} N_P^{10.0968} N_{Re}^{-1.2449} N_{MT}^{-1.0308} N_{Lp}^{-2.1554} N_{OB}^{-3.9113} N_{DT}^{-1.0053} \quad (4.4)$$

From Figure 4.49, the empirical model is fitted with experimental results very well. The R-square from the curve fitting is 0.9691 and the root-mean-square deviation (RMSD) is 0.0151. There is one point deviated from the straight line in Figure 4.49. It is the condition at 1200 rpm of sucrose system. We varied the impeller speeds to determine the effect of them on attrition rate and the result showed at 1200 rpm the attrition rate increased but it is not high enough to get the straight line compared to 800 and 1000 rpm. I think this is the experimental error. If we make more experiments, we can reduce this error.

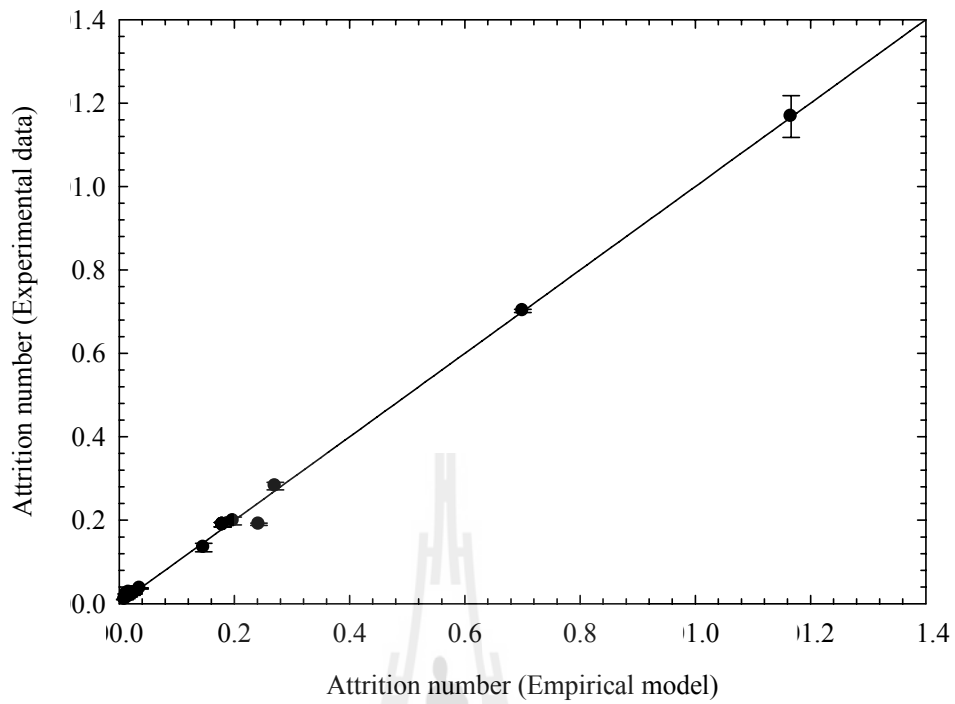


Figure 4.49 Comparison of experimental attrition number with the empirical attrition number estimated by power law model (for sucrose system and NaCl system).

CHAPTER V

CONCLUSIONS AND RECOMMENDATIONS

5.1 Conclusions

Attrition of macroscopic crystals in industrial crystallizers is a significant problem not only due to its degradation of the product crystals, but also due to the creation of large numbers of particles acting as secondary nuclei, thus greatly reducing the mean particle size in the crystallizer. The aim of this study is to understand the attrition behavior and to model the crystal attrition rate equation. The conclusions of this work are presented below.

5.1.1 The attrition fragments size distribution

There are two substances and systems presented in this research to study the attrition. For sucrose, the attrition fragment size distribution had a finite particle size distribution (PSD), and in particular had relatively wide PSDs. The fragments typically had geometric mean sizes in the order of 5 μm , and geometric standard deviations of approximately 0.8-0.9. For sodium chloride, it also had a finite particle size distribution but the mean size is lower than for the sucrose fragments. The mean sizes of NaCl fragment were around 2 μm , and they had geometric standard deviations of approximately 0.4-0.7.

5.1.2 The effect of parameters from crystallizer properties, crystal properties, and solution properties on the attrition rate

For this section, we have to conclude separately between sucrose and NaCl because the effect of solution properties and type of parent crystal are quite different. All parameters varied during the study of sucrose system had a strong effect on the attrition rate. The highest attrition rate is from the condition of resin impeller but unfortunately we cannot take this parameter into the empirical model because we need more investigation about the hardness of the material (resin) and other properties. The same as for the pitch blade impeller, it is difficult to include in a general model because we need the information about the hydrodynamics of different impeller type. So, the parameters that we can use for the model are impeller speed, suspension density, parent crystal size, off-bottom clearance, and draft tube diameter.

The second part, for the sodium chloride system, the effect of parameters on attrition rate is a little bit different from the sucrose system. The highest attrition rate for this system is the condition of highest suspension density (0.1 g/ml). Similar to the sucrose system, resin and pitch blade impeller cannot be included in an empirical model, but for the sucrose system these two parameters show no significant effect on the attrition rate. Another parameter which showed no effect on the attrition from the standard condition is the off-bottom impeller clearance. Therefore, the parameters that we will select for the empirical model are impeller speed, suspension density, parent crystal size, and draft tube diameter.

5.1.3 The effect of scale up on attrition rate

The reason that we should know about the effect of scale up on attrition rate is that we need to ensure that a model based on the current data can be suitably scaled up to an industrial sized crystallizer. From the results and discussion in section 4.3, it has shown that the size of crystallizer has an effect on attrition rate but there are similar trend between the small scale and the large scale. So if we investigate more about the scale of crystallizer and use a better scale up rule we will have the scale-up factor that is suitable for crystallizer design.

5.1.4 The suitable dimensionless groups for data fitting

In section 4.4 and 4.5, the results of the calculation show that the suitable dimensionless groups for modeling of empirical model are attrition number, power number, Reynolds number, parent crystal size number, suspension density number, draft tube number, and off-bottom clearance number. These dimensionless groups are useful for modeling of crystal attrition in industrial crystallizers, but there are a lot of crystallizer types so we have to select the right dimensionless groups for the system.

5.1.5 The empirical engineering model for nucleation rate

The empirical engineering model fits the experimental results very well. Therefore this method can be used to calculate the secondary nucleation in industrial crystallizers of similar geometry to those used here. For the sucrose system and the sodium chloride system in this research, the power law model is very good for modeling because the empirical correlations have very good R-squared and RMSD. There are three empirical models presented in this work. The first one is for the NaCl

system, the second one is for the sucrose system, and the third one is for a combination of both systems.

5.2 Recommendations

5.2.1 Experimental design for study of secondary nucleation

There are a lot of mechanisms of secondary nucleation in crystallization processes. We have to determine the mechanism of secondary nucleation that can occur in the system first and then we can use the best experimental design to study about the secondary nucleation. In this work, we consider other attrition mechanism which always occurs in the crystallization process if the parent crystal is moving and has a chance to contact with other crystal or crystallizer parts. In a real system, we cannot study only one mechanism like attrition because other mechanisms also occur simultaneously so if we want to study the attrition mechanism, we have to separate attrition from other mechanisms, for example, using saturated or slightly supersaturated solution or non-solvent to avoid the effect of supersaturation and dissolution of parent crystals.

5.2.2 Parameters for further study of secondary nucleation

The models for secondary nucleation have been proposed by many investigators but those models are for only one mechanism so it is very difficult to apply in industrial application. If we want to generate the model for secondary nucleation, we should include all mechanisms in the model, for instance, contact nucleation, attrition nucleation, fluid shear nucleation, and fracture nucleation. This research tried to model the attrition nucleation by counting the attrition fragments,

which is the best way to calculate the attrition rate. This method should be used to study other mechanisms and combine all mechanisms to develop a general model for secondary nucleation.

5.2.3 The general equation for secondary nucleation

As we know, a general theory of secondary nucleation to predict the secondary nucleation rates does not exist (Myerson, 2002). This research was studied about only one mechanism of secondary nucleation (the attrition mechanism). The general model needs more investigation about secondary nucleation mechanisms, for instance, contact nucleation, shear, and fracture. If we define the overall mechanisms of secondary nucleation as micro-attrition mechanism (MA) and boundary-layer mechanism (BL) (Grootscholten et al., 1982), the general equation for secondary nucleation should be given by

$$B^0 = B_{MA} + B_{BL} \quad (5.1)$$

where B_{MA} = secondary nucleation from attrition, fracture, contact, and needle

B_{BL} = secondary nucleation from shear and initial breeding

In industrial crystallizers we cannot separate one secondary mechanism from the others, so we have to know every mechanism in the crystallizer because every types of secondary nucleation can be dominant depending on the properties of the crystallization process, for example, for slightly supersaturation and good crystal growth the most important mechanism should be attrition.

REFERENCES

- Aeschbach, S. and J. R. Bourne (1972). The attainment of homogeneous suspension in a continuous stirred tank. **The Chemical Engineering Journal**. 4(3): 234-242.
- Akal, M. M., M. Zakaria, et al. (1986). Secondary nucleation rate of sodium chloride under different stirring conditions. **Journal of Crystal Growth**. 78(3): 528-532.
- Akrap, M., N. Kuzmanić, et al. (2012). Impeller geometry effect on crystallization kinetics of borax decahydrate in a batch cooling crystallizer. **Chemical Engineering Research and Design**. 90(6): 793-802.
- Ang, H. M. and P. I. W. Loh (1990). Kinetics of Secondary Nucleation of Alumina Trihydrate in a Batch Crystallizer. *Crystallization as a Separations Process*, **American Chemical Society**. 438: 329-343.
- Asakuma, Y., T. Honda, et al. (2008). Fragmentation behavior of aggregated crystal in suspension crystallization processes. **Powder Technology**. 181(3): 266-272.
- Asakuma, Y., T. Tetahima, et al. (2007). Attrition behavior by micro-hardness parameters in suspension-crystallization processes. **Powder Technology**. 171(2): 75-80.
- Ayazi Shamlou, P., A. G. Jones, et al. (1990). Hydrodynamics of secondary nucleation in suspension crystallization. **Chemical Engineering Science**. 45(5): 1405-1416.
- Bao, Y., J. Zhang, et al. (2006). Determination of growth and breakage kinetics of l-threonine crystals. **Journal of Crystal Growth**. 289(1): 317-323.

- Beekman, W. J., G. M. H. Meesters, et al. (2002). Measurement of granule attrition and fatigue in a vibrating box. **Particle and Particle Systems Characterization**. 19(1): 5-11.
- Bennett, R. C., Fiedelman, H., and Randolph, A. D., (1997). Crystallizer influenced nucleation. **Chemical Engineering Progress**. 69: 86-93.
- Biscans, B. (2004). Impact attrition in crystallization processes. Analysis of repeated impacts events of individual crystals. **Powder Technology**. 143-144: 264-272.
- Biscans, B., Chemini, R., Guiraud, P., and Laguerie, C. (1996). Design of an attrition experiment to simulate the effect of crystal-wall or crystal-stirrer impacts occurring in a crystallizer. **Powder Technology**. 86: 155-161.
- Biscans, B., Guiraud, P., Laguerie, C., Massarelli, A., and Mazzarotta, B. (1996). Abrasion and breakage phenomena in mechanically stirred crystallizers. **The Chemical Engineering Journal**. 63: 85-91.
- Bravi, M. Cave, S. D., Mazzarotta, B., and Verdone, N. (2003). Relating the attrition behaviour of crystals in a stirred vessel to their mechanical properties. **The Chemical Engineering Journal**. 94: 223-229.
- Briesen, H. (2005). Improving the predictive capabilities of the attrition model according to Gahn and Mersmann. In **Proceeding of the 16th International Symposium on Industrial Crystallization** (pp. 349-354). Dresden, Germany: VDI Verlag.
- Briesen, H. (2007). Model-based analysis of the effect of particle and impact geometry on attrition of brittle material. **Powder Technology**. 178(2): 87-98.
- Briesen, H. (2009). Two-dimensional population balance modeling for shape dependent crystal attrition. **Chemical Engineering Science**. 64(4): 661-672.

- Cayey, N. W. and J. Estrin (1967). Secondary Nucleation in Agitated, Magnesium Sulfate Solutions. **Industrial & Engineering Chemistry Fundamentals**. 6(1): 13-20.
- Clontz, N. A. and McCabe, W. L. (1971). Contact nucleation of $\text{MgSO}_4 \cdot 7\text{H}_2\text{O}$. **Chemical Engineering Progress**. 67: 6-17.
- Daudey, P. J., G. M. Van Rosmalen, et al. (1990). Secondary nucleation kinetics of ammonium sulfate in a CMSMPR crystallizer. **Journal of Crystal Growth**. 99(1-4 pt 2): 1076-1081.
- Denk, E. G. and Botsaris, G. D. (1972a). Fundamental studies in secondary nucleation from solution. **Journal of Crystal Growth** 13-14: 493-499.
- Denk, E. G. and Botsaris, G. D. (1972b). Mechanism of contact nucleation. **Journal of Crystal Growth**. 15: 57-60.
- Evans, T. W., G. Margolis, et al. (1974). Mechanisms of secondary nucleation in agitated crystallizers. **AIChE Journal**. 20(5): 950-958.
- Evans, T. W., A. F. Sarofim, et al. (1974). Models of secondary nucleation attributable to crystal-crystallizer and crystal-crystal collisions. **AIChE Journal**. 20(5): 959-966.
- Fasoli, U and Conti, R. (1976) Secondary nucleation in agitated crystallizers. In **industrial crystallization (6th Symposium, Usti nad Labem)** (pp. 77-87). New York: Plenum Press.
- Flood, A. E. (2009). **Industrial crystallization from solution: A primer**. Thailand: Suranaree University of Technology.
- Gahn, C., Krey, J., and Mersmann, A. (1996). The effect of impact energy and the shape of crystals on their attrition rate. **J. of Crystal Growth**. 166: 1058-1063.

- Gahn, C. and Mersmann, A. (1995). The brittleness of substances crystallized in industrial processes. **Powder Technology**. 85: 71-81.
- Gahn, C. and Mersmann, A. (1999). Brittle fracture in crystallization processes Part A. Attrition and abrasion of brittle solids. **Chemical Engineering Science**. 54: 1273-1282.
- Garside, J. (1985). Industrial crystallization from solution. **Chemical Engineering Science**. 40(1): 3-26.
- Garside, J. and R. J. Davey (1980). Secondary contact nucleation: kinetics, growth and scale-up. **Chemical Engineering Communications**. 4(4-5): 393-424.
- Garside, J. and S. J. Jančić (1979). Measurement and scale-up of secondary nucleation kinetics for the potash alum-water system. **AIChE Journal**. 25(6): 948-958.
- Garside, J., Rusli, I.T., and Larson, M.A. (1979). Origin and size distribution of secondary nuclei. **AIChE Journal**. 25(1): 57-64.
- Genck, W. J. and Larson, M. A. (1972). Temperature Effects of Growth and Nucleation Rates in a Mixed Suspension Crystallization. **AIChE Symposium Series**. 68(121): 57-66.
- Gharidi, M., Yuregir, K. R., Pollock, H. M., Ross, D. J., and Rolfe, N. (1991). Influence of processing conditions on attrition of NaCl crystals. **Powder Technology**. 65: 311-320.
- Ghadiri, M. and Zhang, Z. (2002). Impact attrition of particulate solids. Part 1: A theoretical model of chipping. **Chemical Engineering Science**. 57: 3659-3669.

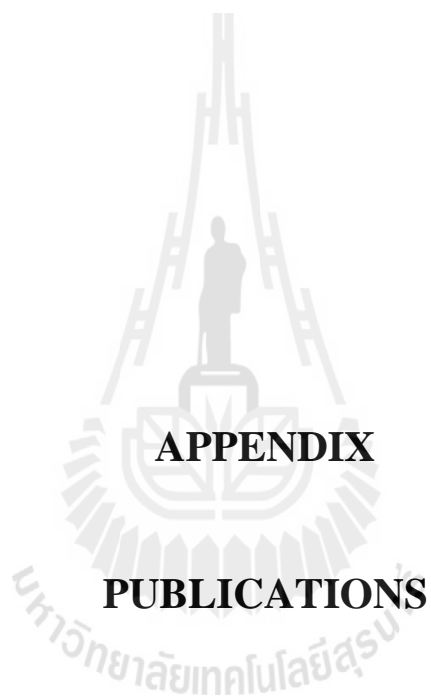
- Grootscholten, P. A. M., B. G. M. De Leer, et al. (1982). Factors affecting secondary nucleation rate of sodium chloride in an evaporative crystallizer. **AIChE Journal**. 28: 728-737.
- Jager, J., de Wolf, S., Kramer, H.J.M. and de Jong, E.J. (1991) Estimation of nucleation and attrition kinetics from CSD transients in a continuous crystallizer. **Chemical Engineering Research and Design**. 69: 53-62.
- Jancic and Grootcholten, (1984) **Industrial crystallization**. University Press, Delft.
- Kubota, N. and H. Ooshima. (2001). Japanese industrial crystallization research: overview. **Powder Technology**. 121: 26-30.
- Kuboi, R., Nienow, A.W. and Conti, R., 1984. Mechanical Attrition of Crystals in Stirred Vessels. In **Industrial Crystallization 84** (pp. 211-216). North Holland, Amsterdam: Elsevier.
- Larson, M. A. and Bendig, L. L. (1976). **AIChE Symposium Series**. 72(153): 11.
- Lieb, A. and Kind, M. (2004). Determination of the attrition behaviour of ammonium sulphate and of pentaerythritol crystals using a Forced Circulation Crystallizer. **Powder Technology**. 143-144: 273-279.
- Marrot, B. and Biscans, B. (2001). Impact of a single crystal in solution, on an immersed target, in conditions which simulate impact attrition in crystallizers. **Powder Technology**. 120: 141-150.
- Marrot, B., Pons, M.N., and Biscans, B. (2000). Identification of impact attrition mechanisms in solution by morphological analysis. **Chem. Eng. J.** 79: 123-131.
- Mazzarotta, B. (1992). Abrasion and breakage phenomena in agitated crystal suspensions. **Chemical Engineering Science**. 47(12): 3105-3111.

- Melia, T.P. and Moffitt, W.P. (1964a). Secondary Nucleations from Aqueous Solutions. **Ind. Eng. Chem. Fund.** 3: 323.
- Melia, T.P. and Moffitt, W.P. (1964b). **Nature** (London) 201, 1024.
- Mersmann, A., R. Sangl, et al. (1988). Attrition and secondary nucleation in crystallizers. **Chemical Engineering and Technology** 11(2): 80-88.
- Mullin, J.W. (2001). **Crystallization**. 4th ed. Butterworth-Heinemann. UK.
- Myerson, A. S. (2002). **Handbook of Industrial Crystallization**. 2nd ed. Butterworth-Heinemann. USA.
- Ness, J.N. and White, E.T. (1976). Collision Nucleation in an Agitated Crystallizer. **AIChE Symposium Series**. 72 (153): 64-73.
- Neumann, A. M., Bermingham, S. K., Kramer, H. J. M., and van Rosmalen, G. M. (1999). The effect of the impeller speed on the product crystal size distribution (CSD) a 22 liter draft tube (DT) crystallizer. **J. of Crystal Growth**. 198/199: 723-728.
- Nienow, A. W. and Conti, R. (1978) Particle abrasion at high solids concentration in stirred vessels. **Chemical Engineering Science**. 33: 1077-1086.
- Nývlt, J. (1968). "Kinetics of nucleation in solutions." **Journal of Crystal Growth** 3-4(C): 377-383.
- Nývlt, J. (1981). Cell. Czech. 46, 79.
- Offermann, H., and Ulrich, J. (1982). On the Mechanical Attrition of Crystals, In **Industrial Crystallization** 81(pp.313-314). North-Holland Publishing Company.

- ÓMeadhra, R. and G. M. Van Rosmalen (1996). Scale-up of ammonium sulphate crystallization in a DTB crystallizer. **Chemical Engineering Science**. 51(16): 3943-3950.
- Ottens, E. P. K. and E. J. De Jong (1973). A model for secondary nucleation in a stirred vessel cooling crystallizer. **Industrial and Engineering Chemistry**. 12(2): 179-184.
- Ottens, E. P. K. and E. J. de Jong (1974). A Model for Secondary Nucleation in a Stirred Vessel Cooling Crystallizer. **Kristall und Technik**. 9(8): 873-886.
- Ottens, E. P. K., A. H. Janse, et al. (1972). Secondary nucleation in a stirred vessel cooling crystallizer. **Journal of Crystal Growth**. 13-14(C): 500-505.
- Papageorgiou, N. A. and G. D. Botsaris (1986). Contact nuclei breeding in motor controlled sliding of crystal seeds. **Journal of Crystal Growth**. 74(1): 225-227.
- Paramanathan, B. K. and Bridgwater, J. (1983). Attrition of solid – I Cell development. **Chem. Eng. Sci.** 38(2): 197-206.
- Ploß, R. and A. Mersmann (1989). A new model of the effect of stirring intensity on the rate of secondary nucleation. **Chemical Engineering & Technology**. 12(1): 137-146.
- Powers, H. E. C., (1963). **Ind. Chemist**. 39: 351.
- Randolph, A. D. and Larson, M. A. (1988). **Theory of particulate processes**. 2nd ed. Academic Press, Inc. USA.
- Reeves, S. M. and P. J. Hill (2012). Mechanisms Influencing Crystal Breakage Experiments in Stirred Vessels. **Crystal Growth & Design**.
- Seader, J. D., and Henley, E. J. (1998). **Separation process principles**. John Wiley & Sons, Inc. USA.

- Shamlou, P. A., A. G. Jones, et al. (1990). Attrition of potassium sulphate crystals in stirred vessels. **Institution of Chemical Engineers Symposium Series**. 121: 309-325.
- Sikdar, S. K. and Randolph, A. D. (1976). **AIChE J.** 27: 1029.
- Synowiec, P., A. G. Jones, et al. (1993). Crystal break-up in dilute turbulently agitated suspensions. **Chemical Engineering Science** 48(20): 3485-3495.
- Strickland-Constable, R. F. (1968). **Kinetics and mechanism of crystallization**. **Academic Press**. London and New York.
- Strickland-Constable, R. F. (1972). **Chem. Eng. Symposium Series**. 68(121): 1.
- Tai, C. Y. and P.-C. Chen (1995). Nucleation, agglomeration and crystal morphology of calcium carbonate. **AIChE Journal**. 41(1): 68-77.
- Tai, C. Y., W. L. McCabe, et al. (1975). Contact nucleation of various crystal types. **AIChE Journal**. 21(2): 351-358.
- Tai, C. Y. and C.-Y. Shih (1996). A new model relating secondary nucleation rate and supersaturation. **Journal of Crystal Growth** 160(1-2): 186-189.
- Tai, C. Y., C.-D. Tai, et al. (2009). Effect of interfacial supersaturation on secondary nucleation. **Journal of the Taiwan Institute of Chemical Engineers**. 40(4): 439-442.
- Tai, C. Y., J. F. Wu, et al. (1992). Interfacial supersaturation, secondary nucleation, and crystal growth. **Journal of Crystal Growth**. 116(3-4): 294-306.
- Tait, S., E. T. White, et al. (2009). A Study on Nucleation for Protein Crystallization in Mixed Vessels. **Crystal Growth & Design**. 9(5): 2198-2206.

- van der Heijden, A. E. D. M. and M. Elwenspoek (1990). Contact nucleation: in situ and ex situ observations of surface damaging. **Journal of Crystal Growth**. 99(1–4, Part 2): 1087-1091.
- van der Heijden, A. E. D. M., J. P. van der Eerden, et al. (1994). The secondary nucleation rate: a physical model. **Chemical Engineering Science**. 49(18): 3103-3113.
- van Laarhoven, B., S. H. Schaafsma, et al. (2010). Development of a new abrasion tester based on planetary motion. **Powder Technology**. 203(2): 167-175.
- Wang, J. and J. Estrin (1996). Secondary nucleation of sucrose by fluid shear in aqueous solutions. **Chemical Engineering Communications**. 152-153: 275-286.
- Wójcik, J. A., Synowiec, P. M., and Opaczynska, K. (2005). Modeling of crystal attrition. In **Proceeding of the 16th International Symposium on Industrial Crystallization** (paper B-9). Dresden, Germany: VDI Verlag.
- Yokota, M., Takezawa, E., Takakusaki, T., Sato, A., and Takahashi, H. (1999). Scale-up effect on the rate of contact nucleation caused by collisions of crystals with an impeller. **Chem. Eng. Sci.** 54: 3831-3838.
- Youngquist, G. R. and A. D. Randolph (1972). Secondary nucleation in a class II system. Ammonium sulfate- water. **AIChE Journal**. 18(2): 421-429.
- Yuregir, K. R., Ghadiri, M., and Clift, R. (1987). Impact attrition of sodium chloride crystals. **Chem. Eng. Sci.** 42(4): 843-853.
- Zhang, Z. and Ghadiri, M. (2002). Impact attrition of particulate solids. Part 2: Experimental work. **Chem. Eng. Sci.** 57: 3671-3686.



APPENDIX

PUBLICATIONS

List of publications

Mueansichai, T., Flood, A. E., Stelzer, T., and Ulrich, J. (2012) Rates of sodium chloride attrition fragment generation in a mixed-suspension crystallizer.

Crystal Research and Technology (Submitted for publication)

Mueansichai, T., Flood, A. E., Stelzer, T., and Ulrich, J. (2009) Scale up effect on attrition of sucrose crystal in batch crystallizer. In **16th BIWIC International Workshop on Industrial Crystallization** (pp. 110-116). Lappeenranta, Finland: (Oral presentation)

Mueansichai, T. and Flood, A. E. (2008) Attrition of sucrose crystals in mixed suspension crystallizers. **15th BIWIC International Workshop on Industrial Crystallization** (pp. 65-72). Magdeburg, Germany: (Oral presentation)

Mueansichai, T. and Flood, A. E. (2011) Rates of sodium chloride attrition fragment generation in a mixed-suspension crystallizer. In **18th International Symposium on Industrial Crystallization (ISIC)**. Zurich, Switzerland: (Poster presentation)

Mueansichai, T. and Flood, A. E. (2010) A study of nucleation by attrition in industrial crystallization. In **11th RGJ – Ph.D. Congress**. Chonburi, Thailand: (Oral presentation)

Attrition of Sucrose Crystals in Mixed Suspension Crystallizers

T. Mueansichai, Associate Professor A.E. Flood
 School of Chemical Engineering, Suranaree University of Technology
 Nakhon Ratchasima, 30000 Thailand
 adrianf@sut.ac.th

Attrition of macroscopic crystals in industrial crystallizers is a significant problem not only due to its degradation of the product crystals, but also due to the creation of large numbers of particles acting as secondary nuclei, thus greatly reducing the mean particle size in the crystallizer. Although there are previous models relating to the phenomenon (notably that of Gahn and Mersmann [1,2] and Biscans [3]) the models require parameters not readily available, and are potentially complex to use in industrial systems. The work presented here is part of a project to describe attrition in industrial crystallizers using an empirical engineering model based on dimensionless groups (derived from Buckingham-Pi theory for example) describing crystal properties, suspension properties, mother liquor properties, and groups describing crystallizer geometry and operation. The current paper describes attrition of sucrose crystals in a small scale mixed suspension crystallizer, varying the following parameters: impeller diameter; draft tube diameter; impeller clearance; impeller speed; blade type; blade material; parent crystal size; suspension density; solution viscosity; and solution density. In all experiments it was found that the attrition fragments had a finite particle size distribution (PSD), and in particular had relatively wide PSDs. The fragments typically had mean sizes in the order of 5 μm , and geometric standard deviations of approximately 0.8-0.9. The initial rate of generation of attrition fragments was far higher than a latter rate of 'steady' attrition. This initial rate is presumably higher due to the sharp edges on the particles at the start of the experiment; after the edges become rounded the rate of attrition drops off significantly, but then stays at a constant rate for the remainder of the batch run. The rate of attrition during the 'steady' attrition allows the different conditions to be compared for differences in attrition rates to high accuracy. All parameters varied during the study had a strong effect on the attrition rate, and some parameters also had a significant effect on the PSD of the attrition fragments.

1. Introduction

Attrition is a process where very fine particles (typically with sizes in the order of 10 μm or less) are fragmented from the surface of parent crystals, and where the size and the shape of the parent crystal is changed only slightly by the process. This makes it distinct from the process of breakage, where the fragments produced are a substantial fraction of the size of the parent, and where the size of the parent crystal changes significantly, or where the parent crystal effectively disappears and is replaced by newly formed fragments. In many ways attrition is a more significant mechanism than breakage in industrial crystallizers. In many cases attrition is the major cause of formation of secondary nuclei, particularly in crystallizers with low supersaturation levels. While attrition does not change the appearance of the parent crystals significantly it does have a very strong effect on the particle size distribution (and therefore the overall appearance of the crystalline product, and its suitability for its intended application) because of the increased nucleation resulting in smaller average particle sizes. In seeded crystallizers it may result in an undesirable bimodal particle size distribution.

Two notable previous models for attrition in industrial crystallization systems have been produced, that of Gahn and Mersmann [1, 2, 4] and Biscans [3, 5, 6]. In other cases attrition data for specific materials in industrial crystallizers has been fitted to models (for example by Lieb and Kind [7]). The models are difficult to use for general industrial crystallizers for two reasons: the parameters required in the model are often unknown (for instance the fracture surface energy and the radius of the circle of contact on the crystal surface) and the fact that they do not take into account the geometry of the crystallizer, which is presumably important in determining the number and type of contacts between crystals and the impeller.

The current research is part of a project to attempt a non-dimensional engineering correlation of attrition data in industrial crystallizers in order to obtain a general model suitable for initial design purposes, and in order to enable designers to predict geometrical and operation conditions to minimize secondary nucleation by attrition. The project has begun with a detailed study of the attrition of sucrose in a small-scale crystallizer with a draft tube and baffles. Due to the scale of the problem and number of variables involved, it was decided to partition the properties which have an effect on the attrition rate into three types; properties of the crystallizer geometry; properties of the suspension, solution, and fluid flow; and crystal properties. The last set of properties is not considered in this study since only one solute species (sucrose) has been tested so far. From a dimensional analysis of the variables expected to be significant in attrition it is expected that the following dimensionless groups should reflect the mechanism best; the Impeller Reynolds number (N_{Re}), which is varied in the current study by variations in fluid viscosity and impeller speed; the Power Number (N_p); the impeller clearance ratio (N_{Cl}); the impeller/draft tube ratio (N_{DT}); and the ratio of suspension density to fluid density (N_{SD}). The rate of attrition is characterized by the attrition number (N_{At} = attrition rate $\cdot V_{imp} / N$), which is original (to the best knowledge of the authors). The material and type of the impeller are also expected to have strong effects on the attrition rate, although these parameters are non-numeric and thus impossible to include into correlations. They are still varied in the current study, which uses marine impellers and pitch blade impellers from both stainless steel and resin.

2. Materials and Methods

All experiments in the current study were performed in a 500 mL batch crystallizer equipped with four vertical baffles, draft tube, and an upflow impeller connected to a variable speed overhead mixer. A schematic figure of the crystallizer is shown in Fig. 1. Experiments were performed via a partial factorial design, with standard conditions (low value : high value) for the experiments being:

Crystallizer properties

- Diameter of draft tube = 64 : 75 mm
- Diameter of impeller = 50 mm
- Impeller clearance = 10 : 20 mm
- Type of blade = *marine type propeller* : 45° pitch blade impeller
- Material of blade = *stainless steel* : resin
- Impeller speed = 800 : 1000 : 1200 rpm

Crystal properties

- Size range of parent crystals (L) = 300 – 425 : 425 – 600 : 600 – 850 μm

- Type of parent crystals = *sucrose*

Solution and suspension properties

- Parent crystal suspension density (m_c) = 10 : 15 g of parent crystal/100 ml solution
- Saturated solution (25 °C, sucrose in 100% MeOH : 90% MeOH : 80% MeOH)
- Reynolds Number = 14,400 : 36,700 : 43,900

The conditions for the standard case (all variables at base level in the factorial design) are indicated by the use of italics. Other conditions were also studied where extra points appeared necessary for model fitting.

When a sampling time was reached the impeller speed was lowered to 200 rpm, which is low enough that the parent crystals (which had sizes in the order of hundreds of micrometers) settled out while attrition fragments remained suspended. 20 mL of suspension was sampled using a pipette for analysis of the suspension density by determination of the weight of particles left after filtration through a 0.45 μm filter. Samples were also taken for particle sizing, which was performed with a Malvern Mastersizer/E with a 300 mm lens and a beam length of 14.3 mm. While it would have been more convenient to use a particle counter (a Coulter Counter for instance) it was found that the PSDs of the fragments were sufficiently wide that it was impossible to count all fragments using a single orifice. Sieve separation followed by sizing is not convenient at the small sizes evident in this work. Volume based PSDs of the fragments varied from approximately 1 – 100 μm (with the larger sized particles still being considerably smaller than the parent crystals), while number based PSDs were typically in the range of 0.5 – 50 μm , although the fraction of particles larger than 20 μm was small. The volume based PSD was log-normal indicating that the number based PSD was also log-normal. The conversion to the number of attrition fragments could then be calculated from the Malvern data and the suspension density via the equations

$$\ln(\mu_{gN}) \equiv \ln(\mu_{gV}) - 3(\ln(\sigma_g))^2 \quad (1)$$

$$\overline{L_{3,0}} = \sqrt{\exp(3 \ln \mu_{gN} + 4.5 \ln^2 \sigma_g)} \quad (2)$$

$$N_T = \frac{M_T}{\frac{\pi}{6} \overline{L_{3,0}}^3} \quad (3)$$

3. Results and Discussion

In each experiment the number of attrition fragments was measured as a function of time, based on the output from the Malvern Mastersizer/E, the measured suspension density of fragments, and equations (1) – (3). The PSD of the attrition fragments was essentially constant with respect to time during the experiments indicating that the attrition only occurred to the parent crystals added to the vessel (not occurring again to fragments) and that the mechanism was maintained throughout the process. Average sizes over time and in triplicate experiments did vary slightly but randomly, and values were taken as averages of the nine PSDs; triplicate experiments over three time periods. The number of attrition fragments vs. time is shown in Fig. 2.

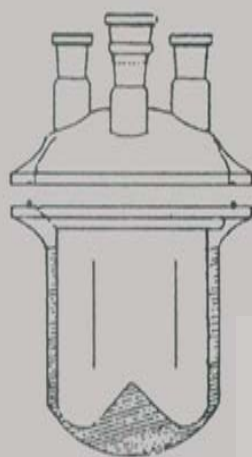


Fig. 1: Schematic diagram of the 500 mL crystallizer used in the study. The impeller and 4 vertical baffles are not shown for reasons of clarity.

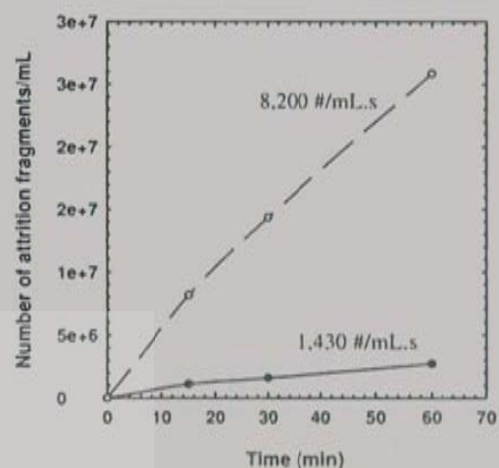


Fig. 2: Number of attrition fragments as a function of time for the stainless steel marine impeller at 1000 rpm • 10%; • 15% suspension density.

Although the size of the fragments produced is constant during an experiment under a particular set of conditions, it varies strongly depending on the condition being investigated, which makes the system more difficult to analyze in terms of the attrition rate. For a particular volume rate of production of attrition fragments the number rate of attrition varies strongly with the size of the fragments produced. Fig. 3 shows the average size of fragments at standard conditions in the crystallizer as the impeller speed is increased from 800 to 1200 rpm. Higher agitation rates (and therefore higher power inputs) clearly produce larger attrition fragments. Fig. 4 shows how the suspension density of the attrition fragments (on the basis of volume fragments per suspension volume) increases over the course of an experiment, for the conditions shown in Fig. 3. Although the increase in the suspension density at 1200 rpm occurs at a higher rate than at the lower stirrer speeds, the average particle size (and also the value of $L_{3,0}$ for the fragments) is also much higher. These effects balance each other out to some extent when the number rate of attrition is calculated from the data.

The effect of the impeller speed on the attrition rate (at standard conditions) is shown in Fig. 5. It is clear that the increased volume rate of production of the attrition fragments more than compensates for the increased size of the attrition fragments at higher speeds, and thus the number based attrition rate increases as the impeller speed increases. Fig. 6 shows the attrition rate as a function of the size of the parent crystals used in the experiment. Although it is expected that the larger parent crystals are more likely to impact the impeller, and therefore more likely to undergo attrition, it was found that smaller parent crystals resulted in higher attrition rates at a particular suspension density of parent crystals. This is due to the much larger number of the smaller parent crystals compared to the larger parent crystals at a constant value of the suspension density (in this case 10%).

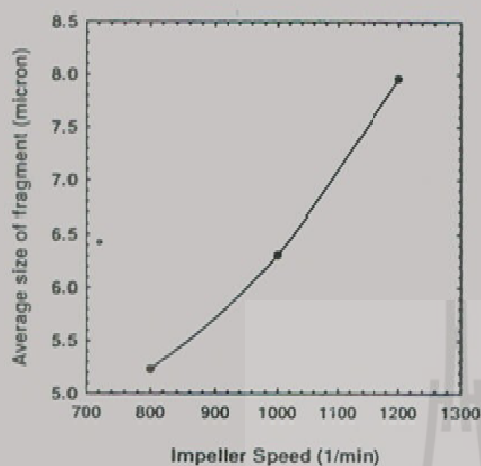


Fig. 3: Attrition fragment size as a function of impeller speed at standard conditions.

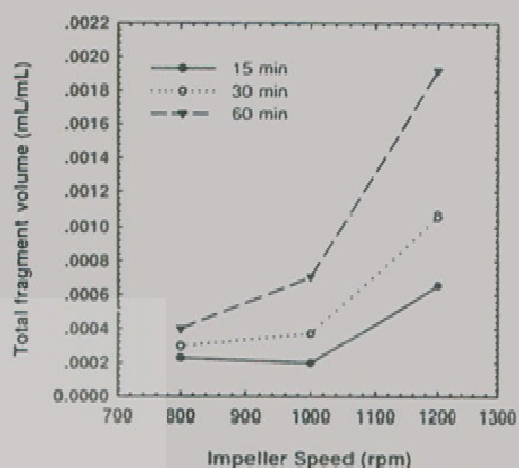


Fig. 4: Rate of increase in fragment volume per mL suspension (at standard conditions).

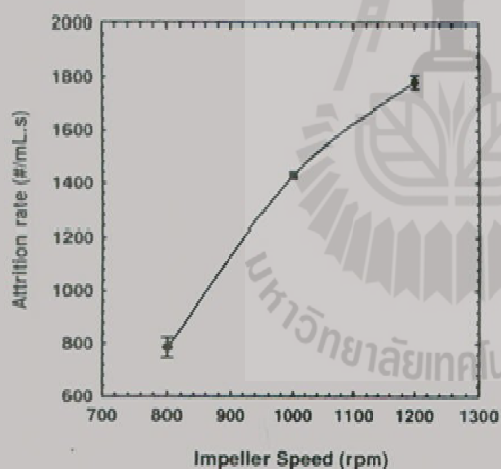


Fig. 5: Attrition rate as a function of impeller speed at standard conditions.

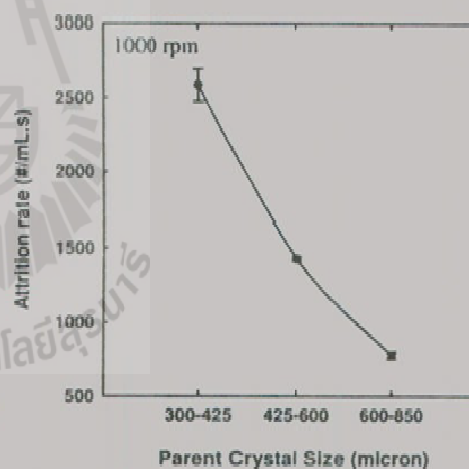


Fig. 6: Attrition rate as a function of parent crystal size at standard conditions.

The attrition rate as a function of suspension density is shown in Fig. 7. The increase in suspension density had a larger than anticipated effect on the rate of production of attrition fragments; much larger than the 50% increase anticipated from the relative magnitudes of the number of parent crystals. It is likely that this increased effect is due to a much larger number of crystal-crystal interactions in the zone of the impeller. As anticipated, the material of construction of the impeller had a significant effect on the rate of fragment generation (Fig.

8), although this effect may be difficult to include in a general model, as it seems unlikely to be entirely due to the differences in hardness of the two materials.

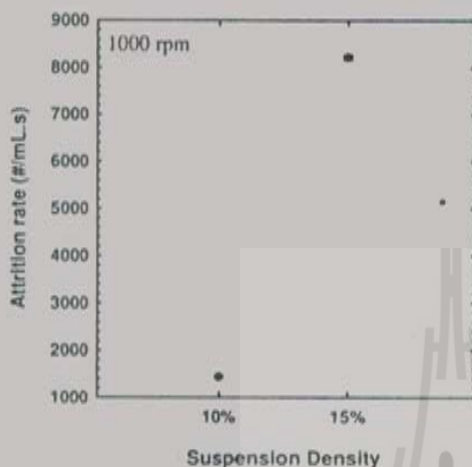


Fig. 7: Attrition rate as a function of suspension density at standard conditions.

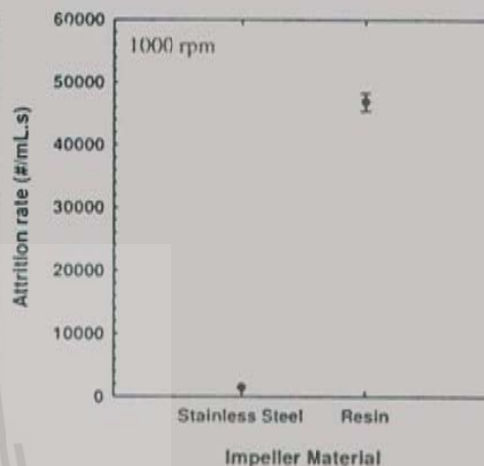


Fig. 8: Attrition rate as a function of impeller material at standard conditions.

Fig. 9 and Fig. 10 show the effect of the impeller speed on the attrition rate for a marine impeller and a pitch blade impeller respectively. In both cases the attrition rate increases strongly with the impeller speed, however the effect of the impeller speed is far more pronounced for the pitch blade impeller. This characteristic also produces difficulty for an entirely general model for the system.

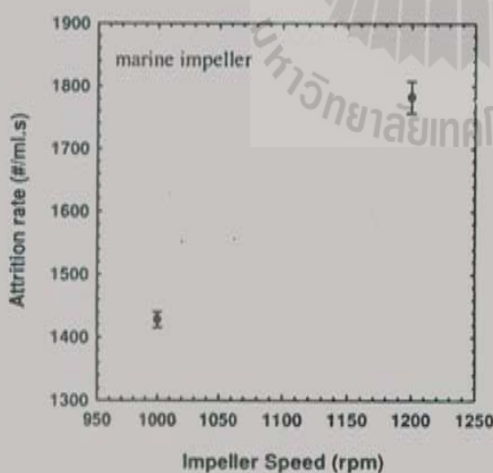


Fig. 9: Attrition rate as a function of impeller speed (marine impeller).

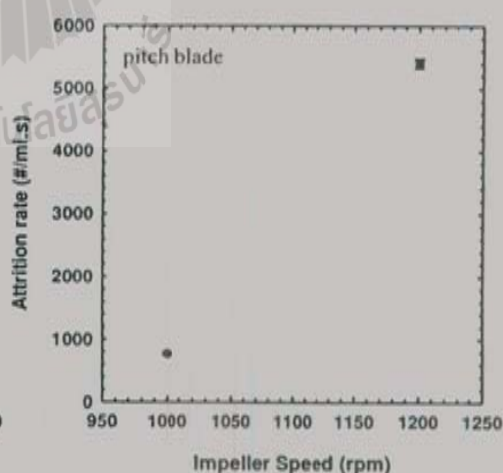


Fig. 10: Attrition rate as a function of impeller speed (pitch blade impeller).

Fig. 11 and Fig. 12 show the effect of the impeller : draft tube ratio and clearance : draft tube ratio respectively on the attrition rate for the standard conditions. The attrition rate decreases strongly as the diameter of the draft tube increases with respect to the impeller diameter. This is presumably due to the added clearance between the impeller tip and the draft tube, allowing more parent crystals to avoid contact with the impeller. An increase in the off-bottom clearance for the impeller also greatly reduces the attrition rate, presumably also because increased clearance allows for a greater proportion of parent crystals to escape contact with the impeller.

Although increased clearance between the impeller and the wall of the draft tube, and increased clearance between the impeller and the crystallizer vessel wall (at the base of the crystallizer) improves the performance of the crystallizer with respect to attrition, it is not possible to allow these parameters to take on any value. These parameters will also have a strong effect on the efficiency of mixing in the crystallizer, and also on the ability of the impeller to fully suspend the particles in the vessel. There is almost certainly a trade-off between improved design with respect to attrition, and improved design with respect to solution and suspension flow within the crystallizer. CFD studies are likely to enable a better understanding of this trade-off, and overall optimum values for clearance and draft tube diameter.

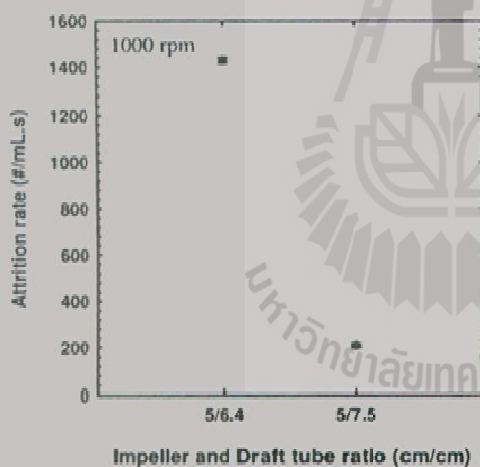


Fig. 11: Attrition rate as a function of impeller : draft tube ratio (marine impeller).

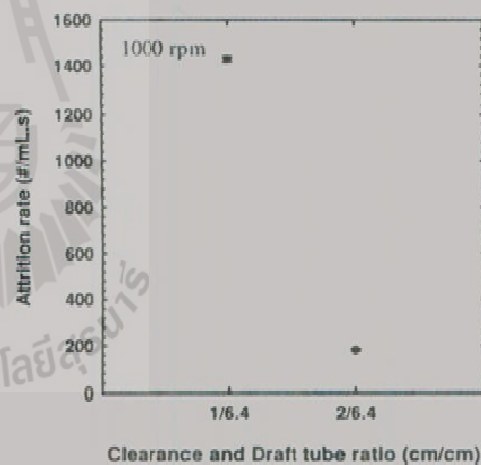


Fig. 12: Attrition rate as a function of clearance : draft tube (pitch blade impeller).

4. Conclusions

The study has produced a large number of measurements of attrition rate in a small-scale crystallizer; only a fraction of the total data can be shown here due to space limitations. These data are sufficient to produce an engineering model of attrition of sucrose in the crystallizer. The system is more complex than first anticipated due to the strong variation in fragment size as the conditions in the crystallizer vary, which has a strong influence on the measured

attrition rate. It is possibly easier to model the system based on a volume rate of attrition. The downside of this approach is that the main problem associated with attrition, the rate of secondary nucleation caused by attrition, is a number based mechanism.

Further research needs to be performed in larger crystallizers to ensure that a model based on the current data can be suitably scaled up to an industrial sized crystallizer. In particular, it is not yet known whether attrition rate correlation based on the impeller : draft tube ratio and the clearance : draft tube ratio will be suitable upon scale-up. It is possible that ratios based on the clearance between the impeller and the draft tube divided by the volume mean particle size, and the off-bottom clearance divided by the volume mean particle size may be more appropriate. Experiments in larger crystallizers should be able to verify which dimensionless groups are most suitable for scale-up studies.

5. Nomenclature

D	Impeller diameter (m)
$\bar{L}_{v,0}$	Number-volume mean particle size (μm)
M_T	Suspension density (kg/m^3) or (m^3/m^3 in eq.3)
N	Impeller speed (s^{-1})
N_{At}	Attrition number: attrition rate $\cdot V_{imp}/N$ (-)
N_{Cl}	Clearance ratio: impeller clearance/draft tube diameter (-)
N_{DT}	Draft tube ratio: impeller diameter/draft tube diameter (-)
N_P	Power number: $P/\rho N^3 D^5$ (-)
N_{Re}	Impeller Reynolds number: $D^2 N \rho / \mu$
N_{SD}	Suspension density ratio: suspension density/fluid density (-)
N_T	Number density of crystals ($\#/mL$)
P	Power (W)
V_{imp}	Volume used by the moving impeller (m^3)
μ_{gN}	Geometric mean of the number particle size distribution (μm)
μ_{gV}	Geometric mean of the volume particle size distribution (μm)
σ_g	Geometric standard deviation of the volume particle size distribution (μm)

6. References

- [1] C. Gahn and A. Mersmann. *Chem. Engng. Sci.* **54** (1999) 1273.
- [2] C. Gahn and A. Mersmann. *Chem. Engng. Sci.* **54** (1999) 1283.
- [3] B. Biscans. *Powder Tech.* **143-144** (2004) 264.
- [4] C. Gahn and A. Mersmann. *Powder Tech.* **85** (1995) 71.
- [5] B. Biscans, R. Chemini, P. Giuraud and C. Laguerie. *Powder Tech.* **86** (1996) 155.
- [6] B. Marrot and B. Biscans. *Powder Tech.* **120** (2001) 141.
- [7] A. Lieb and M. Kind. *Powder Tech.* **143-144** (2004) 273.

Acknowledgements

The authors thank the Royal Golden Jubilee Ph.D. Program fund of the Thailand Research Fund, and also the Ministry of Education (Thailand), for support of this research.

BIOGRAPHY

Mr. Thirawat Mueansichai was born on May 27, 1981 in Loei province. He graduated with bachelor's degree of engineering in chemical engineering in 2004 from Suranaree University of Technology (SUT), Nakhon Ratchasima province. He awarded the Royal Golden Jubilee Ph.D. grant from the Thailand Research Fund (TRF) since 2004 to study the doctoral degree of engineering in chemical engineering at SUT. He also received scholarship for development of new faculty staff from the Ministry of Education through the Commission on Higher Education since 2005. He has a contract with Rajamangala University of Technology Thanyaburi to work at the Department of Chemical Engineering after completing his Ph.D. He has one year's experience in the group of Thermal Process Technology (TVT) at Martin Luther University Halle-Wittenberg in Halle (Saale), Germany in September 2008 to September 2009.